

DTIC FILE COPY

1

Anatomy of a "Bomb"  
Diagnostic Investigation of  
Explosive Cyclogenesis Over the  
Mid-West United States

DTIC  
ELECTE  
FEB 22 1990  
S D

by  
Michael E. Adams

A thesis submitted to the Graduate Faculty of  
North Carolina State University  
in partial fulfillment of the  
requirements for the Degree of  
Master of Science


Department of Marine, Earth, and Atmospheric Sciences

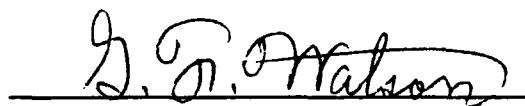
Raleigh  
1989


DISTRIBUTION STATEMENT A

Approved for public release  
Distribution Unlimited

Approved By:

  
Steven Businger  
Co-Chairman of Advisory Committee

  
Gerald F. Watson  
Co-Chairman of Advisory Committee

  
John Morrison

AD-A218 161

90 02 21 062

## REPORT DOCUMENTATION PAGE

Form Approved  
OMB No. 0704-0188

1a. REPORT SECURITY CLASSIFICATION <b>UNCLASSIFIED</b>			1b. RESTRICTIVE MARKINGS <b>NONE</b>		
2a. SECURITY CLASSIFICATION AUTHORITY			3. DISTRIBUTION / AVAILABILITY OF REPORT <b>APPROVED FOR PUBLIC RELEASE; DISTRIBUTION UNLIMITED.</b>		
2b. DECLASSIFICATION / DOWNGRADING SCHEDULE			4. PERFORMING ORGANIZATION REPORT NUMBER(S)		
5. MONITORING ORGANIZATION REPORT NUMBER(S) <b>AFIT/CI/CIA-89-053</b>			6a. NAME OF PERFORMING ORGANIZATION <b>AFIT STUDENT AT NORTH CAROLINA STATE UNIVERSITY</b>		
6b. OFFICE SYMBOL (If applicable)			7a. NAME OF MONITORING ORGANIZATION <b>AFIT/CIA</b>		
6c. ADDRESS (City, State, and ZIP Code)			7b. ADDRESS (City, State, and ZIP Code) <b>Wright-Patterson AFB OH 45433-6583</b>		
8a. NAME OF FUNDING / SPONSORING ORGANIZATION		8b. OFFICE SYMBOL (If applicable)		9. PROCUREMENT INSTRUMENT IDENTIFICATION NUMBER	
8c. ADDRESS (City, State, and ZIP Code)		10. SOURCE OF FUNDING NUMBERS			
		PROGRAM ELEMENT NO.		PROJECT NO.	TASK NO.
				WORK UNIT ACCESSION NO.	
11. TITLE (Include Security Classification) <b>(UNCLASSIFIED)</b> <b>Anatomy of a "Bomb" - Diagnostic Investigation of Explosive Cyclogenesis Over the Mid-West United States</b>					
12. PERSONAL AUTHOR(S) <b>Michael E. Adams</b>					
13a. TYPE OF REPORT <b>THESIS / DISSERTATION</b>		13b. TIME COVERED FROM _____ TO _____		14. DATE OF REPORT (Year, Month, Day) <b>1989</b>	
15. PAGE COUNT <b>102</b>		16. SUPPLEMENTARY NOTATION <b>APPROVED FOR PUBLIC RELEASE IAW AFR 190-1 ERNEST A. HAYGOOD, 1st Lt, USAF Executive Officer, Civilian Institution Programs</b>			
17. COSATI CODES			18. SUBJECT TERMS (Continue on reverse if necessary and identify by block number)		
FIELD	GROUP	SUB-GROUP			
19. ABSTRACT (Continue on reverse if necessary and identify by block number)					
20. DISTRIBUTION / AVAILABILITY OF ABSTRACT <input checked="" type="checkbox"/> UNCLASSIFIED/UNLIMITED <input type="checkbox"/> SAME AS RPT. <input type="checkbox"/> DTIC USERS					
21. ABSTRACT SECURITY CLASSIFICATION <b>UNCLASSIFIED</b>					
22a. NAME OF RESPONSIBLE INDIVIDUAL <b>ERNEST A. HAYGOOD, 1st Lt, USAF</b>			22b. TELEPHONE (Include Area Code) <b>(513) 255-2259</b>		22c. OFFICE SYMBOL <b>AFIT/CI</b>

## Abstract

ADAMS, MICHAEL E. Anatomy of a "Bomb" - Diagnostic Investigation of Explosive Cyclogenesis Over the Mid-West United States (Under the direction of Steven Businger and Gerald F. Watson.)

An in depth study was conducted to investigate the physical processes responsible for the explosive cyclogenesis that took place over the Mid-West United States on 14-15 December 1987. This system is worthy of study because of its explosive development (central pressure dropped 27 mb in 18 hours) totally over land. Statistical studies have shown that the explosive development of land-locked cyclones or "bombs" are a rare event. This study provides a unique opportunity to take advantage of the National Weather Service observation network in analyzing the structure of the explosive cyclogenesis.

The development of this storm is marked by two distinct phases of deepening. During the initial phase (1800 UTC 14 December to 0400 UTC 15 December) the cyclone experienced a pressure fall of  $1 \text{ mb/hr}^{-1}$ . Cyclogenesis was initiated near Houston, Texas at approximately 1800 UTC 14 December. Convection developed in the vicinity of the cyclone center and extended along the cold front with time. Low-level convergence associated with the convection enhanced frontogenesis along the cold front and an associated low-level jet developed in the warm air just ahead of the front in response to thermal wind constraints. The low-level jet aided cyclogenesis through the advection of warm-moist Gulf air into the region of developing low pressure, coincidental with the superposition of the left exit region of a subtropical jet over the surface front.

The second and most rapid phase of explosive development began when a progressive short-wave trough, associated with the polar jet, moved out of the southern Rockies and approached within 400 km of the cyclone center. This rapid phase of development (pressure fall of  $2.5 \text{ mb/hr}^{-1}$  from 0600 to 1200 UTC 15 December) coincides with: i) a merging of the polar and subtropical jets aloft; ii) very strong advection of cyclonic mid-tropospheric vorticity over the cyclone center; iii) vertical coupling of the ageostrophic motion fields associated with the upper and lower level jets; and iv) the intrusion of stratospheric air down to the 700 mb level enhancing the generation of cyclonic vorticity. All of these factors combine to provide a favorable environment for enhanced upward vertical motion and surface deepening.

## Biography

Michael E. Adams is a weather officer in the United States Air Force assigned to the Air Weather Service.

He is a native of Connecticut born in New Haven in 1958. He attended Lyndon State College in up-state Vermont where he received a Bachelor of Science degree in Meteorology with a minor in Mathematics. Upon graduation in the spring of 1981, he was commissioned a Second Lieutenant in the United States Air Force.

His active military career began with the Air Force Global Weather Central at Offutt Air Force Base, Omaha, Nebraska. While there he served as the officer in charge of the Asian forecast section, the upper atmosphere analysis section, and then as the assistant Operations Officer. In 1984, he was reassigned overseas to the Royal Air Force Base Lakenheath, England. There he served as the Wing Weather Officer responsible for the coordination of base wide weather support. He was promoted to the rank of Captain in 1985. In 1987, he was awarded an Air Force Institute of Technology scholarship to pursue an advanced degree in meteorology at North Carolina State University, Raleigh, North Carolina. Upon completion of his masters degree, he will be assigned to Patrick Air Force Base, Florida where his duties will include providing weather support to Space Shuttle operations.

Michael E. Adams is married to the former Susan Jayne Goblen. They have one daughter, Katelyn Christine.

Accession For	
NTIS CRA&I	<input checked="" type="checkbox"/>
DTIC TAB	<input type="checkbox"/>
Unannounced	<input type="checkbox"/>
Justification	
By	
Distribution /	
Availability Codes	
Dist	Avail and/or Special
A-1	



### Acknowledgements

The author would like to thank Dr. Steven Businger and Dr. Gerald Watson for their guidance, expertise, and patience during the preparation of this thesis. The personal time and effort spent in enhancing the quality of this document is truly appreciated.

I would like to express my sincere appreciation to the following individuals who aided my research:

- John Walsh of OL-A Environmental Technical Applications Center (ETAC), USAF, Asheville, North Carolina. His assistance in supplying surface and upper-air data was critical in conducting this research.
- Dr. Arthur V. Douglas, Creighton University, Omaha, Nebraska and Roderick A. Schofield, NESDIS/Satellite Applications Laboratory, Washington D.C. The satellite imagery they supplied provided valuable insight into the storm development. The speed in which data was made available and the willingness to aid were greatly appreciated.
- Mary McVicker for the outstanding artistic and drafting expertise that enhanced the visual presentation of this research. Thanks Mary!
- The U. S. Air Force for allowing me the opportunity to pursue this advance degree.
- My parents, John and Regina; my sisters, Denise and Susan; and my brothers Randy and Chris for the encouragement, support and love they have always provided me. A special acknowledgement to my brother Chris. Without your enthusiasm and introducing me to the world of meteorology this thesis would never have been realized - thanks!

Finally, I would like to express my heartfelt appreciation to my wife Susan and daughter Katelyn. Completion of this thesis would not have been possible without their love, support, and patience!

## Table of Contents

	Page
CHAPTER 1 - LITERATURE REVIEW.....	1
1.1 Brief Historical Perspective.....	1
1.2 Climatology of Rapid Cyclogenesis.....	5
1.3 Influential Physical Processes.....	8
1.4 Current Research.....	11
1.5 Research Objectives.....	14
CHAPTER 2 - DATA AND METHODOLOGY.....	15
2.1 Data Sources.....	15
2.2 The Barnes Objective Analysis Scheme.....	15
CHAPTER 3 - CYCLONE EVOLUTION.....	19
3.1 Synoptic Development.....	19
3.2 Isallobaric Analysis.....	44
CHAPTER 4 - SATELLITE IMAGERY ANALYSIS.....	48
4.1 Evolution of the Synoptic Cloud Pattern.....	48
4.2 Water-Vapor Imagery Interpretation.....	60
CHAPTER 5 - STORM STRUCTURE.....	63
5.1 Conventional Vertical Cross Section Display.....	63
5.2 Stratospheric Influences.....	67
5.2.1 Role of Stratospheric Intrusion in Cyclogenesis.....	67
5.2.2 Conservation of Potential Vorticity.....	69
5.2.3 Eulerian Perspective of Potential Vorticity.....	73
5.2.4 Vertical Cross Section of Potential Vorticity Structure.....	78
5.3 Thermodynamic Omega.....	83
5.3.1 Thermodynamic Calculations of Vertical Motion.....	83
5.3.2 Vertical Cross Section of Thermodynamic Omega.....	86
CHAPTER 6 - SUMMARY AND CONCLUSIONS.....	89
6.1 Summary.....	89
6.2 Conclusions.....	93
6.3 Future Research.....	94
CHAPTER 7 - REFERENCES.....	95

## **CHAPTER 1**

### **LITERATURE REVIEW**

#### **1.1 Brief Historical Perspective**

The study of cyclone development has fascinated scientists for centuries and it was not until the advent of routinely plotted synoptic weather charts that a better understanding of extratropical cyclones could be realized. Nearly a century ago, Fitz-Roy developed a model depicting surface air currents associated with developing cyclones. Through personnel observation and limited availability of synoptic charts he was able to conclude that cyclones developed along a boundary separating two air masses of differing origin (Fitz-Roy, 1863). In the mid 1800's two theories existed to explain the development of extratropical cyclones. Espy is credited with the development of the "convectonal theory" for cyclone development. He hypothesized that cyclone centers were columns of warm ascending air responsible for the formation of precipitation. He attributed cyclone development to the release of latent heat from condensation. In 1876, Hann disputed Espy's claim and proposed the "dynamical theory". Hann pointed out that mountain top observations showed that air is cooler over a developing cyclone and not warm as proposed by Espy. Hann proposed that cyclones developed as eddies in the westerly air current and obtained energy from the current itself (Palmen and Newton, 1969).

In the early 1900's scientists at the Geophysical Institute of Bergen, Norway developed the classical representation of a developing extratropical cyclone known as the "Polar Front Theory". Bjerknes and Solberg (1921) developed a model representing the typical structure of a developing cyclone (Fig. 1.1). They determined that cold air acts like a wedge forcing itself under the less dense warm air. The adiabatic ascent of air resulted in the cloud and precipitation distribution about an extratropical cyclone. Further work by Bjerknes and Solberg (1922) on cyclone development resulted in a model illustrating the life cycle of an extratropical cyclone (Fig. 1.2). Cyclogenesis is depicted as a small perturbation on the boundary of a stationary front (Fig. 1.2a,b). The initiation of a counter clockwise circulation results in a wind component behind the cyclone center from cold to warm air and from warm to cold air ahead of the cyclone center (Fig. 1.2c). This circulation results in a further deformation of the thermal field associated with the

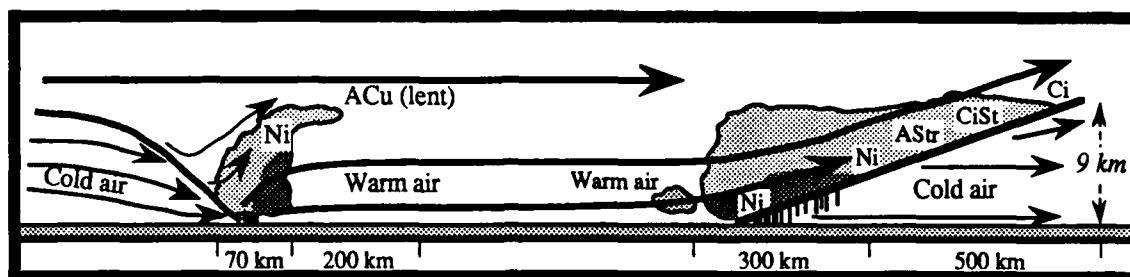


Figure 1.1. Extratropical cyclone model proposed by J. Bjerknes and H. Solberg (1921). The model depicts the vertical cross section passing through the warm sector to the south of a cyclone center. The model shows the adiabatic lifting of warm air resulting in the cloud and precipitation distribution. Arrows depict the relative flow within the plane of the cross section.

developing cyclone. Precipitation forms as a result of the displacement of warm air by the advancing cold front and the adiabatic lifting of warm moist air over the warm front. The cyclone develops as the cold front advances and overtakes the surface warm front as the system becomes occluded. The cyclone is the strongest at this stage (Fig. 1.2d). Figure 1.2e represents the dissipation of the system as the thermal structure weakens to an essentially barotropic whirl of air (Palmen and Newton, 1969). Dissipation occurs as cold air surrounds the cyclone at the lower levels. Without the available potential energy associated with warm air in the lower troposphere the system decays.

The development of the perturbation theory (Bjerknes *et al.*, 1933) allows one to treat the process of cyclogenesis as a small perturbation superposed on the mean zonal wind current. Amplification of a perturbation occurs as the basic flow gives up potential energy to the perturbation in the form of kinetic and potential energy. The energy is derived from the shear of the zonal wind, i.e., the baroclinicity of the atmosphere.

Bjerknes (1937), using the tendency equation, was able to relate the change in surface pressure to tropospheric thermal advection and the divergent patterns of the upper level wind field. This understanding, along with additional research, resulted in linking cyclone development to the vertical motion patterns of a progressive upper-level short wave trough (SWT). Normally, decreasing surface pressure is found in advance of a SWT where the presence of low-level convergence and upper-level divergence are found. The upward vertical motion pattern and the evacuation of mass within the column of air results in a decrease in surface pressure. The strength of this process is dependent on the amplitude and length of the SWT and the strength of the upper-level jet which is determined



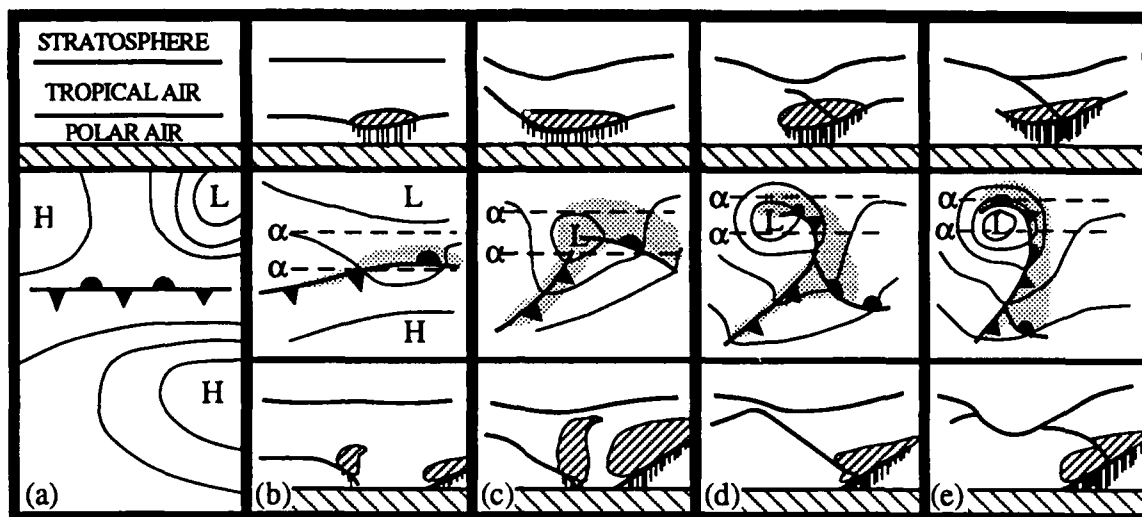


Figure 1.2. Life cycle of an extratropical cyclone developed by J. Bjerknes and H. Solberg (1922). Middle diagram depicts the horizontal development of a mid-latitude cyclone at one day intervals. Solid lines represent isobars and hatched regions correspond to precipitation distribution. Top and bottom diagrams correspond to vertical cross sections positioned north and south of the cyclone center along the axis  $\alpha$ . Depicted are clouds and precipitation while thick lines represent tropopause and frontal surface.

by the baroclinicity of the atmosphere. The mean divergent pattern associated with a sinusoidal wave pattern is given by:

$$\bar{D}_A \approx \frac{16\pi^2 A}{\bar{f} L^3} V(V - V_L) \quad \{1.1.1\}$$

where  $\bar{D}_A$  is the mean horizontal divergence,  $A$  is the amplitude of the wave,  $L$  is the wave length,  $\bar{f}$  is the mean coriolis force,  $V$  is the wind velocity, and  $V_L$  is the wind velocity at the level of nondivergence (Palmen and Newton, 1969). Thus, we can see that significant upper-level divergence is found on the east side of a progressive SWT, and is associated with high amplitude waves of small wavelengths, and a strong jet stream with strong vertical shear. The maintenance and intensification of a surface cyclone is closely tied to the proximity of the SWT and the associated divergent and vertical motion patterns.

Prior to 1945, mathematical theory on cyclone development neglected to incorporate the observed vertical shear in the mean zonal flow or the variations of the vertical component of the earth's angular velocity. Work conducted by Charney (1947) incorporate

both conditions leading to a more exact analytical solution similar to that observed in the real atmosphere. His work consisted of an analytical model in which the zonal wind speed increased at a constant rate with height. The solution yielded an eastward progressing sinusoidal wave pattern with a maximum growth rate for wavelengths of 3000 km. This solution is consistent with observed wavelengths in the mid-latitude troposphere.

The German school has been credited for first emphasizing the link between surface development and changes in the upper air flow. World War II brought about an increase in the number of upper air reports available for analysis. The availability of routine upper air charts confirmed many of the earlier theories on the relationship between cyclogenesis and the upper air flow which stimulated new research (Charney *et al.*, 1947).

In the 1950's, Petterssen concluded that the initiation of cyclogenesis was related to the advection of cyclonic vorticity over a surface baroclinic zone. Figure 1.3 depicts the stages of cyclone development as an area of cyclonic vorticity advection moves over a surface front and initiates cyclogenesis. The vertical motion and divergent patterns associated with the cyclonic vorticity advection result in the evacuation of mass and development of the surface cyclone.

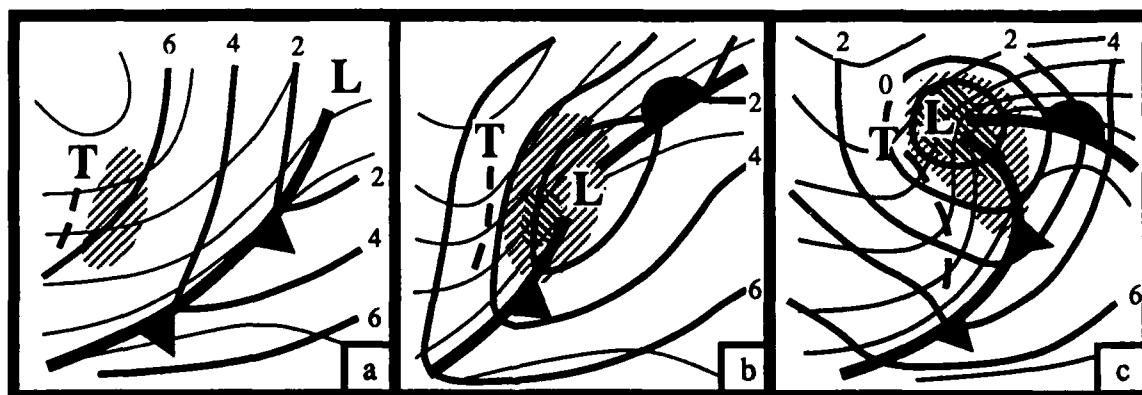


Figure 1.3. Stages of cyclone development in association with an advancing trough (denoted as "T" and depicted as dashed line) and its cyclonic vorticity advection (depicted as hatched area). As the trough approaches, cyclonic vorticity advection overtakes the front and initiates cyclone development. Thin solid lines depict isotherms, heavy solid lines depict isobars, and conventional symbols used to depict surface cyclone and front (After Petterssen, 1956).

Petterssen's scenario for cyclogenesis consists of two primary requirements: 1) The existence of a 500 mb SWT and 2) a surface front lying in a trough of low pressure. The surface trough is a local region of concentrated cyclonic shear and cyclonic vorticity. The approach of 500 mb cyclonic vorticity advection enhances the surface vorticity which results in a further deformation of the wind field. The deformation of the wind field leads to increased thermal advection patterns resulting in further development.

Work conducted by Sutcliffe and Petterssen (Petterssen, 1956) resulted in a mathematical description of the development of a cyclone. This equation provides a diagnostic tool for understanding cyclone development, making use of the relationship between geostrophic relative vorticity and circulation intensity. This mathematical representation shows cyclone development is enhanced by the advection of 500 mb cyclonic vorticity, tropospheric warm advection, an unstable atmosphere, and local diabatic heat sources. Though this model is based on a simple two level geostrophic flow, many of its applications are used today in discussing cyclone development.

## 1.2 Climatology of Rapid Cyclogenesis

In recent years, increased emphasis has been placed on understanding the factors that influence explosive deepening. Sanders and Gyakum (1980) credit Tor Bergeron for defining a rapidly deepening cyclone as one that has a decrease in central sea-level pressure of at least  $1\text{ mb hr}^{-1}$  for 24 hrs (normalized to  $60^{\circ}\text{N}$ ). This criteria has been defined as "one-bergeron" by Sanders and Gyakum (1980) and they refer to the resulting storm as a "bomb" due to its explosive development and capability for devastation.

Studies on the geographical distribution of explosive cyclogenesis show that they tend to be tied to the western portion of great ocean basins primarily during the cold winter months (Sanders and Gyakum, 1980; Roebber, 1984). Their position during the maximum deepening phase of development (Fig. 1.4) shows a particularly strong tie to the Atlantic's Gulf Stream and to the Pacific's Kuroshio Current (Roebber, 1984). Here the environment provides a strong baroclinic zone, low static stability, and a rich source of moisture in the boundary layer for the production of latent heat to be transported into the mid and upper levels of the developing cyclone. The distribution is in agreement with earlier work conducted by Sanders and Gyakum (1980) in depicting a high occurrence in the western ocean basin, while a minimum number of bombs are experienced over land.

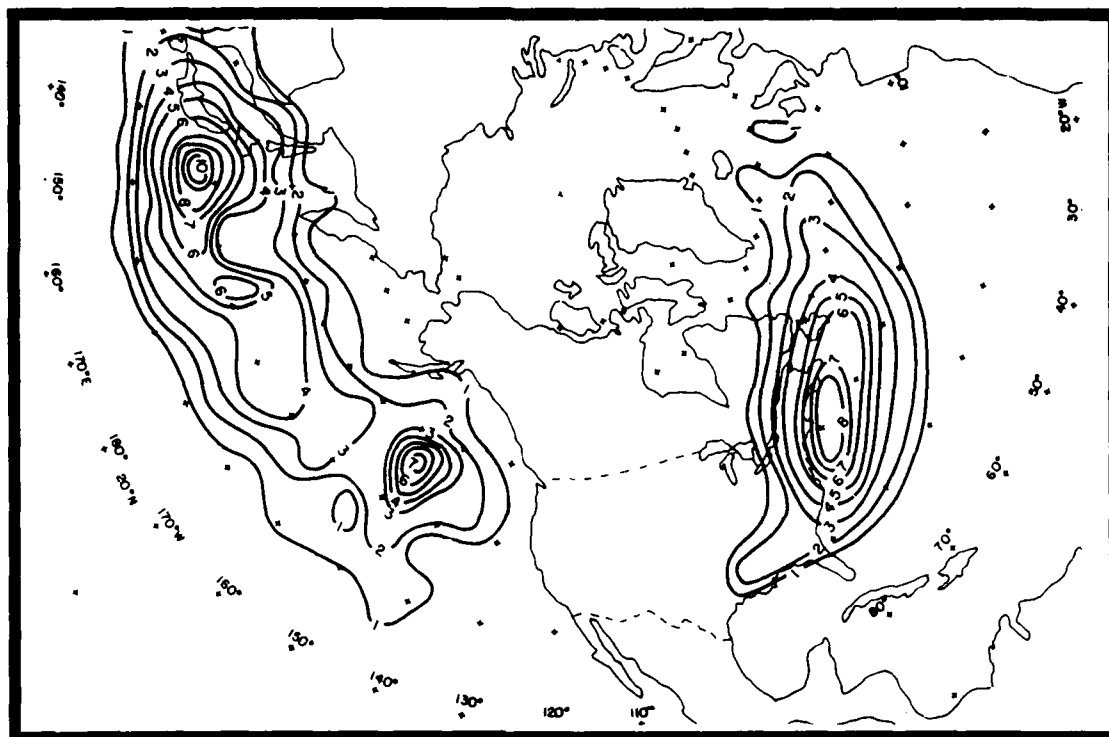


Figure 1.4. Geographical distribution of the maximum deepening positions for meteorological "bombs" for the period 1976-1982 (Roebber, 1984).

A synoptic climatology for bombs has been compiled by Sanders and Gyakum (1980) and Roebber (1984). Statistical studies by Roebber (1984) suggest that additional physical processes separate from ordinary baroclinic instability may be responsible for the observed explosive deepening. Figure 1.5 shows a one year distribution of 24 hour deepening rates for cyclones over an area bound by 130°E eastward to 10°E. The distribution resulted in a mean deepening rate being artificially pulled towards the rapid deepening side of the curve. To compensate, two normal curves of differing means and standard deviations are fit to the distribution. The result shows a maximum deepening rate of  $-3.75 \text{ mb } 24 \text{ hrs}^{-1}$  associated with typical baroclinic development, with a secondary maximum located at  $-22.3 \text{ mb } 24 \text{ hrs}^{-1}$ . The second maximum indicates that the definition of a bergerson is adequate in defining a bomb. The results provide statistical evidence that a group of mid-latitude cyclones, known as "bombs", tend to develop as a result of some additional or enhanced process(es) of baroclinic instability.

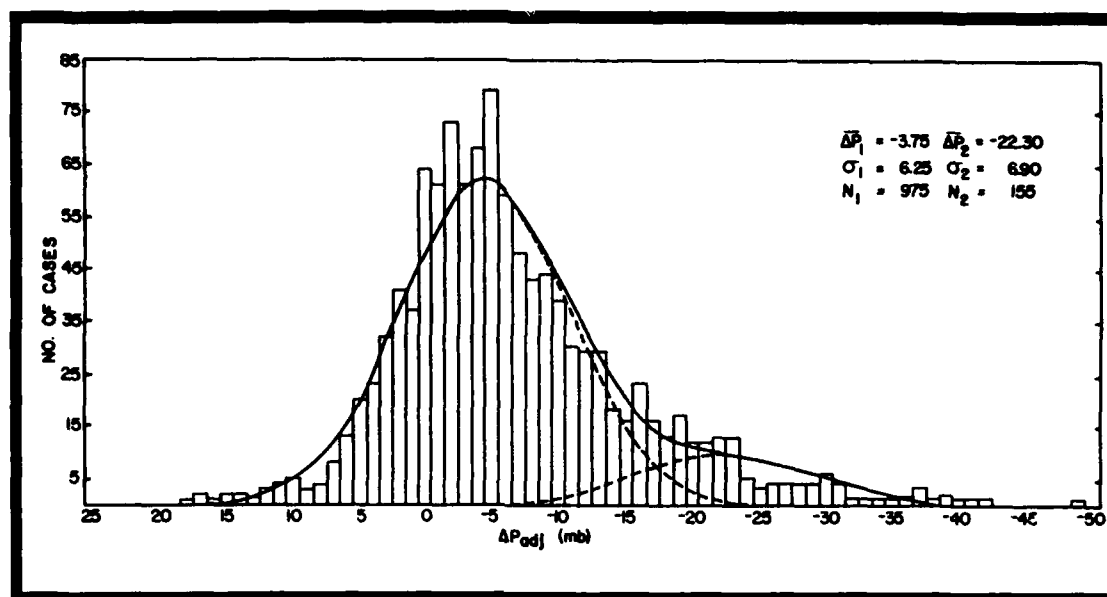


Figure 1.5. Twenty-four hour distribution of pressure falls for all cyclones during the period February 1980 to January 1981. Dashed lines represent two separate curves calculated for the distribution and the solid line represents the sum of these two normal curves (Roebber, 1984).

Examination of the upper-level pattern in relation to the surface cyclone by Sanders and Gyakum (1980) for a three year period, 1977-79, revealed that rapid development began in 78% of all bombs when the SWT was within 400 NM to the west-southwest of the surface cyclone. In 256 cases, 93% of the bombs developed in or poleward of the main jet streak and out ahead or within the advancing SWT. Konrad and Colucci (1988) noted that the rapid development associated with bombs normally have a small effect in changing the circulation pattern seen at the 500 mb level. Sanders' (1987) examination of 500 mb vorticity centers in relation to bombs along the east coast of the United States found them to be associated with a cyclonic vorticity maximum  $\geq 22 \times 10^{-5} \text{ s}^{-1}$ . Sanders' (1986) investigation into explosive cyclogenesis in the northwest Atlantic noted the presence of a 500 mb cyclonic vorticity center 24-36 hours prior to surface development in all cases. However, he points out that initial surface development, in a number of the cases, seemed to occur prior to the arrival of any upper-level support.

### 1.3 Influential Physical Processes

A variety of processes have been suggested as being responsible for stimulating an explosive response in the atmosphere (Bosart, 1981; Gyakum, 1983; Uccellini *et al.*, 1984, 1985; Reed *et al.*, 1986, 1988; Young, 1987). Detailed case studies of the synoptic and dynamic structure of an explosive cyclogenetic event have provided significant insight into the processes involved. The relative importance of each process, in the boundary layer and upper troposphere, in initiating the explosive development remains in question.

#### Upper-Level Forcing

Work conducted by Reed and Sanders (1953), Newton (1954), and Reed (1955) on tropopause folding resulted in an increased acceptance of the importance of subsidence in the upper and mid troposphere as a mechanism for upper-level frontogenesis. Tropopause folding is a mechanism that can transport stratospheric air to the mid and lower troposphere along the jet-stream axis. Reed and Danielsen (1959) are one of the first to emphasize that the advection of high values of stratospheric potential vorticity associated with a low tropopause level is an important ingredient to cyclone development. Further work (Danielsen, 1968; Bosart, 1970; Shapiro, 1976) reinforces the importance of tropopause folding in the transport of air between the stratosphere and troposphere.

To show the relationship between stratospheric intrusion and cyclogenesis, the principal of conservation of potential vorticity is employed (Hoskins *et al.*, 1985; Uccellini *et al.*, 1985; Young *et al.*, 1987). Potential vorticity ( $\zeta_0$ ) calculated on an isentropic surface can be written:  $(\zeta_0 + f)(-\partial\theta/\partial p)$  (Holton, 1979). Where,  $f$  is the coriolis parameter,  $\theta$  is potential temperature, and  $p$  represents pressure.

As stratospheric air protrudes into the troposphere along an isentropic surface, vortex tube stretching occurs as the static stability decreases significantly (stratosphere is a much more stable environment than the troposphere). Thus, absolute vorticity measured along an isentropic surface is generated following parcel trajectories as long as stratospheric values of potential vorticity are conserved resulting in increased cyclonic development.

Most studies have shown that the development of tropopause folds occur as cyclogenesis progresses. Others have related upper-level frontogenesis and tropopause folding to subsequent surface development. Uccellini (1985) found tropopause folding to

occur 1500 km upstream, 12 to 24 hours prior to explosive development. Geostrophic deformation associated with a polar jet resulted in subsidence transporting stratospheric air, marked by high values of potential vorticity, into the lower troposphere to 800 mb.

Cross sections constructed by Bosart *et al.* (1984) across the surface cyclone center in the case of the Presidents' Day storm (18-19 February 1979) visually depict the evolution of a tropopause fold and associated surface development (Fig. 1.6). Bosart hypothesizes that the production of cyclonic vorticity in the boundary layer in the incipient cyclogenesis phase is vital to the eventual rapid storm spinup phase. The juxtaposition of the powerful cyclonic vorticity advection aloft sets the stage for the rapid spinup of the cyclonic vorticity rich air in the lower troposphere. The stable lower troposphere along the coastal plane associated with the cold-air damming and the destabilization of air over the open ocean waters sets up a strong static stability gradient. This gradient allows vortex tube stretching to be particularly effective in "spinning up a cyclone" as the potential vorticity aloft reaches the coast.

### **Boundary Layer Processes**

Bosart (1981) credits initial cyclone development of the Presidents' Day storm to increased convergence in the boundary layer associated with the developing coastal front. Cyclonic vorticity in the boundary layer was generated as the coastal front intensified, though mid and upper level advection of vorticity was minimal. This is consistent with work conducted by MacDonald and Reiter (1988) where they compared the development of a number of land based explosive cyclogenesis cases over the eastern United States with that of typical cyclogenesis. They found that prior to explosive development, the boundary layer was typically rich in cyclonic vorticity and the advection of cyclonic vorticity decreased rapidly with height. During the explosive phase of development, strong cyclonic vorticity advection aloft was found. Regular cyclones tend to exhibit cyclonic vorticity advection throughout the atmosphere.

### **Convective Processes**

Cyclone development by baroclinic processes seems to be significantly enhanced by convective processes (Tracton, 1973). The onset of convection near the center of a rapidly developing cyclone has been cited as an important factor in a number of rapid cyclogenesis

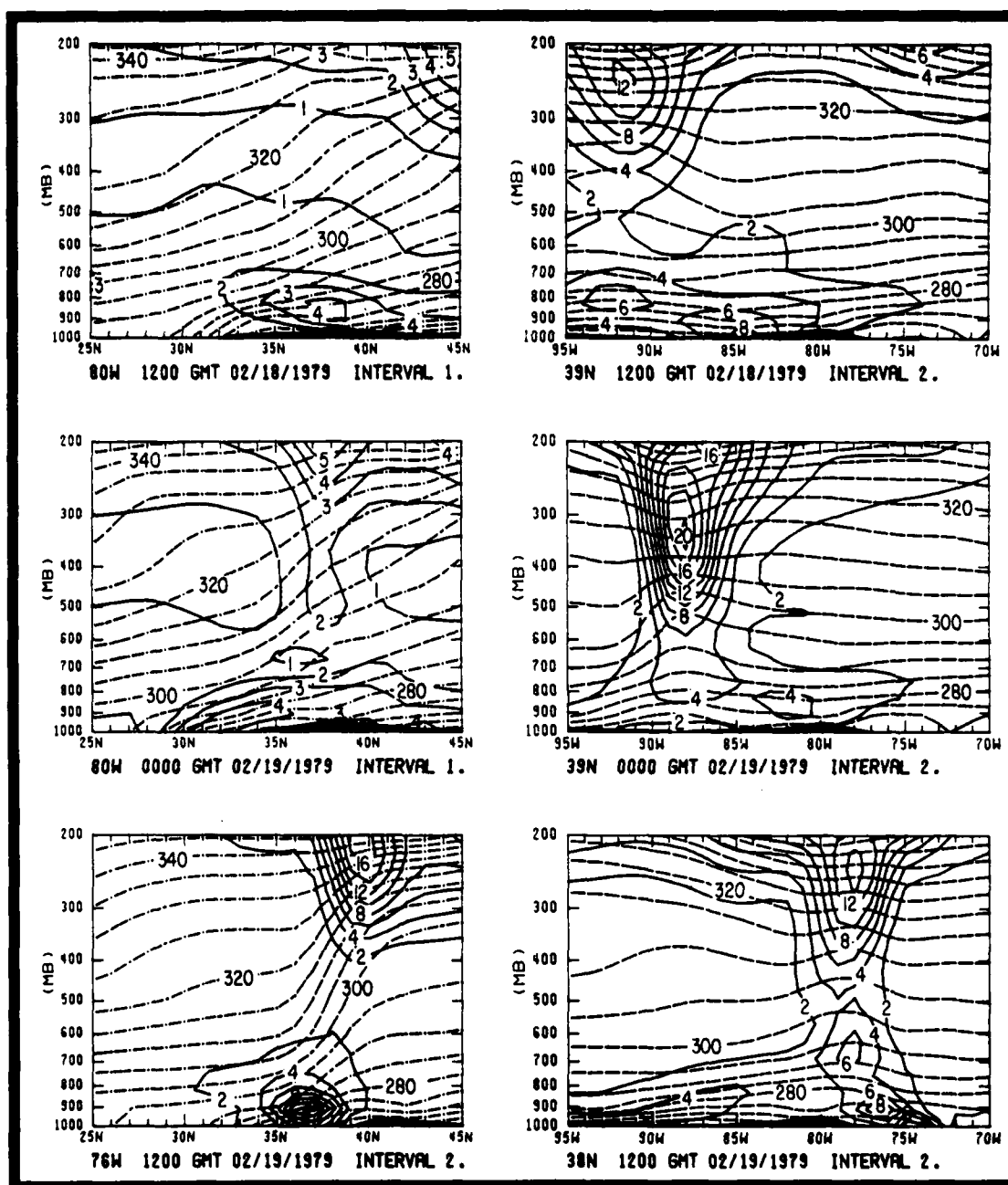


Figure 1.6. Vertical cross sections of semi-geostrophic potential vorticity ( $10^{-4} \text{ s}^{-1}$ , solid) and potential temperature (every 5 °K, dashed) along selected longitudes and latitudes for 1200 UTC 18 February through 1200 UTC 19 February 1979. The potential vorticity contour interval is indicated below lower right corner of each panel (Bosart *et al.*, 1984).



events. Bosart (1981) points out that deep convection broke out coincident with the rapid development of the Presidents' Day storm. The influence of the convective processes appeared to act as a positive feed back mechanism to the overall circulation pattern. Gyakum and Barker's (1988) research of a land based bomb attribute the first of two phases of rapid deepening to convection. Gyakum (1983) placed high significance in the role of convection in the development of the Queen Elizabeth II storm of 10-11 September 1978. He sites the interaction of a mesoscale convective complex and the incipient cyclone resulted in explosive development.

The explosive deepening of an extratropical cyclone has been associated with a variety of processes - all of which have a role in development. The extent to which each physical process plays in the cyclone's explosive development remains in question and will fuel further debate.

#### 1.4 Current Research

This research explores the processes responsible for the explosive cyclogenesis that took place over the Mid-West United States during 14-15 December 1987. Climatology shows that a high frequency of "bombogenesis" occurs over the ocean. Contrary to climatology, this storm's development occurred entirely over land. During an 18 hour period of deepening the cyclone experienced a central pressure drop of 27 mb. Moreover, within that time period the cyclone experienced a six hour pressure drop of 15 mb.

The track of the cyclone is shown in Figure 1.7. Initially, the cyclone moved towards the northeast at a speed  $>25 \text{ m s}^{-1}$ , consistent with steering by the thermal wind (Pettersen, 1956). For the first 10 hours the storm moved towards the north-northeast deepening at a average rate of  $1 \text{ mb hr}^{-1}$ . During the period of most rapid deepening 0600-0900 UTC 15 December, a three hour pressure fall of 9 mb was observed as the storm curved northwestward towards the cold air aloft. O'Hare International Airport, experienced its all time record low surface pressure (981 mb) when the storm was still 100 km to the southwest. After 1200 UTC, the surface cyclone filled as it moved eastward. The surface system continued to weaken and decelerate ( $10\text{-}15 \text{ m s}^{-1}$ ) while curving towards the north within the circulation of the deepening upper-level low.

In the course of the storm's development blizzard warnings were posted, along with a variety of other warnings, as heavy snow, record temperatures, high winds, and

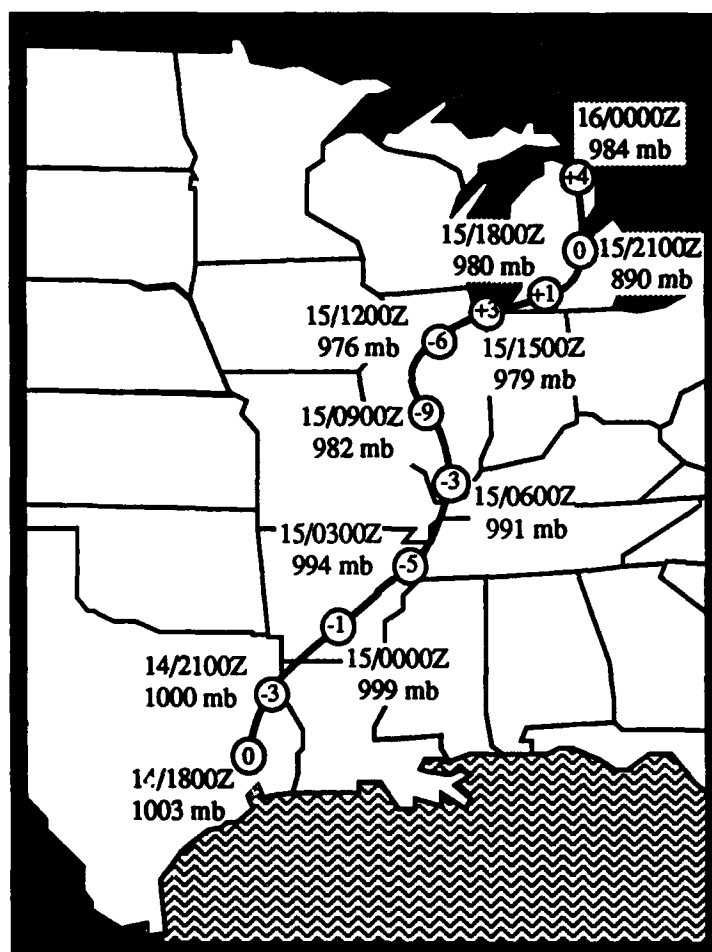


Figure 1.7. Storm track with three hourly positions and central pressure for the developing cyclone during the period 1800 UTC 14 December 1987 through 0000 UTC 16 December 1987. Number within circle depicts three hour pressure change.

severe weather were experienced by a large portion of the nation. The analysis, prepared by the University of Chicago (Fig. 1.8), of the snowfall distribution deposited by this storm system shows an extensive band of heavy snow extending from the southern Rockies northeastward towards the Great Lakes. Snowfall totals of a foot or more were common throughout this area. El Paso, Texas saw a new 24 hour snowfall record when 16.8 inches fell and Kansas City, Missouri broke their 24 hour snowfall record for December by receiving 10.8 inches of new snow.

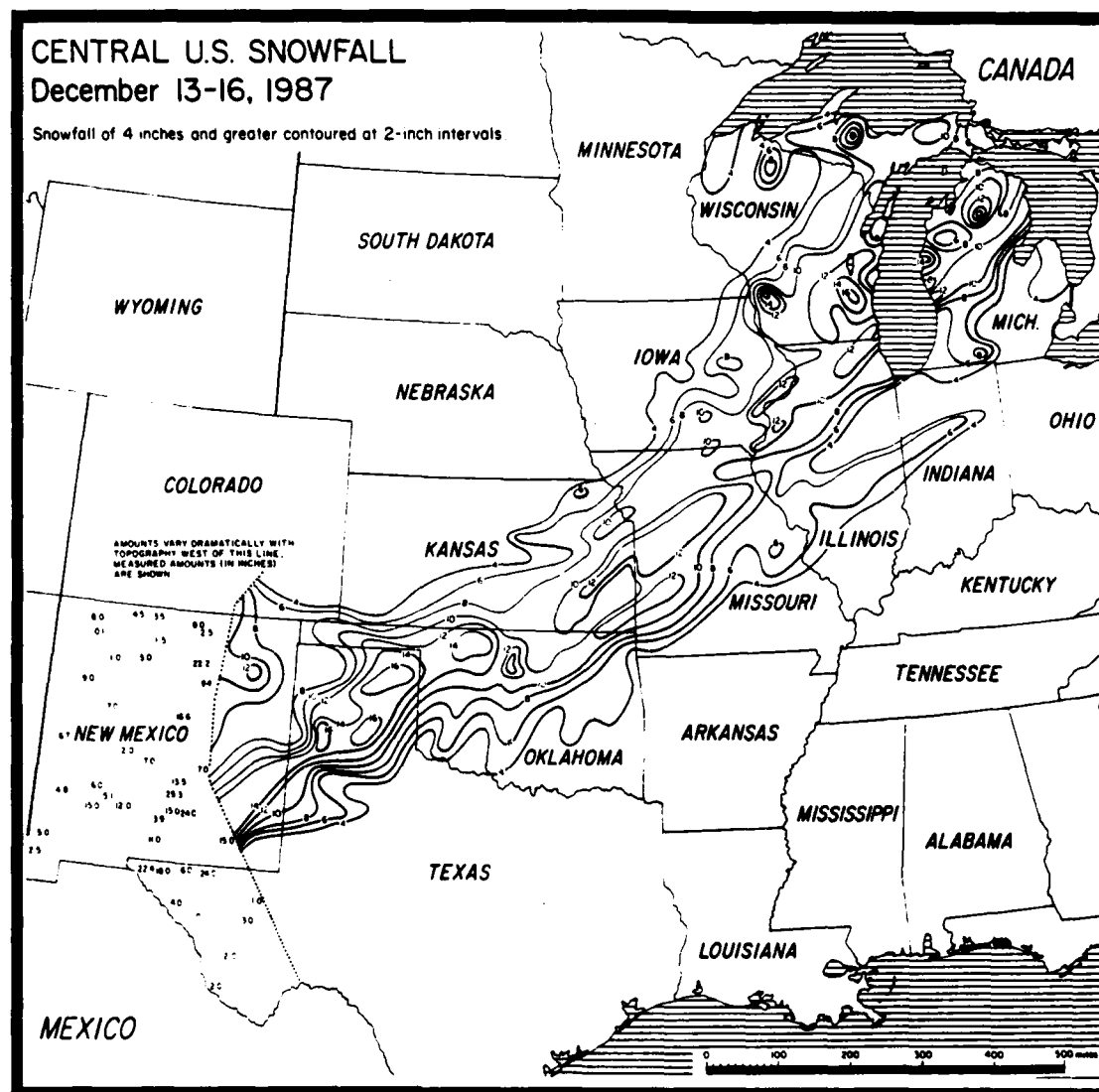


Figure 1.8. Snowfall distribution for the period 13-16 December 1987. Map prepared by the University of Chicago (Storm Data, December 1987).

The strong baroclinicity of the system was reflected in a large contrast in surface temperatures east of the Rocky Mountains. Record high temperatures were experienced in the southeast with a record high of 27°C observed in Baton Rouge, Louisiana. To the north and west, exceptionally cold weather resulted in record low temperatures as cold air poured out of Canada in the wake of the advancing cyclone. Lubbock, Texas broke their previous record low of -12°C, set in 1917, when the mercury fell to -17°C.

Damaging high winds were felt from the Rockies eastward to the Appalachians causing extensive damage. In Illinois, wind gusts of approximately  $35 \text{ m s}^{-1}$  were observed. High winds downed trees and power lines causing power outages effecting over 165,000 people in the Chicago area alone. For just the fourth time in the past 20 years O'Hare International Airport halted operations due to inclement weather. Straight line winds were sited as the cause in over turning nine tractor-trailer trucks on the interstate highway between Lafayette and Lebanon Indiana.

Additionally, severe weather was spawned as the cyclone matured. Hail up to 1 3/4 inches in diameter was reported in Hot Springs, Arkansas with the passage of the cold front. At 0340 UTC 15 December an F-3 tornado touched down four miles southwest of West Memphis, Arkansas. The tornado traveled 25 miles northeastward into Tennessee, just north of Memphis. The tornado devastation resulted in six fatalities, 221 injuries, damaged 300 homes, and displaced 1,529 people.

### 1.5 Research Objectives

The development of this storm system, over the mainland United States, provides a convenient opportunity to study processes that promote explosive cyclogenesis from the perspective of data coverage. The use of the operational National Weather Service (NWS) network provides a relatively good density of hourly surface and 12 hourly upper-air data with which to study the synoptic processes taking place.

The objectives of this research are:

- Examine the process(es) resulting in two observed phases of cyclone deepening.
- Detail the synoptic aspects of the explosive cyclone development.
- Develop conceptual models depicting important aspects of the storm development.

## CHAPTER 2

### DATA AND METHODOLOGY

#### 2.1 Data Sources

Hourly surface observations from National Weather Service (NWS) sites across the continental United States were subjectively analyzed and compared with surface charts prepared and transmitted by the National Meteorological Center (NMC). Routine upper air data, collected from standard NWS sites, were processed to construct a variety of meteorological fields in the vertical and horizontal planes. Visual, infrared and water vapor satellite data from the GOES-East (Geostationary Operational Environmental Satellite) satellite were obtained from the Satellite Application Laboratory of the National Environmental Satellite, Data, and Information Service and the United States Air Force, Air Weather Service, satellite data archives.

#### 2.2 The Barnes Objective Analysis Scheme

During the course of this research a number of meteorological fields were analyzed to represent the development of the 14-15 December 1987 explosive cyclogenesis event. In order to make finite-difference calculations, grid point data at regularly spaced intervals are required. Due to the irregular placement of NWS upper air reporting stations across the United States an objective analysis scheme is employed to interpolate data to the grid point locations. The development of the desired two-dimensional grid array is aided by the Barnes (1964, 1973) objective analysis method. This scheme is used to obtain values at points in a two-dimensional grid array (Fig. 2.1) used in finite-difference calculations.

If  $Q$  represents any meteorological variable, calculations of grid point values are obtained by:

$$\bar{Q} = \sum_{i=1}^N w_i Q_i / \sum_{i=1}^N w_i \quad \{2.2.1\}$$

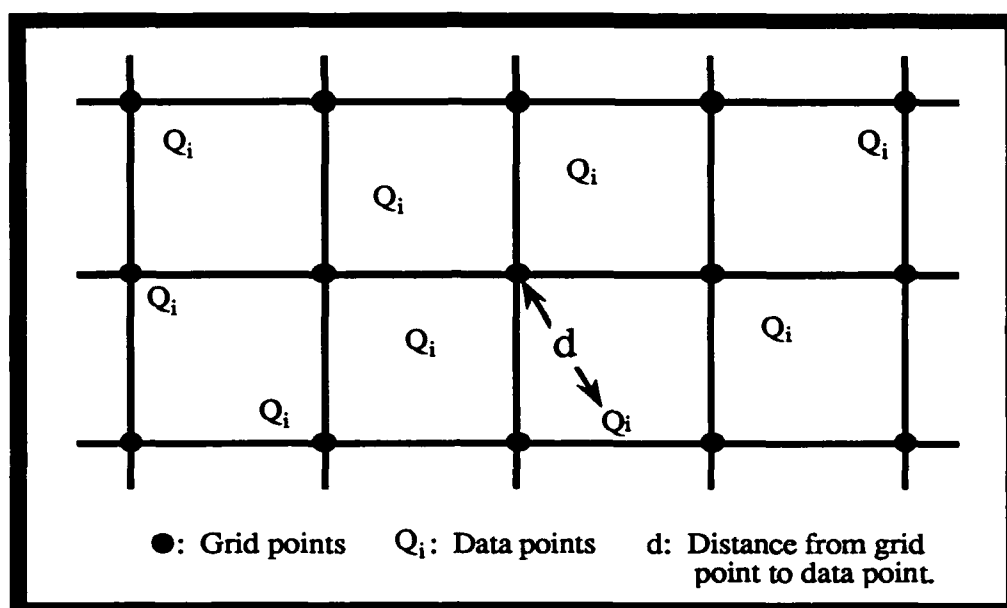


Figure 2.1. Representation of a two-dimensional grid array used by the Barnes objective analysis scheme. The solid circle denotes calculated grid point position, "Q<sub>i</sub>" represents observation sites, and the dashed line indicates the distance "d" from the observation site to grid point.

The interpolated grid point value is just the weighted mean ( $\bar{Q}$ ) of observations surrounding the point. Here,  $N$  is the total number of stations influencing a given grid point,  $w_i$  is the observation weight, and  $Q_i$  is the observed value. The observation weights ( $w_i$ ) are inverse-distance ( $d$ ) dependent and are defined by:

$$w_i = \exp(-d^2 / 4k_0) \quad \{2.2.2\}$$

Here,  $k_0$  is the "weight parameter" which controls the rate at which the weight value decreases outward from the point of interpolation. Hence,  $k_0$  determines the degree of smoothing of the data field. If  $k_0$  is small, there is little smoothing. If  $k_0$  is large, there is greater smoothing (Fig. 2.2).

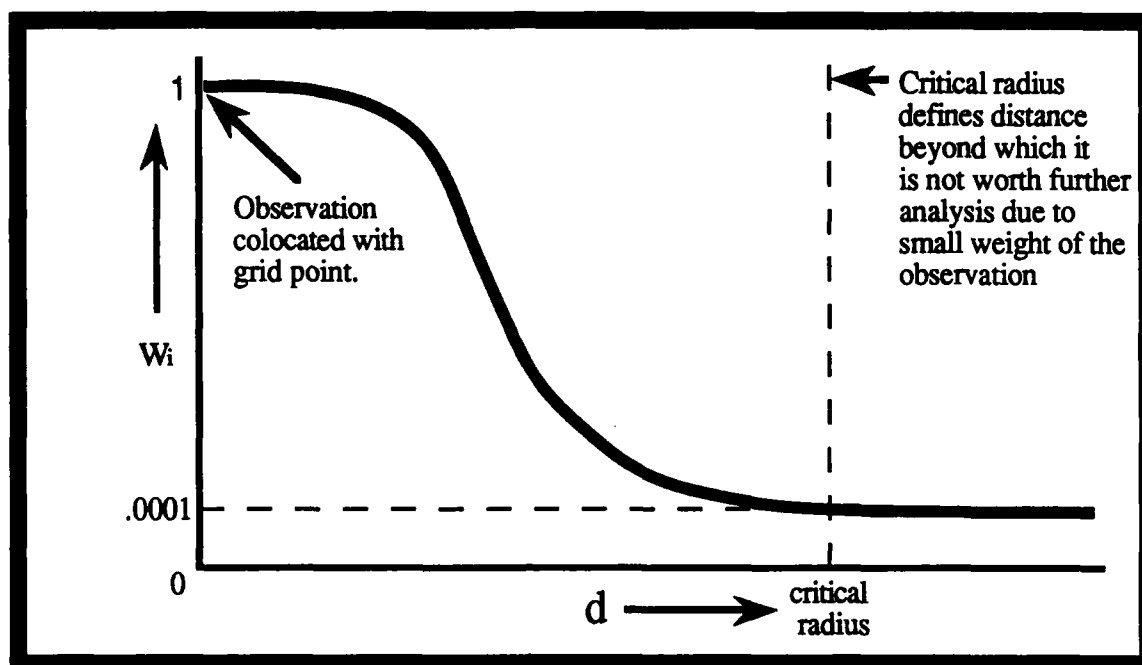


Figure 2.2. Distribution of observation weight versus distance of observation point from grid point. Horizontal axis is distance of grid point to observation. Vertical axis is observation weight. Closer the observation is to the grid point the more weight placed on value. Observations located beyond the critical radius from the grid point are weighted less than  $10^{-4}$ .

The selection of  $k_0$  is crucial to the structural detail remaining in the interpolated field. The choice of this parameter value must strike a balance between retaining as much detail as the observation network density allows, and filtering out sources of random error. Structural detail is limited by the minimum resolvable wavelength. The standard NWS upper-air network has a mean spacing of about 400 km. Theoretically, the upper air network can resolve features twice the mean station separation, or 800 km.

The weight parameter ( $k_0$ ) is selected to reflect the degree of credibility given the amplitudes of the minimally-resolved waves, that is, the signal to noise ratio of the observations at small wavelengths. Sources of "error" include turbulent fluctuations with periods of several minutes (especially near the ground), biases introduced by local topography and obstacles at observation sites (again, especially important for surface stations), and features on scales smaller than the station spacing (e.g. gravity waves). To suppress this noise in the observations a total response of 0.18 in the minimally resolved

waves is adopted. This degree of amplitude suppression is generally consistent with some recent applications of the Barnes scheme, including Barnes (1985) and Moore and Blakley (1988). With a convergence parameter of 0.3, the weight parameter is 99,000 km<sup>2</sup>. The wind components and temperature are interpolated to a mesh of points constructed on a 15 row by 19 column grid spaced at 180 km (60°N, polar stereographic).

This analysis scheme provides a useful means of establishing a two-dimensional grid of data for analysis and computation. It is advantageous because:

- (i) The scheme is computationally simple and assigns weights solely as function of distance between datum and grid point.
- (ii) The weight parameter, which determines the degree of smoothing, can be chosen prior to the analysis.
- (iii) Since the weight function approaches zero asymptotically, the influence of data may be extended any distance to ensure a sufficient number of observations affect each grid point without changing the weight function or the response characteristic.
- (iv) Only two passes through the data are needed to achieve the desired pattern.
- (v) Noise is adequately filtered from the analysis so further smoothing by application of additional numerical filters is unnecessary.

In spite of apparently strong smoothing, the interpolated fields still reflect features one would be inclined to accept if done subjectively by a skilled analyst. In particular, a sharp discontinuity, like frontal zones, are still represented in wind and temperature fields.



## CHAPTER 3

### CYCLONE EVOLUTION

#### 3.1 Synoptic Development

Surface and upper-air charts in this section were prepared by subjectively analyzing routine NWS observational data. Calculations of 500 mb vorticity, from the front range of the Rockies eastward to the Atlantic coast, were made using the Barnes objective analysis scheme as described in section 2.2. Vorticity displays for the inner mountain region of the Rockies were obtained from the computer generated analysis output from the NWS Nested Grid Model (NGM).

The early part of December 1987 was marked by unseasonably warm and dry conditions throughout most of the country. A strong zonal upper-level jet in excess of  $90 \text{ m s}^{-1}$  stretched across the Pacific from southern Japan eastward to the Pacific Northwest. Here the jet splits with the main branch moving into the western provinces of Canada resulting in a ridge over the western United States while a series of SWT's dropped down into the southwest United States. To the east, a trough is situated over the Great Lakes. This pattern resulted in substantial precipitation and cool conditions over the coastal region of the Pacific Northwest and over an area from the Great Lakes into the Mid-Atlantic States up towards New England (Weekly Wea. & Crop Rep., No. 49, 1987).

Early in the second week of December, an upper-level trough entering the coast of California propagated eastward breaking down the ridge over the Rockies. This trough intensified and developed into an upper-level low as it moved into the Great Lakes. The resultant upper-level pattern redirected the incoming Pacific jet stream down along the coast of California.

On 12 December, a weak SWT with a cyclonic vorticity maximum of  $14 \times 10^{-5} \text{ s}^{-1}$  was located over British Columbia. During the day, it progressed southward down the back side of an intensifying trough. The associated jet streak had a wind max of  $35 \text{ m s}^{-1}$ . A long-wave ridge pattern observed earlier over the Rockies was now being replaced by an intensifying trough.

By 1200 UTC 14 December, the SWT was approaching the base of the trough resulting in a sharp positively tilted trough over the Rockies. At the 200 mb level (Fig.

3.1), a broad maximum in wind speeds extends from Baja California through Texas and northeastward into the Mississippi Valley. The combination of a polar and subtropical jets at the base of the trough coincides with a jet maximum of  $75 \text{ m s}^{-1}$ . A second jet streak of  $75 \text{ m s}^{-1}$  is observed over southern Missouri. The ageostrophic circulations associated with the exit region of the jet streak provided conditions conducive for the initiation of a large convective complex extending from northeast Texas into Oklahoma.

A review of the vertical motion distribution associated with a progressive jet streak is presented (Fig. 3.2). The vertical motion distribution associated with a progressive jet streak is due to the constraint of the atmosphere to maintain thermal-wind balance. The thermal advection patterns produced by the geostrophic flow acts to upset thermal-wind balance resulting in an atmosphere that is neither in hydrostatic or geostrophic balance. If the geostrophic wind field parallels the thermal field the flow is in hydrostatic and geostrophic equilibrium. However, the progression of a jet streak requires an increase in the winds ahead and decrease behind. Since the height field does not change in the absence of thermal advection the wind speed is larger than geostrophy will allow. Thus, the wind is

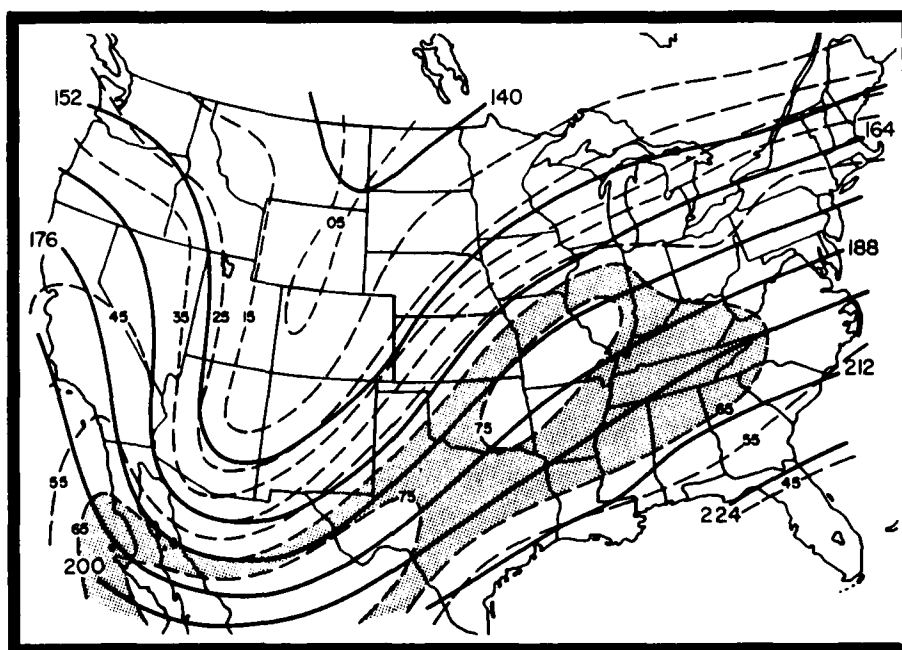


Figure 3.1. 200 mb analysis for 1200 UTC 14 December 1987. Solid lines depict geopotential height field (decameters) and dashed lines are isotachs in  $\text{m s}^{-1}$ .

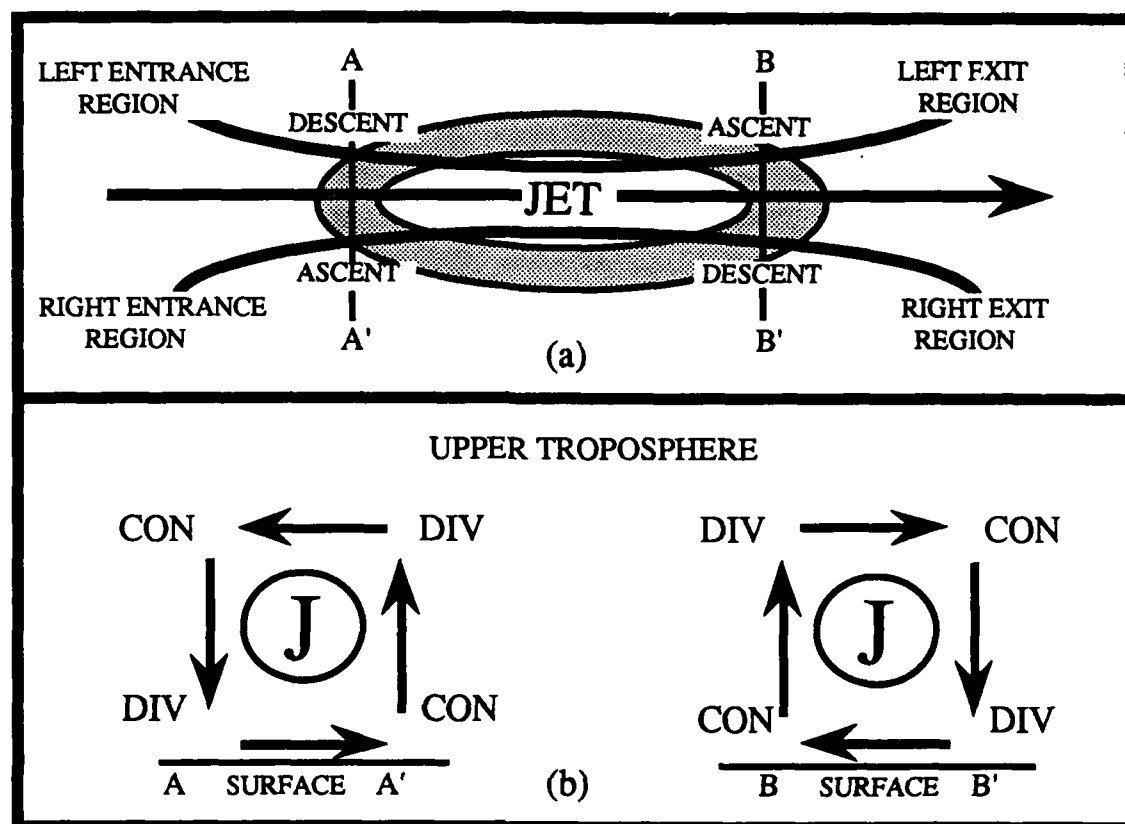


Figure 3.2. (a) Horizontal depiction of the vertical motion patterns associated with a straight jet streak. Solid lines depict the height field and the shaded region are isotachs (b) Vertical cross section in the plane A-A' and B-B' depicting the vertical motion pattern associated with the jet entrance and exit regions, respectively. Cross sections contain the jet position (marked "J"), the vertical motion (vertical arrows) and the ageostrophic wind component (horizontal arrows).

not in thermal-wind balance (Fig. 3.2a). An ageostrophic flow develops to restore the atmosphere to thermal and geostrophic wind balance. The ageostrophic circulation patterns in the plane of the cross sections A-A' and B-B' in Figure 3.2a are depicted in Figure 3.2b. In the entrance region of the jet we find the upper branch of the ageostrophic flow directed poleward of the jet and equatorward in the exit region. The resultant pattern of ascending/descending vertical motion act to adiabatically cool/warm the air increasing the horizontal temperature gradient. The horizontal ageostrophic wind component acts to decrease the wind shear in the vertical. The combination of these processes work towards maintaining a balance in the thermal and geostrophic wind field. This scenario uses a simple straight line flow. The effect of curvature on the ageostrophic flow and vertical

motion pattern is complicated due to the three-dimensional variations in the upper-level divergence and ageostrophic flow (Uccellini and Johnson, 1979; Uccellini, 1980; Durran and Snellman, 1987; Uccellini and Kocin, 1987). Studies relating the position of cyclone development to jet-streak quadrants have shown a high correlation of development to the left exit and right entrance region of a jet streak (Riel and Teweles, 1953; Hovanec *et al.*, 1975; Achtor *et al.*, 1986).

At 300 mb, a  $65 \text{ m s}^{-1}$  jet streak is observed over Mexico and extending into Texas (Fig. 3.3). The SWT that dropped down the back side of the long-wave trough is now situated over the Mexico/Arizona border. The 500 mb analysis (Fig. 3.4a) reveals that the cyclonic vorticity maximum has reached the base of the trough. Its magnitude had doubled during the past 12 hours to  $28 \times 10^{-5} \text{ s}^{-1}$  due to increased directional and speed shear and a closed height contour is noted for the first time. However, vorticity advection into the southern and central Plains is small at this time. The cyclone over Arizona at 1200 UTC is a reflection of the upper-level low. A band of heavy snow in the foot hills of the Rockies is due to the abundant low-level moisture and upslope flow conditions (Fig. 3.4b).

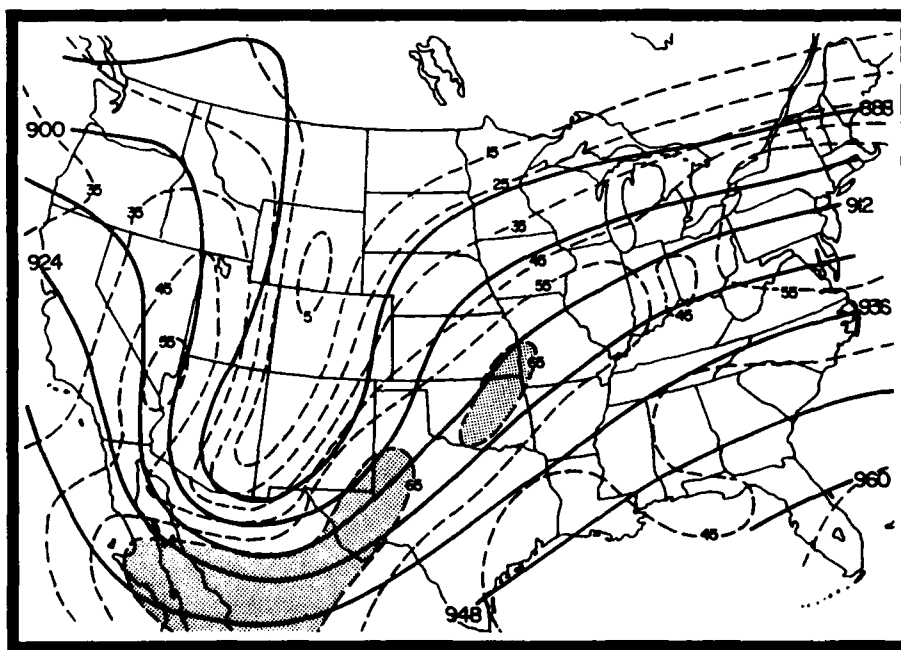


Figure 3.3. 300 mb analysis for 1200 UTC 14 December 1987. Solid lines depict geopotential height field (decameters) and dashed lines are isotachs in  $\text{m s}^{-1}$ .

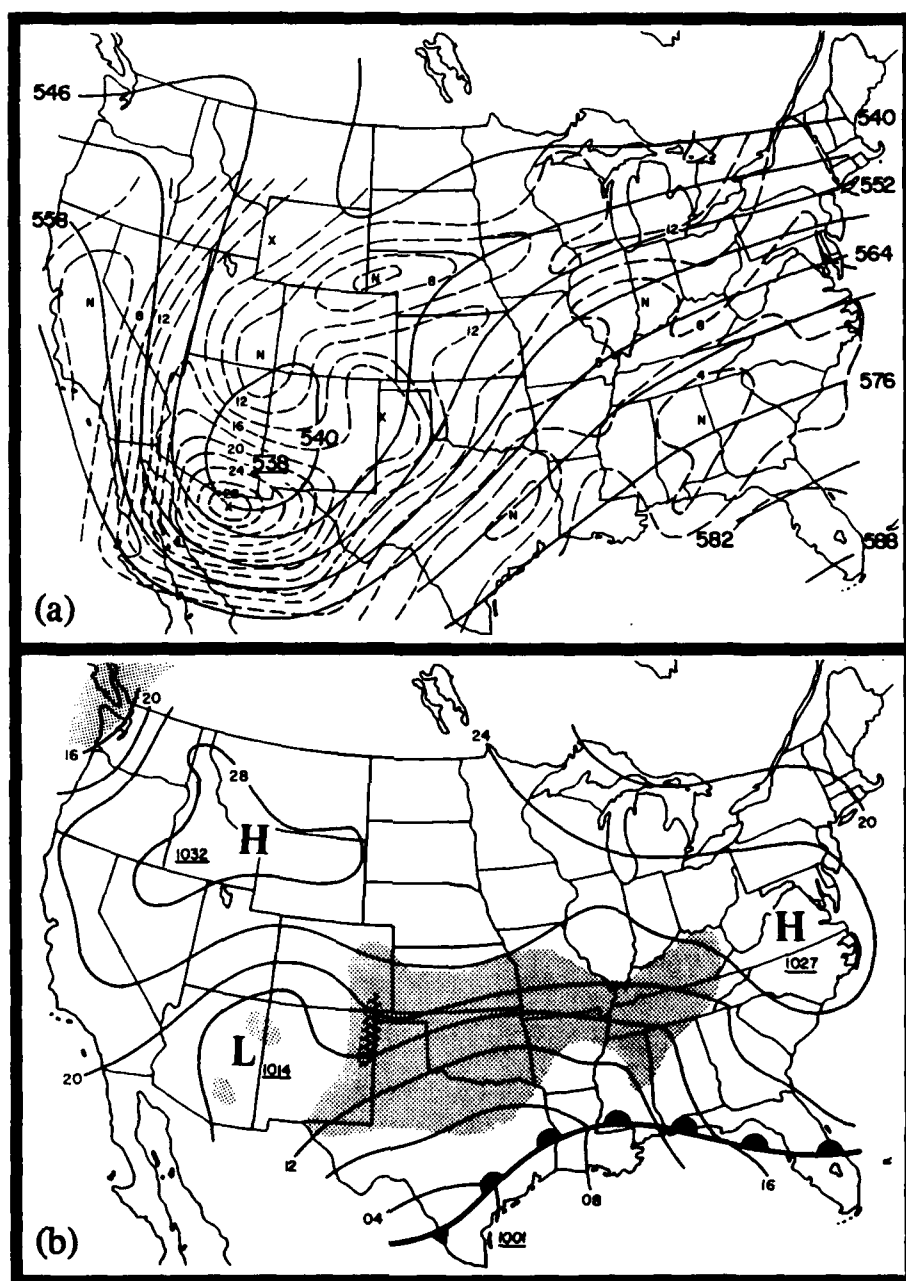


Figure 3.4. a) 500 mb analysis for 1200 UTC 14 December 1987. Solid lines depict geopotential height field (decameters) and dashed lines depict absolute vorticity ( $10^{-5} \text{ s}^{-1}$ ). "X" denotes vorticity maximum and "N" is a vorticity minimum. b) Surface analysis for 1200 UTC 14 December 1987. Solid lines are sea level isobars in millibars, conventional symbols used to depict fronts and pressure centers. Precipitation is represented by the shaded regions and non-convective heavy precipitation is depicted by cross hatching.

The bulk of the precipitation can be attributed to low-level moisture overrunning the warm front found along the Gulf coast. Warm-moist air at the surface, in the warm sector, is associated with the 295°K isentropic surface (Fig. 3.5). The moisture content of the air is  $\approx 14.5 \text{ g kg}^{-1}$  along the coast. Assuming that the air parcel flows along an isentropic surface, Holton (1979), the  $15 \text{ m s}^{-1}$  southerly flow along the 295°K surface advects the surface air to the 750 mb level by the time it reaches the Oklahoma central Missouri region. This adiabatic ascent is consistent with the observed precipitation shield. The northern extent of the precipitation occurs where the orientation of the streamlines asymptotically approach the orientation of the pressure contours indicating reduced ascent.

At 1800 UTC 14 December a surface cyclone, with a central pressure of 1003 mb, developed 100 km north of Houston, Texas (Fig. 3.6a). Cyclogenesis is initiated coincident with the development of convection over eastern Texas. Cyclogenesis and convection are both encouraged by the vertical motion field associated with the subtropical

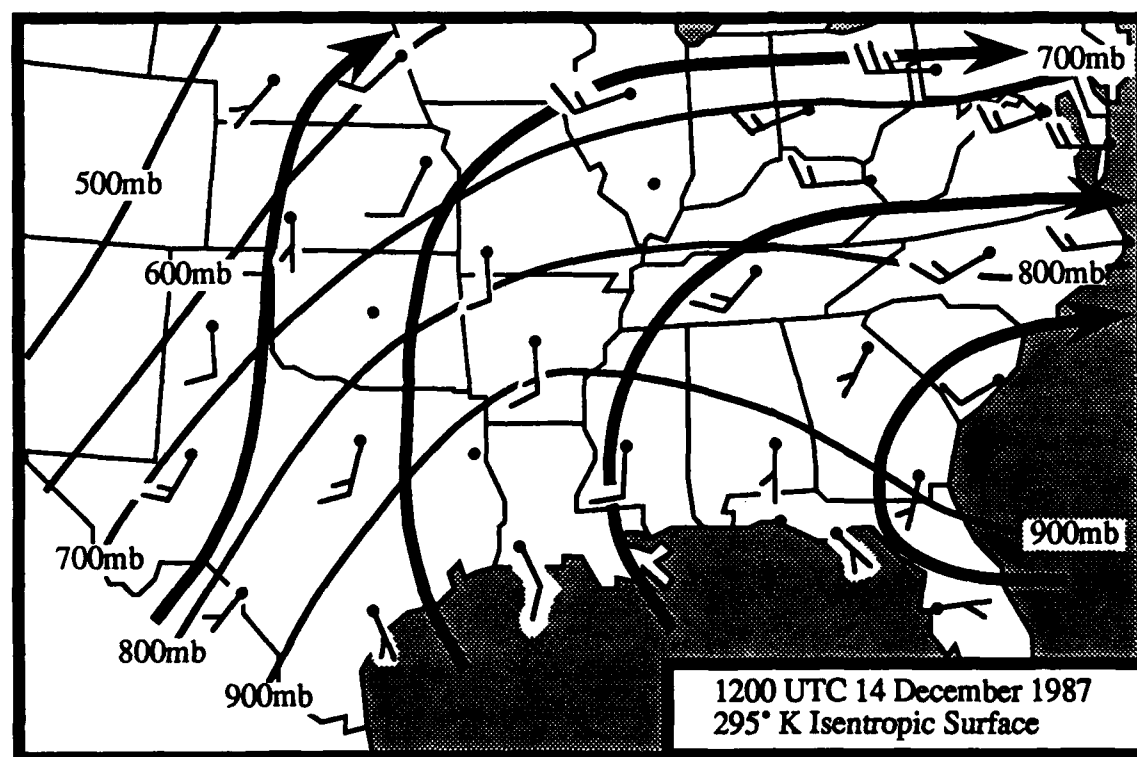


Figure 3.5. 295°K Isentropic surface for 1200 UTC 14 December 1987. Thin lines are isobars (mb). Thick arrows are streamlines along the isentropic surface. Wind barbs in  $\text{m s}^{-1}$ .

jet streak approaching the region. In Figure 3.6b an area of precipitation is beginning to develop in the panhandle of Texas as the upper-level system over the southern Rockies moves into the southern Plains. Heavy rain shower activity is observed in the vicinity of the surface cyclone center with tops reported at 5 km, while heavier thunderstorm activity has developed just to the north with tops extending to 9-11 km. The cells are observed to be moving toward the northeast at  $20 \text{ m s}^{-1}$ . The initiation of cyclogenesis appears to be enhanced by the presence of convection in the region of developing low pressure. This phase of development may be enhanced by the process of conditional instability of the second kind (CISK) (Charney and Eliassen, 1964). The CISK process occurs if the convection is sufficiently organized to provide a positive feedback between the cloud scale and the developing vortex scale. Here, the vortex scale provides the necessary low-level moisture convergence for the convective scale and the convective scale provides heating that can intensify the large-scale disturbance. Additionally, the development of the surface cyclone results in the deformation of the boundary layer winds enhancing the developing thermal advection patterns. This aids the "self-development" process and the generation of cyclonic vorticity in the lower troposphere (Petterssen, 1956).

By 0000 UTC 15 December the upper-level trough is becoming negatively tilted as the jet streak rounds the base of the trough and moves into the southern Mississippi Valley. Figure 3.7a shows an expansive area of winds in excess of  $75 \text{ m s}^{-1}$  at the 200 mb level. The existence of two separate wind maxima (Fig. 3.7b) are consistent with satellite imagery (discussed in chapter 4). The satellite imagery shows that the  $75 \text{ m s}^{-1}$  isotach over the Texas/Oklahoma boarder is associated with the polar jet and the embedded SWT that has advanced from the Pacific Northwest during the past 24 hours. A second  $75 \text{ m s}^{-1}$  isotach near the Texas coast is associated with the subtropical jet stream. The jet streak that initiated convection over Oklahoma at 1200 UTC has advanced into the Mid-Atlantic coastal region at this time.

The 500 mb vorticity pattern in Figure 3.7c shows the cyclonic vorticity center has progressed eastward into north-central Texas while maintaining a magnitude of  $28 \times 10^{-5} \text{ s}^{-1}$ . The developing negative tilt of the upper-level trough favors enhanced cyclonic vorticity advection which is strongest in central Texas. At 0000 UTC the surface cyclone has moved northeastward into Arkansas and deepened to a 999 mb low (Fig. 3.7d). The NWS radar summary depicts two distinctive types of precipitation at this time (Fig. 3.7e). A

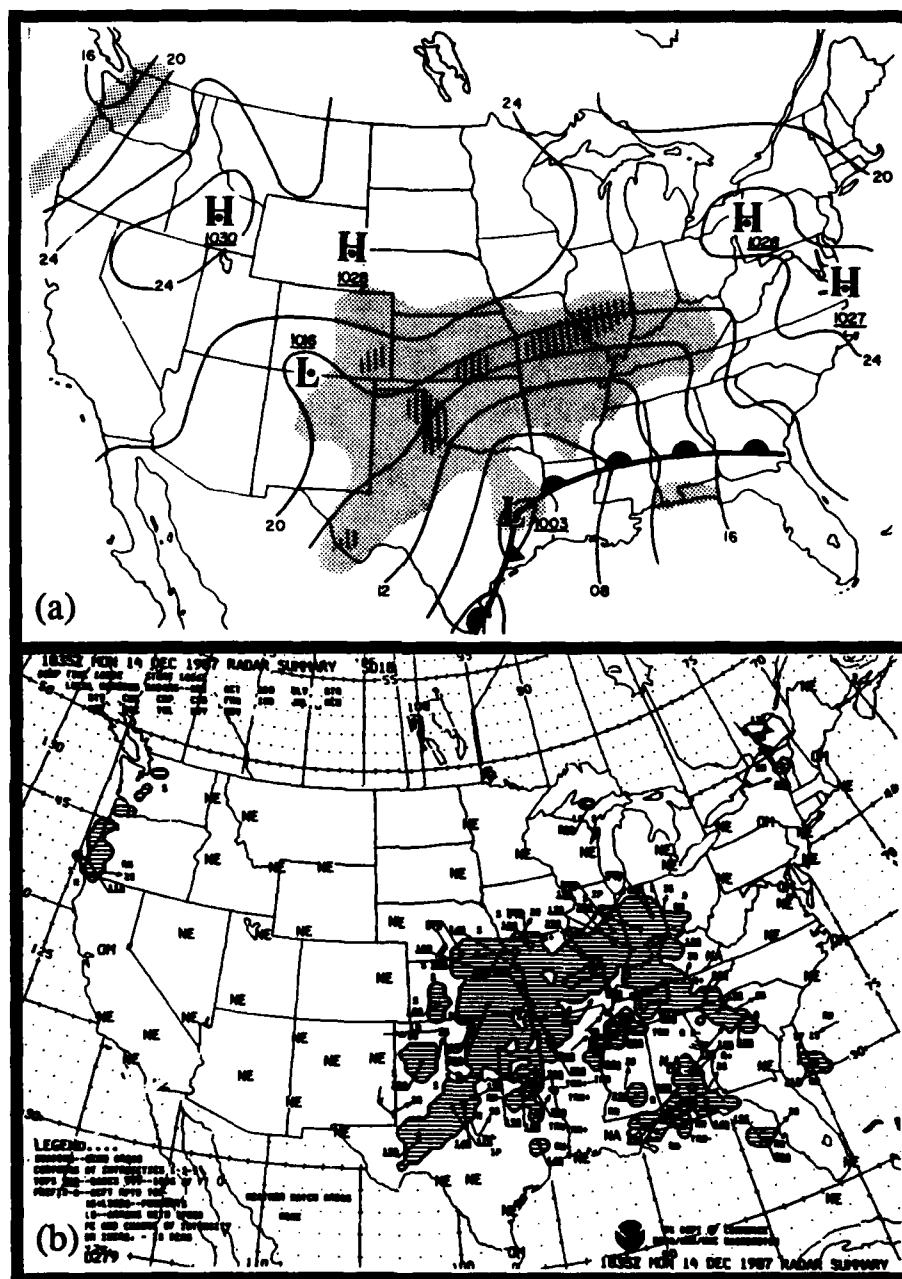


Figure 3.6. a) Surface analysis for 1800 UTC 14 December 1987. Solid lines are sea level isobars in millibars, conventional symbols used to depict fronts and pressure centers. Precipitation is represented by the shaded regions and non-convective heavy precipitation is depicted by cross hatching. b) NWS radar summary for 1835 UTC 14 December 1987.



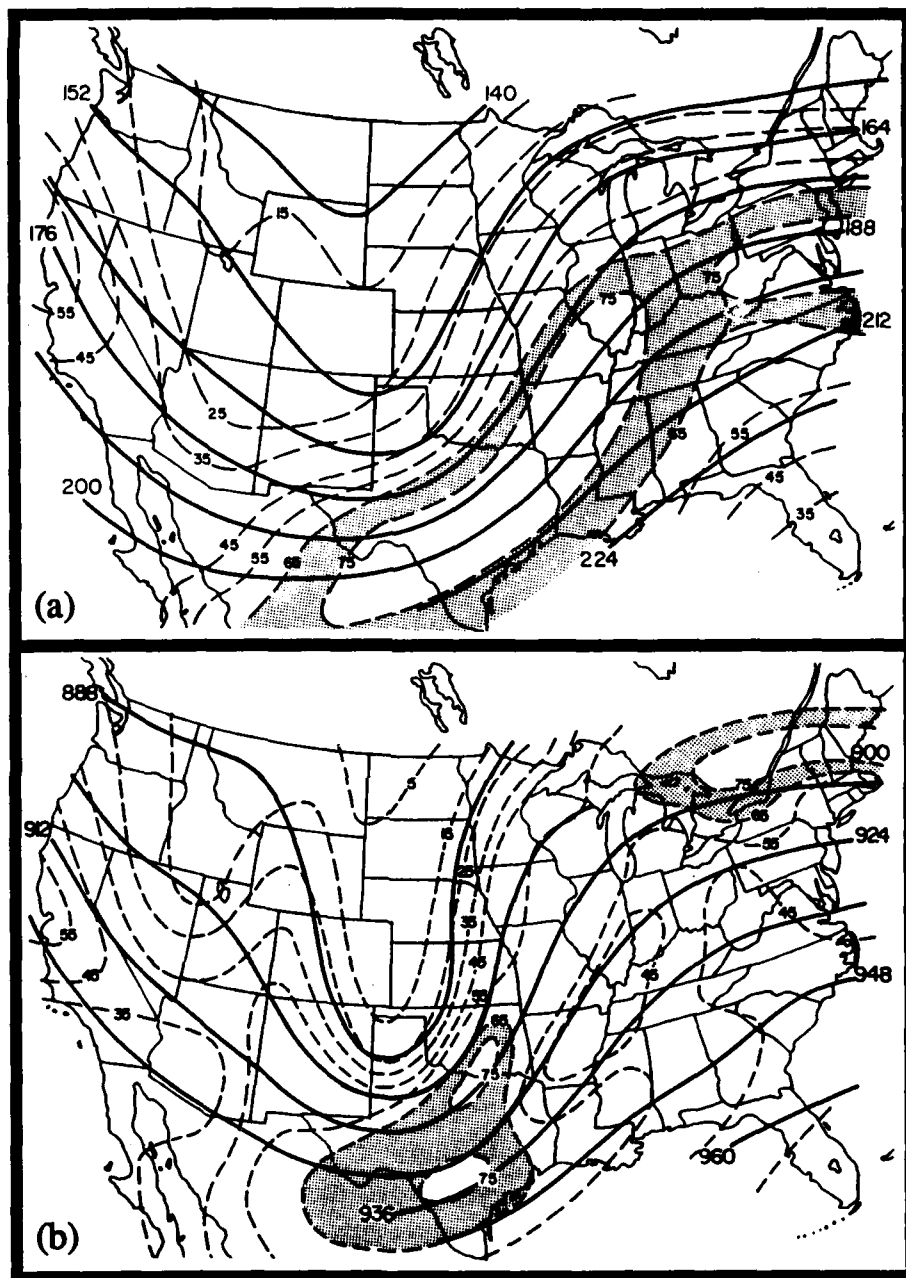


Figure 3.7. a) 200 mb analysis and b) 300 mb analysis for 0000 UTC 15 December 1987. Solid lines depict geopotential height field (decameters) and dashed lines are isotachs in  $\text{m s}^{-1}$ .

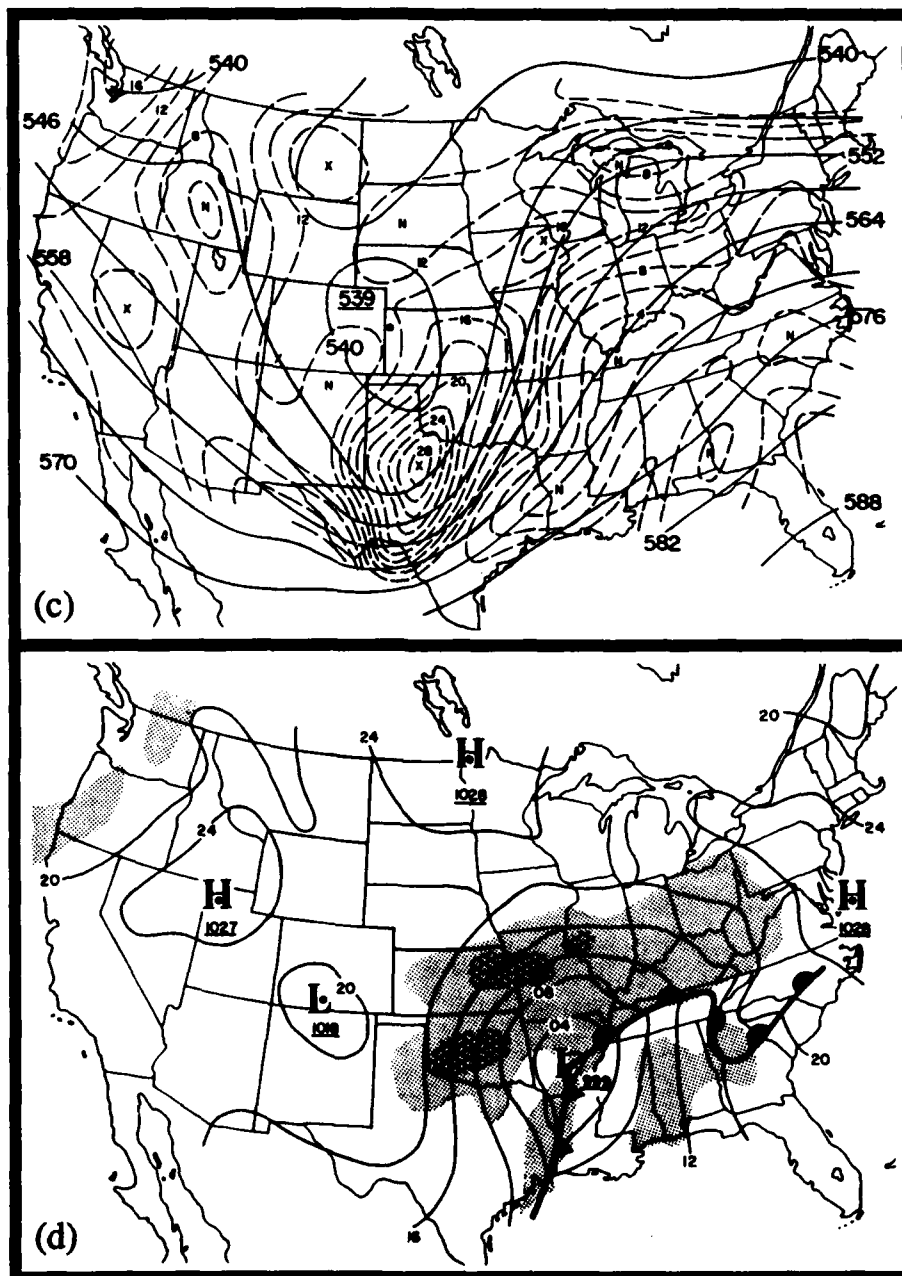


Figure 3.7. c) 500 mb analysis for 0000 UTC 15 December 1987. Solid lines depict geopotential height field (decameters) and dashed lines depict absolute vorticity ( $10^{-5} \text{ s}^{-1}$ ). "X" denotes vorticity maximum and "N" is a vorticity minimum. d) Surface analysis for 0000 UTC 15 December 1987. Solid lines are sea level isobars in millibars, conventional symbols used to depict fronts and pressure centers. Precipitation is represented by the shaded regions and non-convective heavy precipitation is depicted by cross hatching.

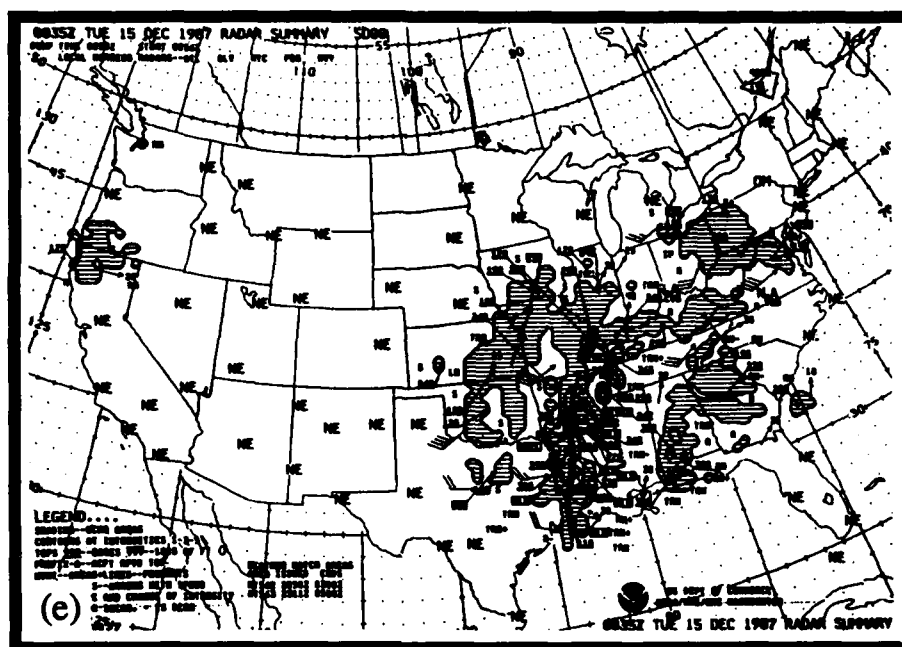


Figure 3.7e. NWS radar summary for 0035 UTC 15 December 1987.

broad regions of stratiform precipitation west and north of the surface cyclone and a concentrated line of deep convection along the cold front are observed. The broad shield of stratiform precipitation northeast of the cyclone is associated with continued overrunning. The areas of heavier stratiform precipitation to the northwest of the surface cyclone are associated with the SWT that has moved out of the Rockies. Very weak cyclonic vorticity advection at 500 mb (Fig. 3.7c) overlie the areas of heavier stratiform precipitation falling in Oklahoma, Kansas, Missouri, into Illinois, as well as over the surface cyclone.

Forecasters rely on the advection of 500 mb vorticity by the 500 mb geostrophic flow to evaluate regions of ascent in synoptic weather systems. However, this practice, based on quasi-geostrophic theory (Holton, 1979), assumes small vorticity advection at low levels and neglects thermal advection factors.

Trenberth (1978) shows that there is partial cancellation between the two terms on the right hand side of the omega equation: i) differential vorticity advection and ii) laplacian of the thermal advection. His work shows that the omega equation can be reduced to:

$$\left( \sigma \nabla^2 + f_0^2 \frac{\partial^2}{\partial p^2} \right) \omega = 2f_0 \frac{\partial V_g}{\partial p} \cdot \left( \nabla \frac{1}{f_0} \nabla^2 \phi \right) + \left( \text{TERMS INVOLVING THE DEFORMATION OF THE WIND FIELD} \right) \quad (3.1.1)$$

LAPLACIAN OF  
OMEGA

ADVECTION OF VORTICITY  
BY THE THERMAL WIND

MINIMAL AFFECT

Where  $\sigma$  is the static stability parameter,  $\phi$  is the geopotential height,  $\omega$  is vertical motion,  $p$  is pressure,  $V_g$  is the geostrophic wind, and  $f_0$  is the coriolis parameter at  $45^\circ\text{N}$ .

Thus, the estimation of vertical motion can be made by simply noting the advection of absolute vorticity by the thermal wind which can be approximated by the thickness field assuming thermal-wind balance.

Figure 3.8 depicts the mid-tropospheric (500 mb) vorticity advection by the 700-300 mb thermal wind. A concentrated area of upward vertical motion can be inferred

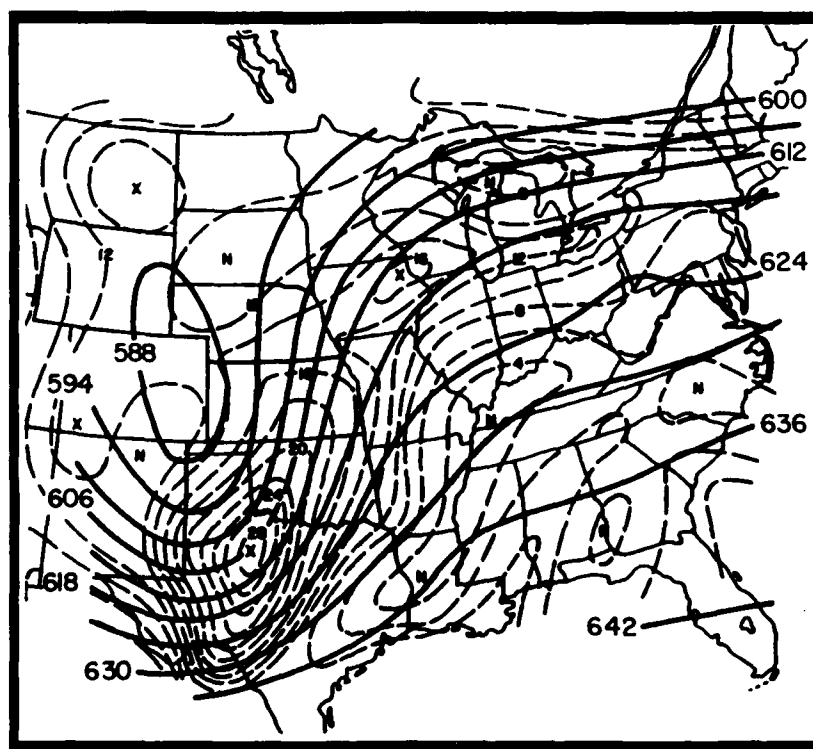


Figure 3.8. Mid-tropospheric vorticity advection by the thermal wind for 0000 UTC 15 December 1987. Dashed lines are 500 mb absolute vorticity isopleths ( $10^{-5} \text{ s}^{-1}$ ). Solid lines depict the 700-300 mb thickness field (decameters) which represents the thermal wind field.

from Oklahoma into eastern Kansas associated with the vortex moving out of the southern Rockies. The correlation of the inferred vertical motion pattern to that of heavy stratiform precipitation is much improved than that seen in Figure 3.7c. Over the region of developing low pressure we continue to see small cyclonic vorticity advection.

A solid line of convective activity along the cold-frontal boundary, extends from the Gulf coast northward to Little Rock, Arkansas. Thunderstorm cells within the line have tops of 11 km. It will be shown in chapter 5 that a low-level jet develops just ahead of the cold front in the warm sector of the cyclone. The rapid expansion of convection along the frontal zone resulted in increased low-level convergence and enhanced frontogenesis. It is suggested that the formation of a low-level jet occurred in response to this frontogenesis, restoring thermal-wind balance (Uccellini, 1987; Mailhot and Chouinard, 1988). Numerical simulations of rapidly deepening cyclones by Mailhot and Chouinard (1988) show that a low-level jet acts to accelerate cyclone development through the advection of warm-moist air over the region of developing low pressure.

To evaluate the stability of the environment in the vicinity of the developing surface cyclone, the Skew-T plot for Little Rock, Arkansas at 0000 UTC 15 December is shown (Fig. 3.9). A strong frontal inversion ( $13^{\circ}\text{C}$  in only 0.5 km) is observed between 952 mb to 906 mb, with significant low-level moisture from the surface to 565 mb at which point a substantial dry intrusion is found. This configuration is consistent with soundings that are observed in conjunction with tornadic outbreaks (Miller, 1972).

A plot of the equivalent potential temperature with height (Figure 3.10) depicts the convective instability present in the environment of the cyclone center. The rapid decrease in equivalent potential temperature from the top of the frontal zone to 565 mb indicates that the atmosphere is conditionally unstable to moist upright convection in this layer.

To further evaluate the stability of the environment in which the surface cyclone developed at 0000 UTC, lifted and K indices were calculated. The examination of both the K and lifted indices help to determine if there is sufficient low-level moisture and dry air aloft to promote convective activity.

At 0300 UTC the cyclone has moved into western Tennessee (Fig. 3.12a). The western edge of the stratiform precipitation shield associated with the mid-tropospheric vortex is now located over Kansas and Oklahoma and is advancing towards the northeast at  $17\text{ m s}^{-1}$ . The squall line extends from the Gulf coast to the cyclone center at this time

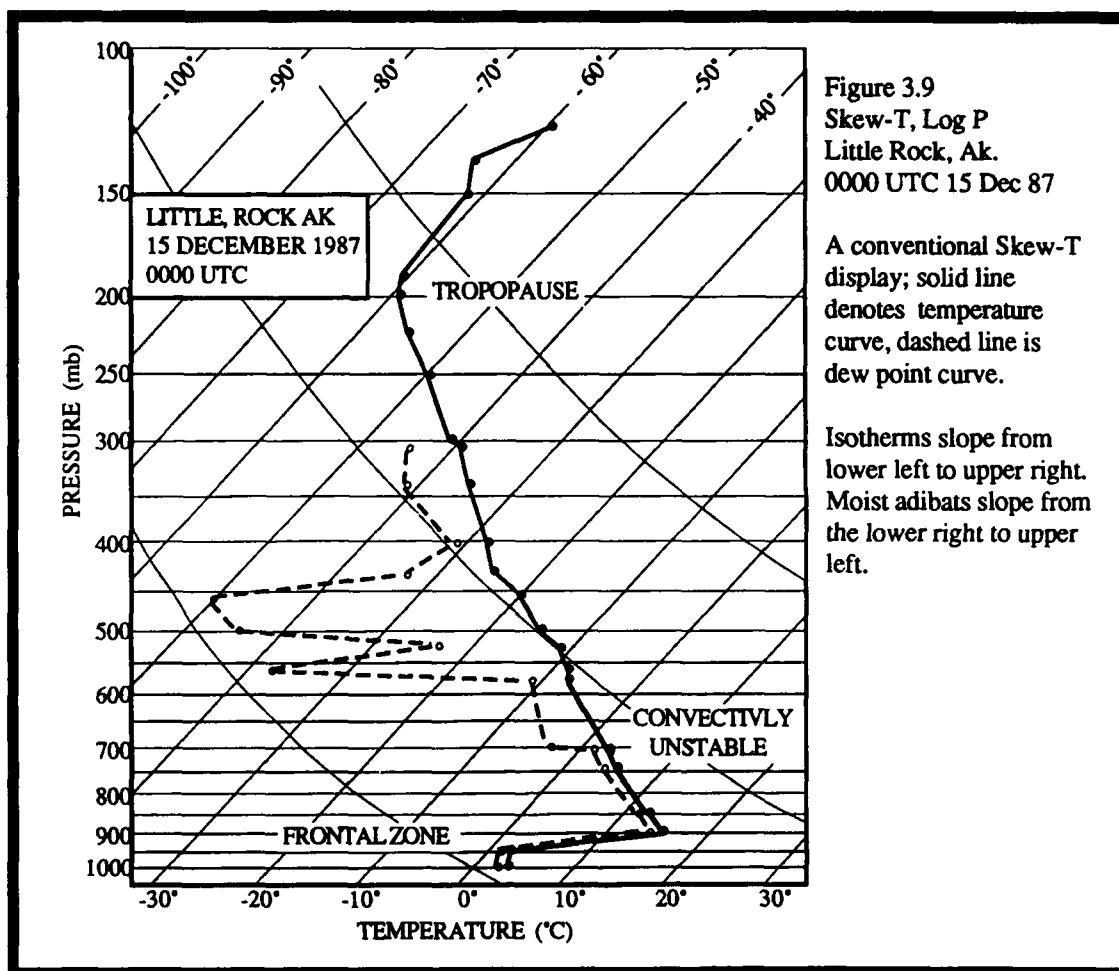


(Fig. 3.12b). Reflectivity tops are reported at 12 km and are moving towards the northeast at  $30 \text{ m s}^{-1}$ . At 0340 UTC an F-3 tornado touched down four miles southwest of West Memphis, Arkansas. The tornadic activity developed 50 km to the south of the cyclone center, reflecting the volatile environment in which cyclogenesis is taking place.

The K-index was developed by George (1960) to help forecast continental summertime air-mass thunderstorm potential. George defined air-mass thunderstorms as "those developing in areas of weak winds without apparent frontal or cyclonic influence". The K-index is calculated from the relation (all temperatures in °C):

$$K = (T_{850} - T_{500}) - T_{d850} - (T_{700} - T_{d700}) \quad \{3.1.2\}$$

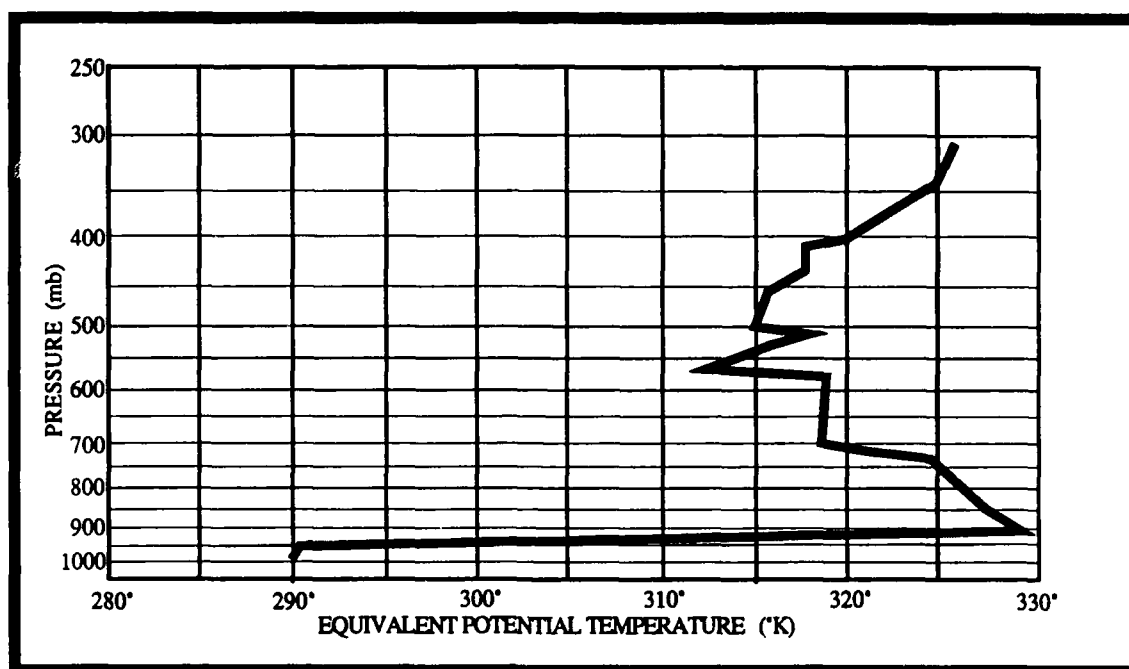


Figure 3.10. Plot of equivalent potential temperature with pressure for Little Rock, Arkansas, 0000 UTC 15 December 1987.

The K-index arithmetically combines the 850-500 mb temperature difference, the 850 mb dewpoint (which directly measures the low-level moisture content), and the 700 mb dewpoint depression (which indirectly measures the vertical extent of the moist layer) (Peppler, 1988). Factors that contribute towards higher K-index values are; i) cold air at 500 mb, ii) warm air at 850 mb, iii) warm moist air at 700 and 850 mb.

The lifted index is calculated to assess the potential for severe thunderstorm activity. The stability is affected by the availability of low-level moisture and the temperature distribution of the atmosphere. The lifted index is calculated by taking a mean boundary layer parcel up to the Lifted Condensation Level (LCL) then moist adiabatically to 500 mb. The lifted temperature is then subtracted from the ambient 500 mb air temperature. Lifted index values of -3 to -6 are associated with moderate to heavy thunderstorms and values <-6 are favorable for severe weather (Miller, 1972).

The combination of warm moist air at the surface and cold air at 500 mb result in lower lifted-index values. The results of the calculations for 0000 UTC are displayed in

Figure 3.11. The combination of low level advection of warm-moist air, and advection of cold-dry air aloft results in an large area of K-index values greater than 35 over the Gulf States. This contour outlines the area within which the probability of thunderstorm activity is  $> 80\%$ . The  $K=35$  contour passes over the developing cyclone (Fig. 3.11a) indicating that the environment that cyclogenesis is occurring is of a highly convective nature.

Figure 3.11b shows a tongue of low values of lifted index extending north eastward from the Gulf of Mexico, indicative of the advection of warm-moist air ahead of the advancing cold front. The solid line of convective activity is aligned along the tight western gradient of stability isopleths.

At 0600 UTC, observed pressure falls of  $2.5 \text{ mb hr}^{-1}$  is indicative of the very explosive development that is occurring. The cyclone has deepened to 991 mb and is located over southern Illinois (Fig. 3.13a). The precipitation pattern associated with the mid-tropospheric vortex has taken on the shape of a comma pattern as the vortex develops (Fig. 3.13b). This vortex is positioned within 400 km of the surface cyclone. The associated cyclonic vorticity advection by the thermal wind is becoming superposed over the region of developing low pressure aiding in the rapid spinup of the system.

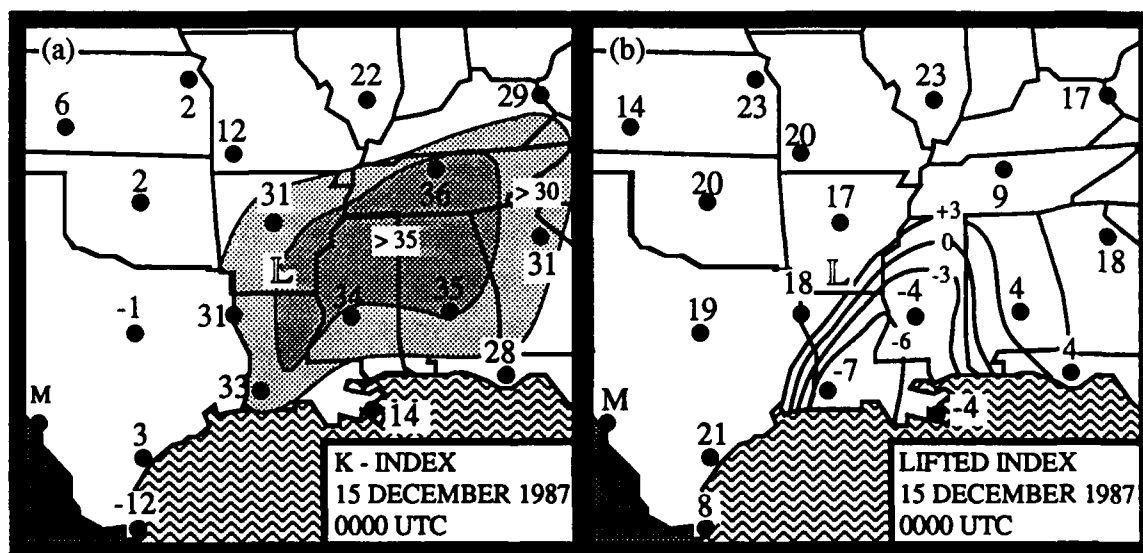


Figure 3.11. 0000 UTC 15 December 1987 stability parameters (a) K-index. Lightly stippled area reflects values  $>30$  and the darker region is  $>35$ . (b) Lifted index. Thin solid lines are lifted index isopleths. Cyclone center denoted as "L". Stations with missing data are denoted with an "M".



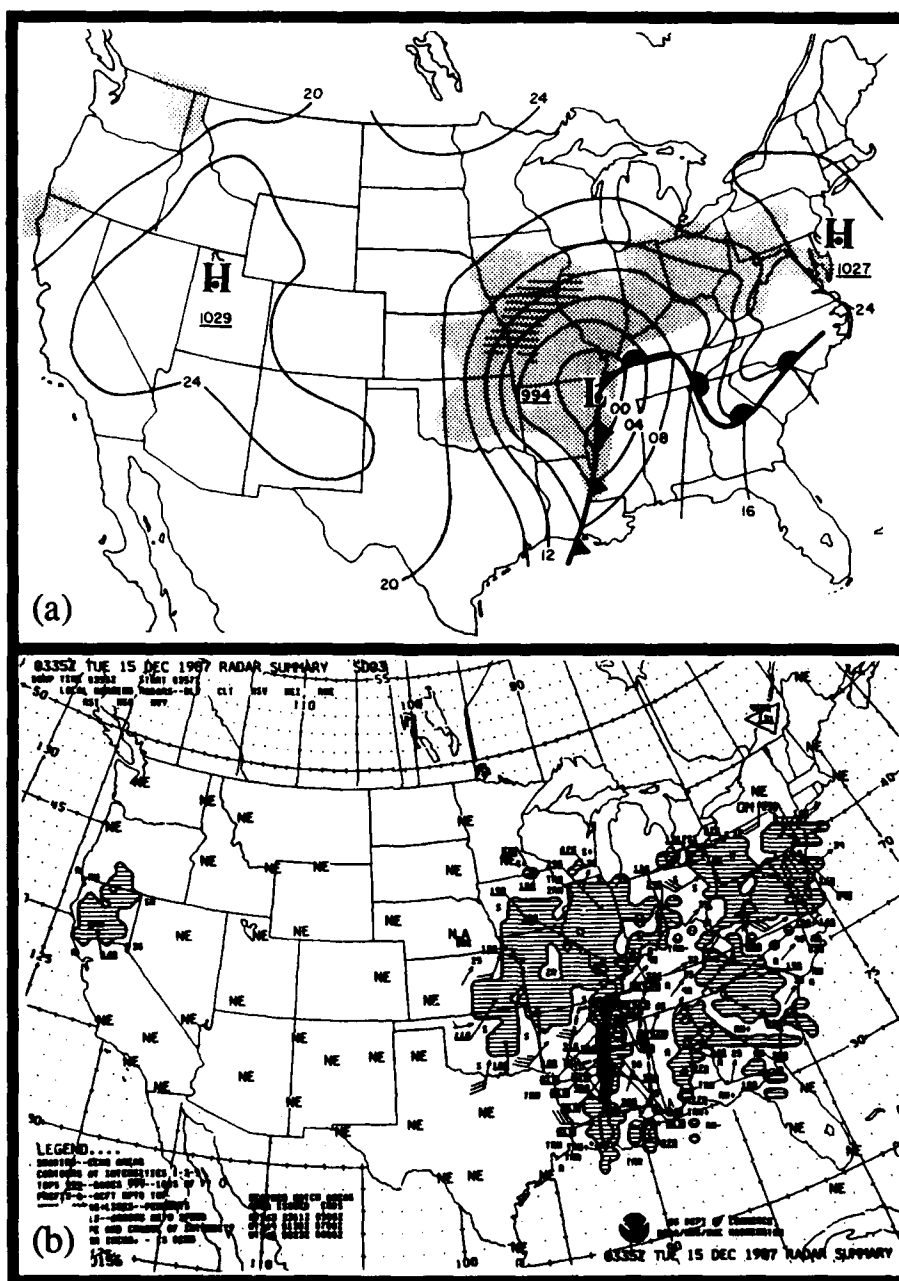
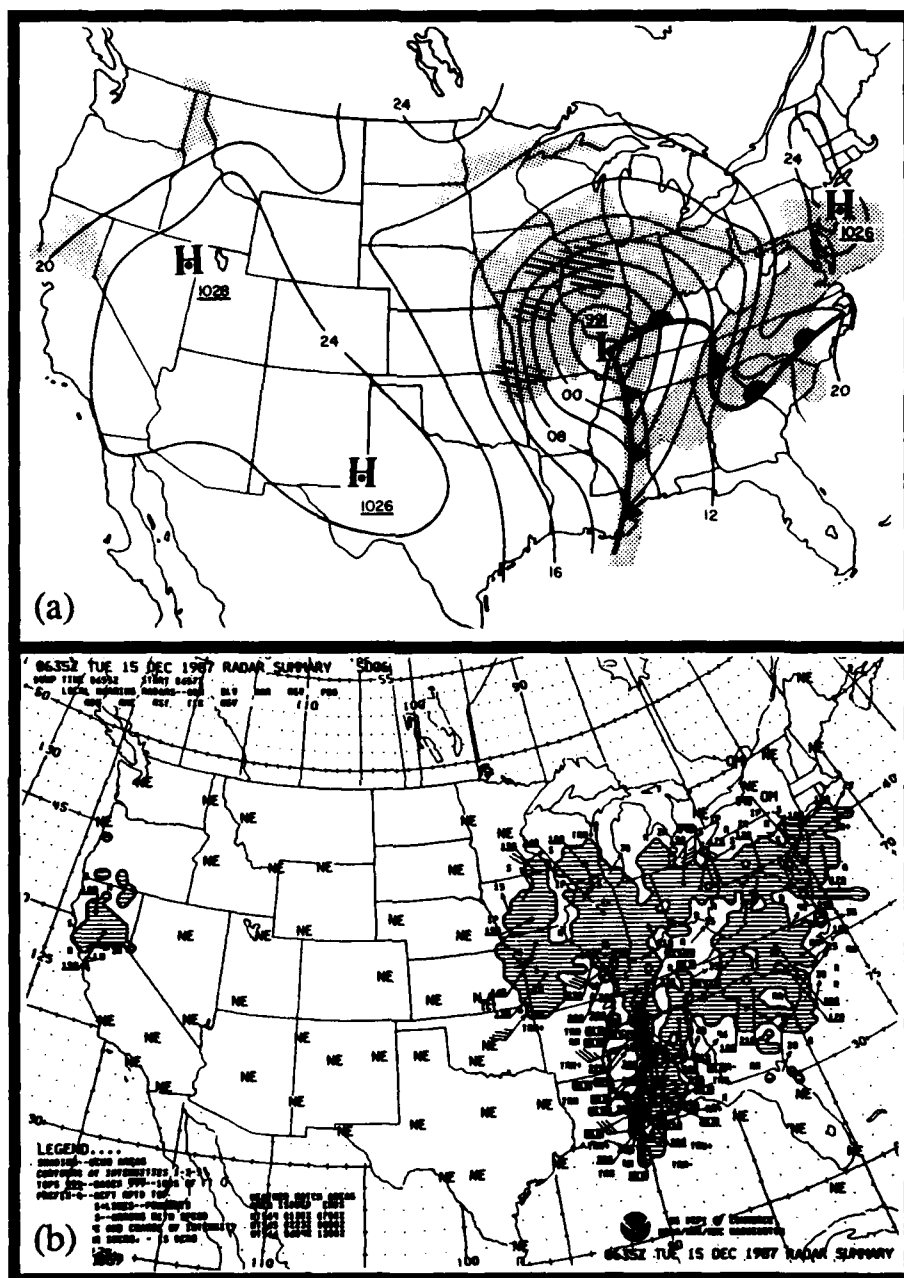


Figure 3.12. a) Surface analysis for 0300 UTC 15 December 1987. Solid lines are sea level isobars in millibars, conventional symbols used to depict fronts and pressure centers. Precipitation is represented by the shaded regions and non-convective heavy precipitation is depicted by cross hatching. b) NWS radar summary for 0335 UTC 15 December 1987.



**Figure 3.13. a) Surface analysis for 0600 UTC 15 December 1987. Solid lines are sea level isobars in millibars, conventional symbols used to depict fronts and pressure centers. Precipitation is represented by the shaded regions and non-convective heavy precipitation is depicted by cross hatching. b) NWS radar summary for 0635 UTC 15 December 1987.**

Convection near the cyclone center has been cited as an important mechanism contributing to the explosive development of a number of oceanic cyclones (Sanders and Gyakum, 1980; Bosart, 1981; Gyakum, 1983). During this storm's development convective activity was most pronounced in the initial stages of cyclone development. However, during this period of most rapid development only isolated cells of convection, maximum tops of 11 km, were found to the north and west of the cyclone center. The significant thunderstorm activity is suppressed to the south of the cyclone center as the surface cyclone crosses to the north of the upper-level jet axis. The northern extent of the thunderstorm activity coincides with the jet axis aloft.

The 0900 UTC analysis shows a mature occluded cyclone (982 mb) over central Illinois (Fig. 3.14a). The radar depiction shows a uniform band of stratiform precipitation wrapping around the cyclone center (Fig. 3.14b). Surface pressure falls of  $3 \text{ mb hr}^{-1}$  were observed between 0600 and 0900 UTC. Convective activity has gradually diminished along the surface cold front to the south.

By 1200 UTC the upper-level pattern shows that the SWT axis, aligned north-south along the front range of the Rockies at 0000 UTC, has swung around and is orientated from the northern Plains to the Mid-Atlantic coast (Fig. 3.15). It is evident that the polar and subtropical jets have merged. At the 200 mb level winds have increased to  $85 \text{ m s}^{-1}$  (Fig. 3.15a), while at 300 mb winds of  $75 \text{ m s}^{-1}$  are observed (Fig. 3.15b). The left exit region of the jet streak is located in the vicinity of the surface cyclone. A well defined closed low appears at the 500 mb level, with a vorticity maximum of  $26 \times 10^{-5} \text{ s}^{-1}$  (Fig. 3.15c).

The surface cyclone is located 90 km south of Chicago Illinois with a central pressure of 976 mb, the lowest observed in the storm's history (Fig. 3.15d). The surface cyclone begins to weaken as it becomes vertically stacked with the upper-level low. The surface pattern shows a strong pressure gradient in the upper midwest supporting wind gusts of  $20\text{--}25 \text{ m s}^{-1}$ . An extensive band of stratiform precipitation about the cyclone results in heavy snow from the Great Lakes southwestward to Missouri. Cold-air drainage down the Atlantic coastal plain is reflected hydrostatically by a surface ridge over Virginia and the western Carolinas. The radar shows that the precipitation is breaking up in the vicinity of the cyclone center and an expanding dry slot is located over the upper Tennessee Valley (Fig. 3.15e). A remnant line of convective activity is located near the Gulf coast.



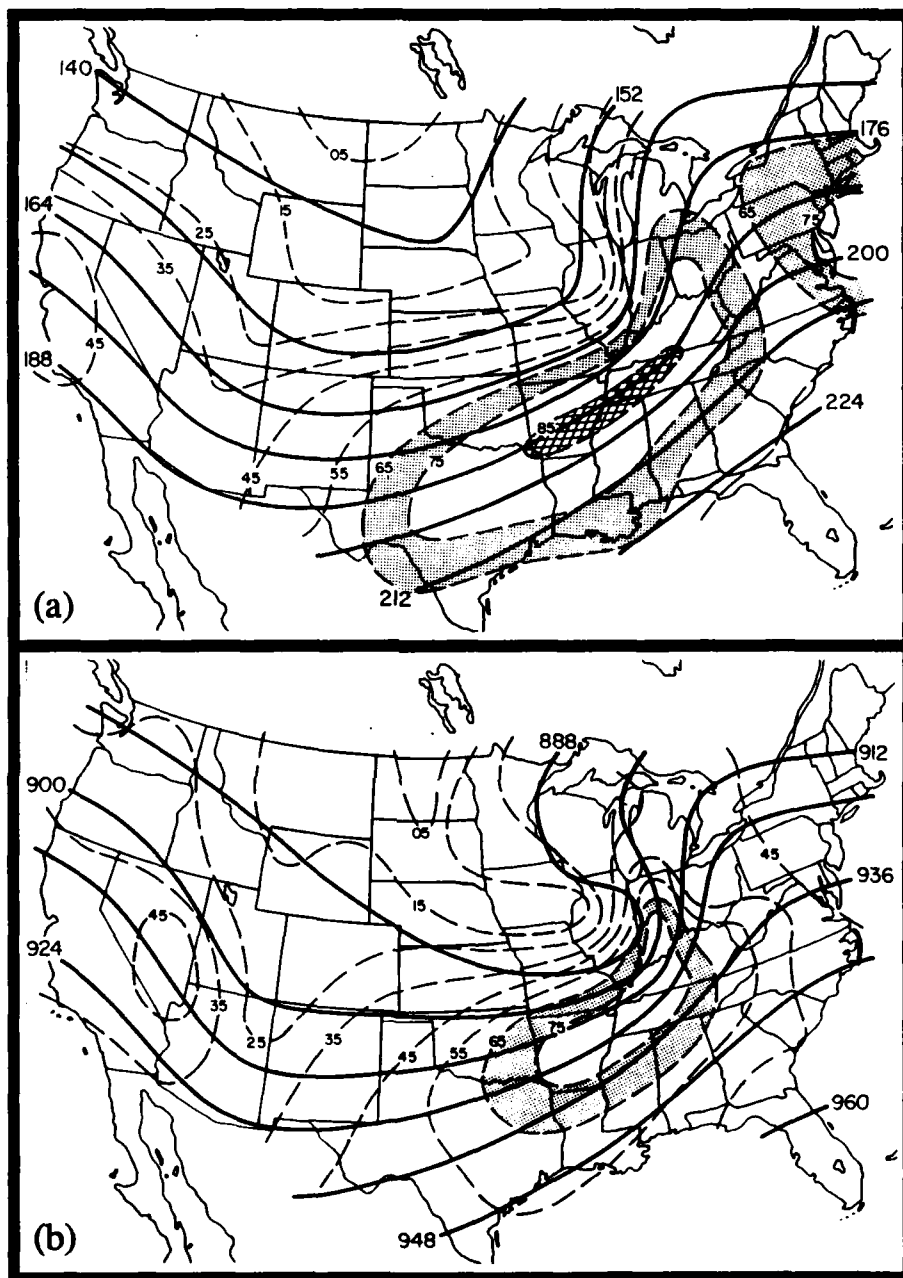


Figure 3.15. a) 200 mb analysis and b) 300 mb analysis for 1200 UTC 15 December 1987. Solid lines depict geopotential height field (decameters) and dashed lines are isotachs in  $\text{m s}^{-1}$ .

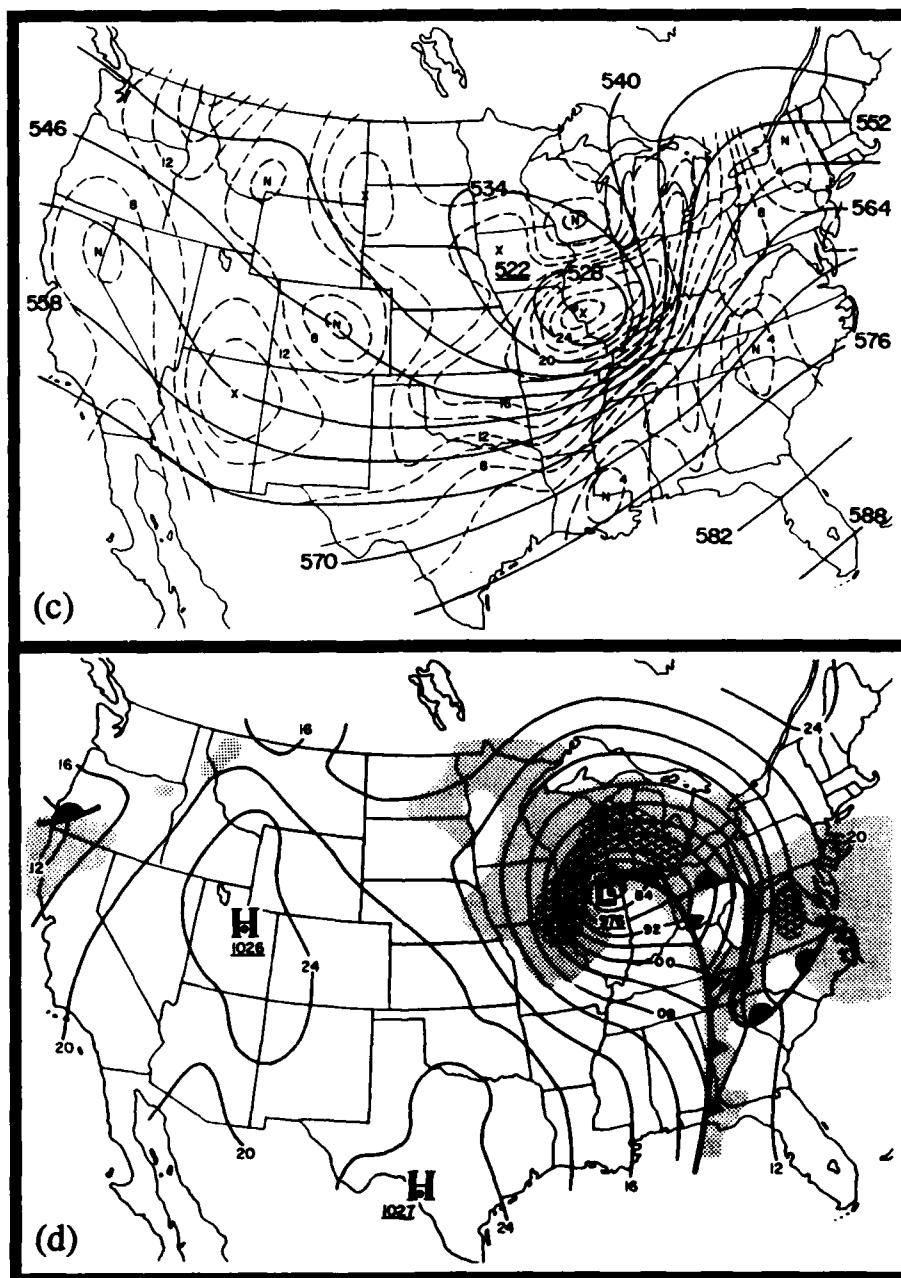


Figure 3.15. c) 500 mb analysis for 1200 UTC 15 December 1987. Solid lines depict geopotential height field (decameters) and dashed lines depict absolute vorticity ( $10^{-5} \text{ s}^{-1}$ ). "X" denotes vorticity maximum and "N" is a vorticity minimum. d) Surface analysis for 1200 UTC 15 December 1987. Solid lines are sea level isobars in millibars, conventional symbols used to depict fronts and pressure centers. Precipitation is represented by the shaded regions and non-convective heavy precipitation is depicted by cross hatching.

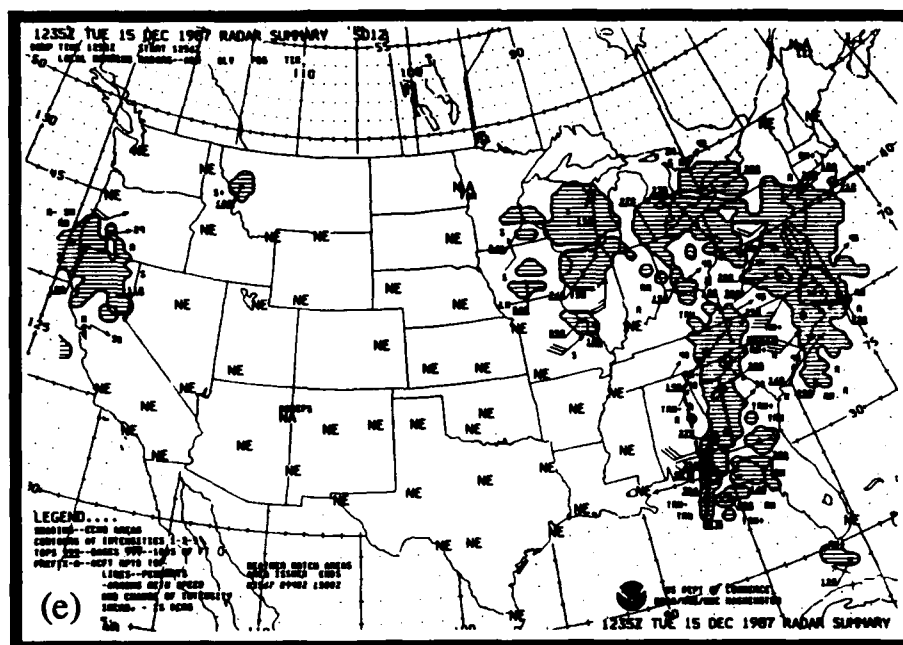


Figure 3.15e. NWS radar summary for 1235 UTC 15 December 1987.

During the next 12 hours the cyclone weakens and slowly moves northeastward with the upper-level low. A broad upper-level jet is evident at 200 mb (Fig. 3.16a). At 300 mb the exit region of the jet streak is crossing the Mid-Atlantic coast (Fig. 3.16b). The 500 mb pattern shows an deep upper low located over the Great Lakes, with a cyclonic vorticity maximum of  $30 \times 10^{-5} \text{ s}^{-1}$ . A second cyclonic vorticity maximum is approaching the coast associated with the jet streak (Fig. 3.16c).

At the surface (Fig. 3.16d) we see the development of a Miller "type B" pattern at 0000 UTC on 16 December. The primary cyclone has continued to weaken as it moved northward west of the Appalachians, while a secondary development has occurred along the New Jersey coast (Miller, 1946). The secondary development is occurring in a strong baroclinic zone, and in the favorable environment produced by the advancing jet streak.

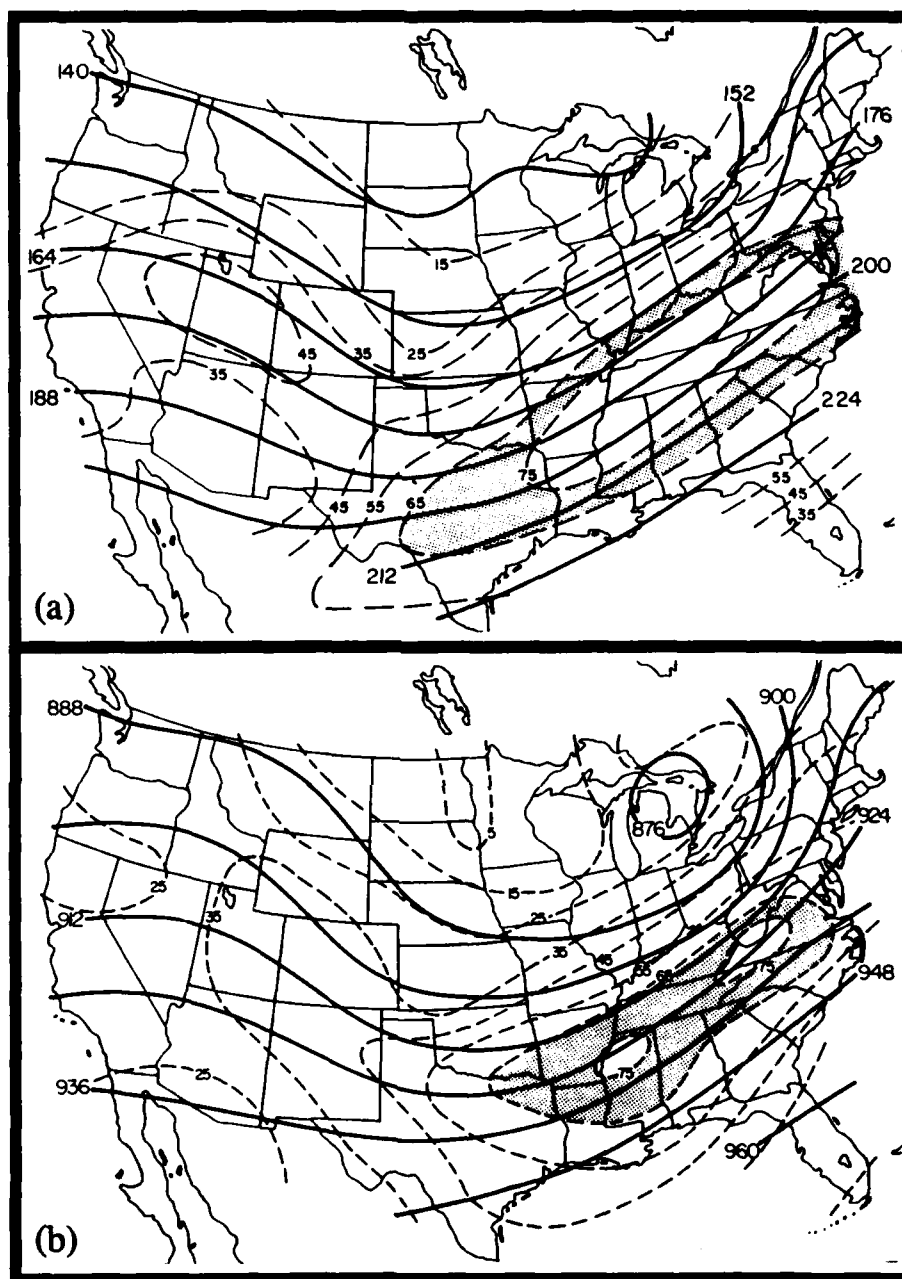


Figure 3.16. a) 200 mb analysis and b) 300 mb analysis for 0000 UTC 16 December 1987. Solid lines depict geopotential height field (decameters) and dashed lines are isotachs in  $\text{m s}^{-1}$ .



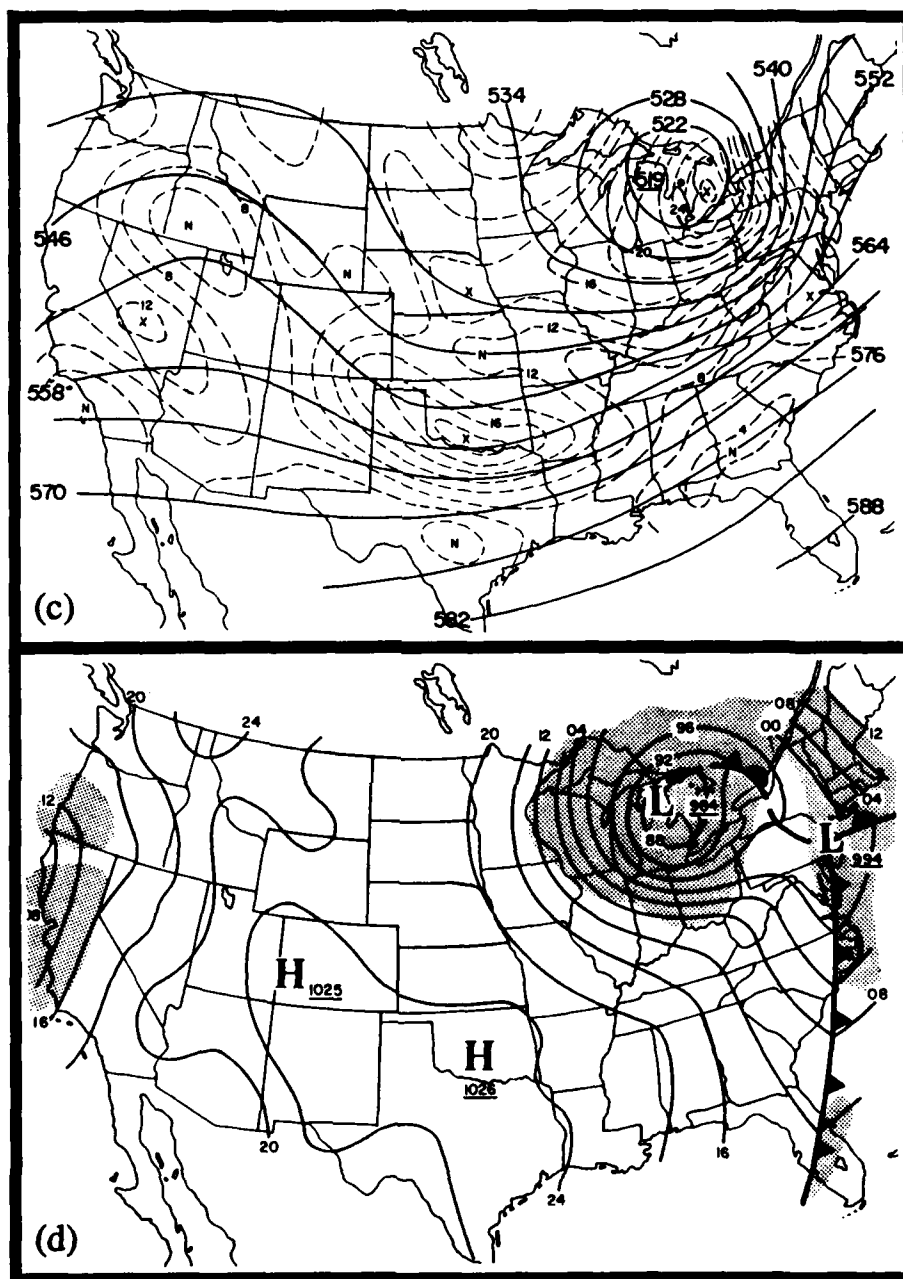


Figure 3.16. c) 500 mb analysis for 0000 UTC 16 December 1987. Solid lines depict geopotential height field (decameters) and dashed lines depict absolute vorticity ( $10^{-5} \text{ s}^{-1}$ ). "X" denotes vorticity maximum and "N" is a vorticity minimum. d) Surface analysis for 0000 UTC 16 December 1987. Solid lines are sea level isobars in millibars, conventional symbols used to depict fronts and pressure centers. Precipitation is represented by the shaded regions and non-convective heavy precipitation is depicted by cross hatching.

### 3.2 Isallobaric Analysis

The most rapid phase of development occurs during the 12 hour period between synoptic reports. In order to gain some insight into the complex atmospheric changes taking place during this time a detailed analyses of the 3 hourly surface-pressure tendencies were constructed between the 0000 and 1200 UTC radiosonde reports. Through inspection of the surface-pressure tendencies we can analyze how the integrated mass divergence in the atmosphere is changing between synoptic reporting periods.

If we integrate the hydrostatic equation from the surface to the top of the atmosphere and take the partial derivative with respect to time we obtain equation 3.2.1.

$$(\partial p / \partial t) = g \int_z^{\infty} (\partial \rho / \partial t) \delta z \quad \{3.2.1\}$$

From this expression we see that the surface pressure tendency is effected only by the change in integrated mass above that point. The pressure change reported on surface observations provide a reasonable estimate to the magnitude of the local pressure changes due to storm development and motion. However, local changes in surface pressure due to the developing storm system can be masked by a number of processes including, diurnal variations in temperature, variability of cloud cover effecting changes in radiative transfers through the atmosphere, and orographic effects. These effects can be minimized by taking integrated 3 hour pressure tendencies (Saucier, 1955).

We can obtain a pressure tendency equation by substitution of the continuity equation into 3.2.1, and expanding  $\nabla_H \cdot (\rho V)$  to get (Haltiner and Martin, 1957):

$$\frac{\partial p}{\partial t} = -g \int_z^{\infty} \rho \nabla_H \cdot V \delta z - g \int_0^{\infty} (V \cdot \nabla_H \rho) \delta z + gpw \quad \{3.2.2\}$$

This equation describes the local change in pressure. The first term on the right side of the equation represents the horizontal mass divergence. The second term represents the horizontal advection of the mass and the third term is the vertical advection of the mass. This equation tells us that a decrease in surface pressure is the result of a net mass decrease

in the column of air over some point. A net mass loss is achieved either from an integrated horizontal divergence above the surface or the advection of less dense air (warm advection) into the area and vertical mass divergence.

Figure 3.17 displays the three hourly isallobaric analysis during for the storm's history. The maps were constructed using reported pressure tendencies from the National Weather Service observations and using graphic subtraction techniques of the sea level pressure pattern in data void areas (Saucier, 1955).

The isallobaric analysis for 2100-0000 UTC 14-15 December 1987 clearly shows the presence of two distinctive pressure fall regions (Fig. 3.17a), with two associated pressure tendency troughs. The surface cyclone is located at this time near the western Arkansas/Louisiana border where a tight isallobaric gradient exists. Pressure falls of  $6 \text{ mb } 3 \text{ hrs}^{-1}$  are occurring over southern Missouri. These pressure reductions are in response to a combination of storm motion and strong warm advection throughout the troposphere over this region.

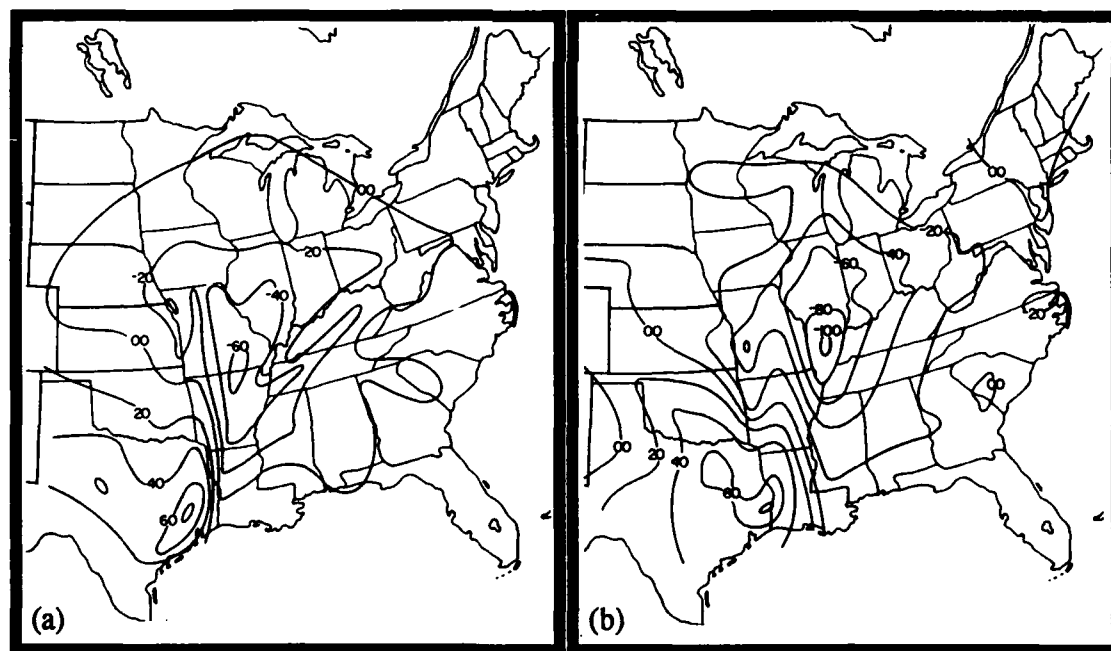


Figure 3.17. Surface isallobaric analysis. Isopleths are in 2 mb/ 3 hr increments. Time period of analysis a) 2100-0000 UTC 14-15 December 1987, b) 0000-0300 UTC 15 December 1987.

A second maximum pressure fall ( $2 \text{ mb } 3 \text{ hrs}^{-1}$ ) is observed over the northwest corner of Missouri, with a pressure tendency trough extending down toward Texas. This pattern of pressure falls is associated with the mid-tropospheric vortex moving into the Plains. The pressure-tendency trough aligns well with the axis of strongest cyclonic vorticity advection by the thermal wind (see Figure 3.8 for 0000 UTC). The thermal wind pattern extends northward and is superposed over the divergent wind field of the polar jet resulting in maximum pressure falls in northwest Missouri.

The two pressure fall regions are still distinguishable during the period from 0000 UTC to 0600 UTC (Figs. 3.17 b and c). The pressure falls increase in magnitude with the western maximum exhibiting falls of  $8 \text{ mb } 3 \text{ hrs}^{-1}$ , while falls of  $10 \text{ mb } 3 \text{ hrs}^{-1}$  are observed over southern Illinois (Figs. 3.17 b and c). The cyclone central pressure has seen a steady drop of  $1 \text{ mb hr}^{-1}$  between 1800 UTC on 14 December and 0400 UTC 15 December. From 0400 UTC to 0600 UTC little or no change in central pressure is observed. During this latter period, it is suggested that the position of the polar and subtropical jets were such that the surface cyclone was in a relative minimum of thermal advection and net mass divergence aloft.

By 0600-0900 UTC, Figure 3.17d, a merging of the two maximum pressure fall regions begins as the developing mid-tropospheric vortex comes within 400 km of the surface cyclone. An explosive decrease in the surface pressure tendencies is observed as the surface cyclone undergoes its most rapid development (falls of  $14 \text{ mb } 3 \text{ hrs}^{-1}$ ). An exceedingly tight isallobaric gradient is seen over southern Illinois. The cyclone central pressure continues to deepen at a rate of  $2.5 \text{ mb hr}^{-1}$  until 1200 UTC. It will be suggested in Chapter 6 that the observed isallobaric pattern results from the merging of the polar and subtropical jets, producing enhanced upper-level divergence and thermal advection patterns.

The 0900-1200 UTC isallobaric pattern, Figure 3.17e, shows a single maximum in pressure falls centered over the Chicago area. In Chapter 4 it will be shown that a marked dry intrusion observed in the water-vapor imagery corresponds well to the strong pressure rises of  $8 \text{ mb } 3 \text{ hrs}^{-1}$  in southern Illinois.



## CHAPTER 4

### SATELLITE IMAGERY ANALYSIS

#### 4.1 Evolution of the Synoptic Cloud Pattern

The cloud signature associated with the explosive development of 14-15 December is similar to that observed with other explosively developing systems (Carleton, 1985). Such storms are marked by an expansive baroclinic cloud shield associated with an upper-tropospheric cyclone and a separate comma cloud, located to the west, associated with an upper-tropospheric disturbance. The phasing of these two features coincide with the explosive development of the surface cyclone as rapid pressure falls are observed (Mullen, 1983).

Roger Weldon (1979) has observed that the development of intense midlatitude cyclones have certain common cloud signatures. Weldon has developed conceptual models depicting the development of such systems after reviewing numerous satellite sequences. Figure 4.1 represents the cloud signatures of two types of cyclone that have reached their maximum stage of development.

Figure 4.1a depicts the development of a type A system. The development of this type storm is considered to be a lower tropospheric phenomena, initiated at the surface and building into the upper atmosphere. The baroclinic cloud shield (labeled "A" in Fig. 4.1a) represents the cirrus shield associated with the upper-tropospheric baroclinic zone and the related jet stream. The cloud formation is primarily the result of convective processes that transport moisture to the upper levels producing cloud debris. The jet axis lies close to the northern and western edge of the baroclinic-zone cirrus. The correspondence between the position of the jet axis aloft and the cloud edge is found along the anticyclonic side of the cloud shield. The "comma cloud" pattern labeled "B" in Fig. 4.1a is associated with a mid-tropospheric vorticity center. Here, the lower cloud pattern is partially masked by the higher cirrus shield. A small amount of deformation zone cirrus, labeled "C", is located near the comma cloud head and is distinct from the baroclinic zone cirrus.

The type B system represents one that is well developed both horizontally and vertically. A substantial circulation is found throughout the troposphere with this type system. Consequently, a type B storm is normally a more intense system associated with

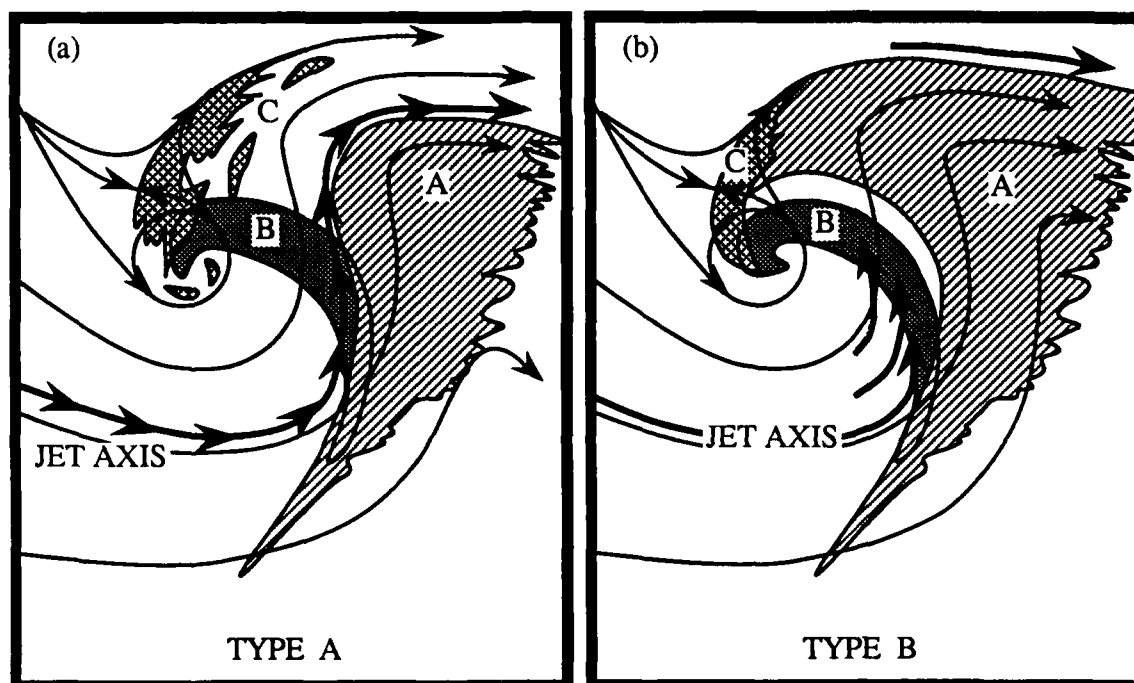


Figure 4.1. Mid and upper-level cloud structure for two types of mature cyclones as defined by Weldon (1979). Type A cyclone builds up from the lower troposphere while a type B storm will develop within the mid levels and build in either direction. The type B storm is normally a more intense system. Region "A" depicts baroclinic zone cirrus, "B" represents the vorticity comma cloud, and "C" is the deformation zone cirrus. Thick arrows represent the axis of the upper level-jet and thin arrows depict upper-level streamlines.

Midwest blizzards. The cloud pattern for a type B system is shown in Figure 4.1b. Here, the cirrus of the baroclinic zone merges with that of the deformation zone and wraps around to the north and west of the comma cloud. The ridge tends to build back and wrap further around the cyclone and the jet is found over a broad region in the cyclonic air just west of the cirrus deck. Winds drop off through the ridge but increase on the leading edge of the cirrus shield on the north side of the ridge due to frontogenesis aloft. Often, the comma cloud pattern is to the west of the cirrus deck. This is a result of the faster moving baroclinic zone cirrus out racing the slower mid-level cloud pattern associated with the vorticity comma cloud. Since a type A system is a mid and lower tropospheric event, a type A system may become a type B system once upper-level support over takes the low-level development.

Weldon developed the D.A.V.E. (Deformation, Advection, and Vertical Exchange) model to describe the evolution of the cloud pattern associated with cyclogenesis. This model depicts the evolution of the cyclone cloud shield in three phases of development (Fig. 4.2). Phase I is the "frontogenetic" or "organizational" phase of development (Fig. 4.2a). During this phase, a jet streak is embedded within the jet stream at position "A". A new jet streak begins to form at position "C" in response to warm advection between areas "B" and "C". Tropospheric frontogenesis begins in response to deformation in the northern-left quadrant in advance of the cold air. As the vertical motion patterns increase, the baroclinic zone intensifies resulting in a cloud element described as a "baroclinic leaf".

Phase II depicts the "initial cyclogenetic" phase of development (Fig. 4.2b). The cloud element has evolved into a "comma" pattern as the surface cyclone begins to form. The jet streak at position "C" increases in magnitude, while the jet streak at "B" decreases, as significant upper-tropospheric warm advection occurs.

Figure 4.2c shows the third phase of development referred to as the "open comma" phase. Here, the jet streak at "C" has become well defined in response to the vertical exchange and upper-tropospheric warming. The jet streak at "A" is primarily induced by horizontal thermal advection. The head of the comma cloud gradually moves towards the center of circulation as a result of deformation. A dry slot develops in response to the horizontal and vertical motion taking place. The surface cyclone experiences significant deepening while amplification of the upper-level trough and ridge are observed.

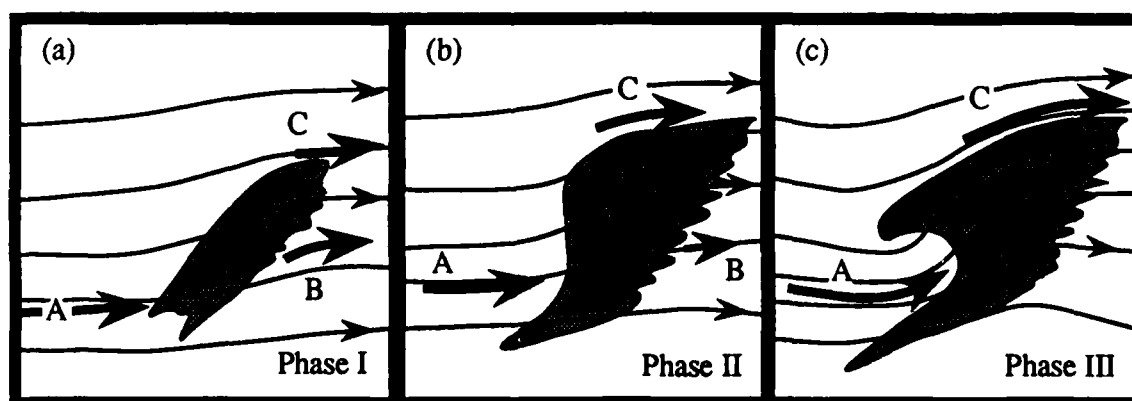


Figure 4.2. The D.A.V.E. model depicting the three phases of evolution of the cloud shield associated with cyclone development. Shaded region depicts the high cloud signature, thin arrows depict upper-level streamlines, thick arrows are jet streak positions, black dot is surface cyclone position (Weldon, 1983).



Weldon (1987) empirically categorized cyclone development by making modifications to the D.A.V.E. model. The following categories of cyclone development are in terms of structure and jet stream configuration.

- i. In stream cyclogenesis -- Development occurs within a jet stream core.
- ii. Left track cyclogenesis -- Jet streak and development occur left of the jet axis.
  - a. *Cold air development* -- Development totally within the cold air.
  - b. *Induced wave* -- Initial development in cold air near jet axis. This induces a wavy pattern on the baroclinic shield.
  - c. *Enhanced cumulus* -- Primarily an oceanic event, convection develops under a cold trough and organizes into a comma pattern.
- iii. Right track cyclogenesis -- Jet streak located to the right of the jet stream.
  - a. *Base of trough development* -- Cyclogenesis takes place at the base of a high amplitude trough.
  - b. *Rear of trough development* -- Cyclogenesis is initiated on the west side of a trough in response to a rapidly building upstream ridge.
  - c. *Digging jet stream* -- Similar to the "rear of trough" type development, however development begins within a zonal jet stream.
- iv. Branching jet cyclogenesis -- Upstream jet stream splits into two branches initiating cyclogenesis between the two.

The explosive cyclogenesis that was observed during the 14-15 December 1987 resulted from a combination of "rear of trough" and "in stream" cyclogenesis. The development of the cyclone over the southern Rockies on 14 December was the result of the "rear of trough" type cyclogenesis.

During the second week of December, a high amplitude ridge developed over the eastern Pacific with a trough situated over the Rockies. On the 13th, a SWT dropped down out of Pacific Northwest and moved into the southern Rockies resulting in a significant mid-tropospheric circulation. Satellite reveals the development of a tight vortex over southern Arizona by 0000 UTC 14 December (not shown). This system had a very short wavelength ( $\approx 500$  km). An area of deformation zone cirrus was located over the four corners region while a vorticity comma cloud developed over New Mexico. The cloud tops

of the deformation zone cirrus is associated with temperatures of  $-50^{\circ}\text{C}$  while the comma cloud is associated with temperatures of  $-40^{\circ}\text{C}$ . An  $85\text{ m s}^{-1}$  jet streak at the 200 mb level passed just south of the developing comma cloud. The jet axis extends from the base of the trough westward up along the back side of the trough.

During the next 12 hours the upper-level trough axis is orientated north-south near  $108^{\circ}\text{W}$ . The 1331 UTC 14 December infrared satellite photograph reveals that the cloud pattern has become more complex (Fig. 4.3). The initial comma cloud has moved out of the base of the trough and moves northeastward into Colorado and decays (labeled "A").

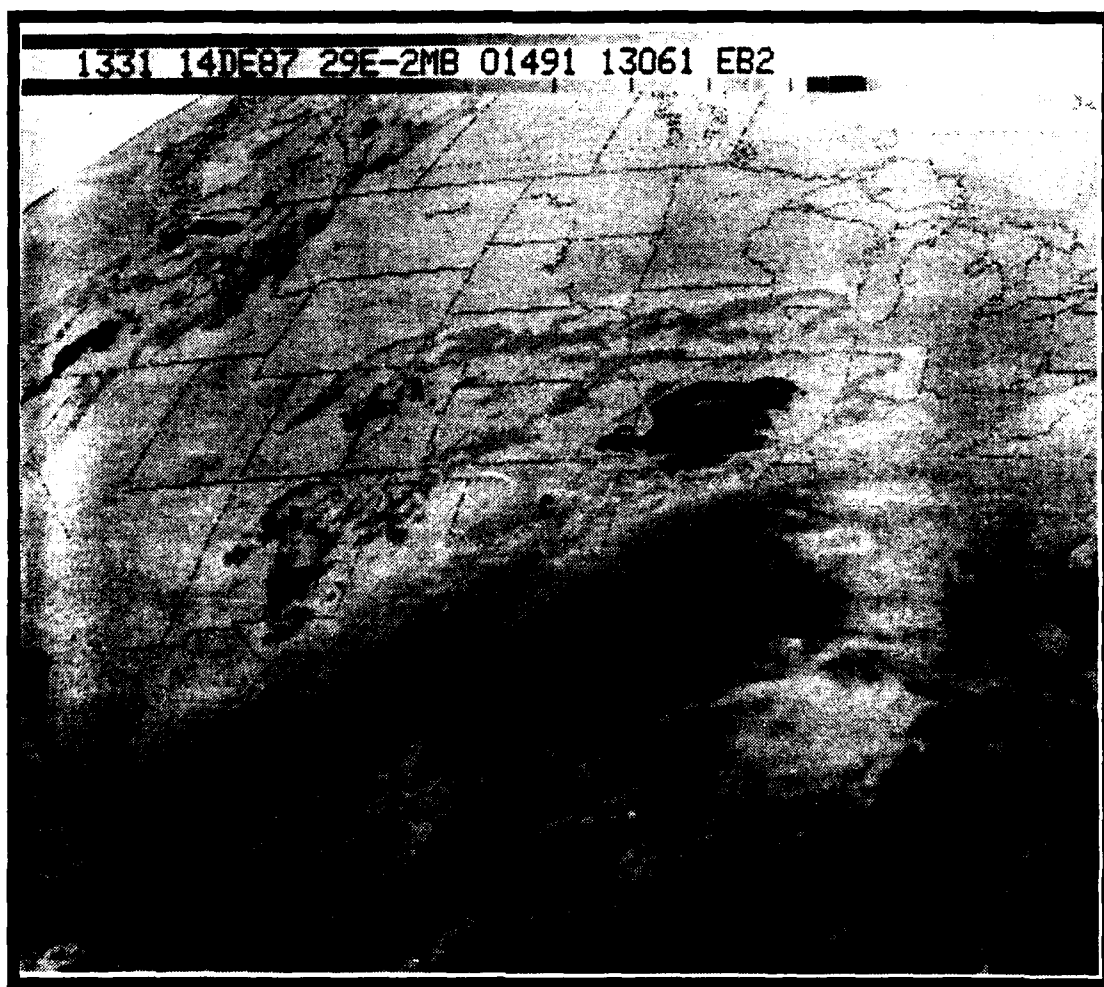


Figure 4.3. GOES-East infrared satellite imagery for 1331 UTC 14 December 1987. Lettered areas are referenced in the text.

A second vorticity lobe has entered the base of the trough and results in the formation of a new comma cloud over New Mexico (labeled "B"). Deformation zone cirrus is observed over eastern New Mexico. Visible imagery clearly shows the existence of the vorticity induced comma cloud, below the thin cirrus deck, extending from eastern New Mexico into north-central Mexico. The cirrus shield over the Plains reveals the presence of a broad upper-level ridge. The northern edge of the cirrus shield corresponds to the region of maximum horizontal wind shear associated with the polar jet axis. A second band of strong winds at the 200 mb level, associated with the subtropical jet, extends from central Mexico into Oklahoma. The vertical motion of the left exit region of a subtropical jet streak over Oklahoma has initiated convection in this area (labeled "C"). Cloud top temperatures of the convection approaches  $-60^{\circ}\text{C}$ . The low-level flow out of the Gulf provides abundant low-level moisture throughout the southern and central Plains. The flow results in a large shield of low stratus and stratocumulus cloud as the warm-moist air ascends adiabatically overrunning the colder surface air.

During the next few hours the upper trough progresses eastward into the foot hills of the Rockies. The cirrus shield indicates a positively tilted upper-level trough of large meridional extent with the upper flow extending from central Mexico into the Mid-West United States. The flow is similar to the pattern associated with Weldon's "in stream" cyclogenesis. By 1800 UTC 14 December, a jet streak associated with the subtropical jet is situated over eastern Texas. Visual satellite imagery shows a north/south line of convection developing coincident with cyclogenesis near Houston, Texas at 1800 UTC.

The satellite photograph for 0031 UTC 15 December (Fig. 4.4) shows two distinct bands of clouds. A cloud mass associated with the upper trough and the polar jet is found over the central Plains. This system is entering the second phase of development (as described by the D.A.V.E. model) as the jet core rotates cyclonically about the trough axis. A region of deformation zone cirrus is located in region "A". The extent of deformation zone cirrus extends over a large area due to the displaced moisture by the initial comma cloud dissipating over Nebraska. The western edge of the cirrus lines up along the 250 mb trough axis. A vorticity induced comma cloud extending from eastern Oklahoma southward into Texas can be seen as a mid-level cloud mass marked by position "B". A  $75 \text{ m s}^{-1}$  polar jet max at 300 mb has rounded the base of the trough and is located over central Oklahoma. The jet is located in the developing dry slot of the vortex at point "C".

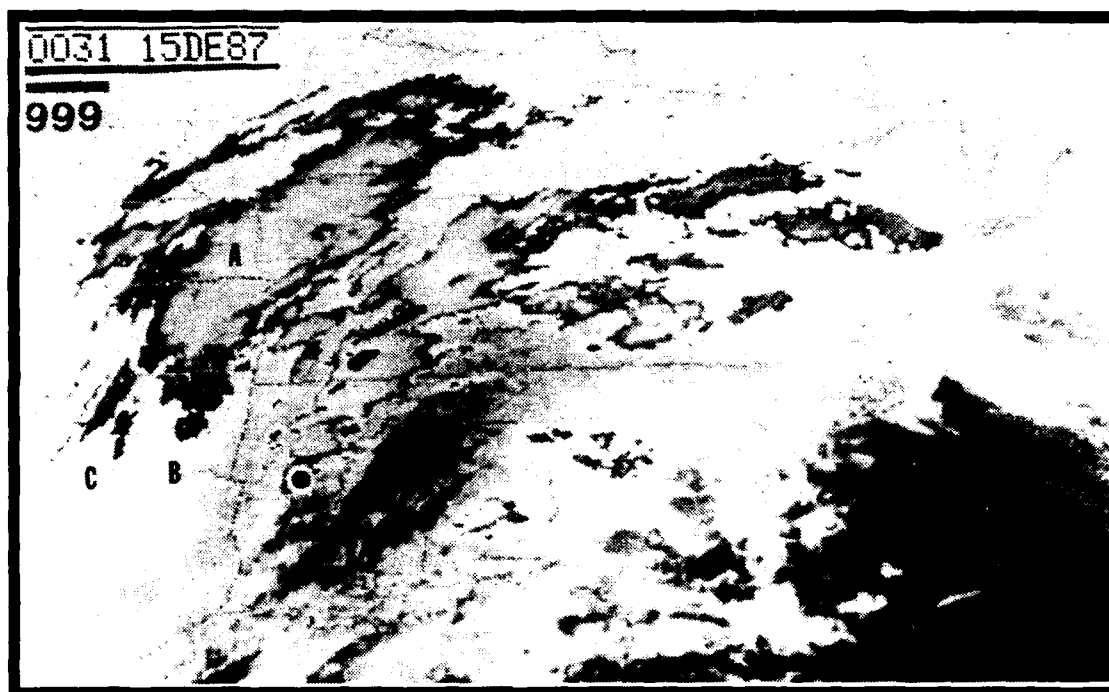


Figure 4.4. GOES-East infrared satellite imagery for 0031 UTC 15 December 1987. Surface cyclone position indicated by the black dot over southern Arkansas while the sea-level pressure value is located beneath the date/time in the upper left. Lettered areas are referenced in the text.

Since 1800 UTC, a line of convection has exploded along the frontal boundary from Louisiana northward into Missouri as the subtropical jet progresses northward. The convection transports moisture 10 km into the troposphere. The surface cyclone located over south central Arkansas has a central pressure of 999 mb. The upper-level trough runs north/south at this time with a  $75 \text{ m s}^{-1}$  subtropical jet located at the 200 mb level. The jet axis runs cyclonically through central Texas up along the western edge of the convective activity in Arkansas and Missouri.

The 0701 UTC 15 December imagery shows the dramatic development that has taken place in approximately six hours (Fig. 4.5). The transport of moisture in the upper atmosphere and strong upper-level jet winds has resulted in the rapid horizontal expansion of cloud cover over the Midwest. A tight upper-level vortex has produced a comma cloud over the central Plains (area "A"). At this point, the surface cyclone is undergoing its most rapid phase of deepening with the central pressure dropping  $2.5 \text{ mb hr}^{-1}$ . The center of the

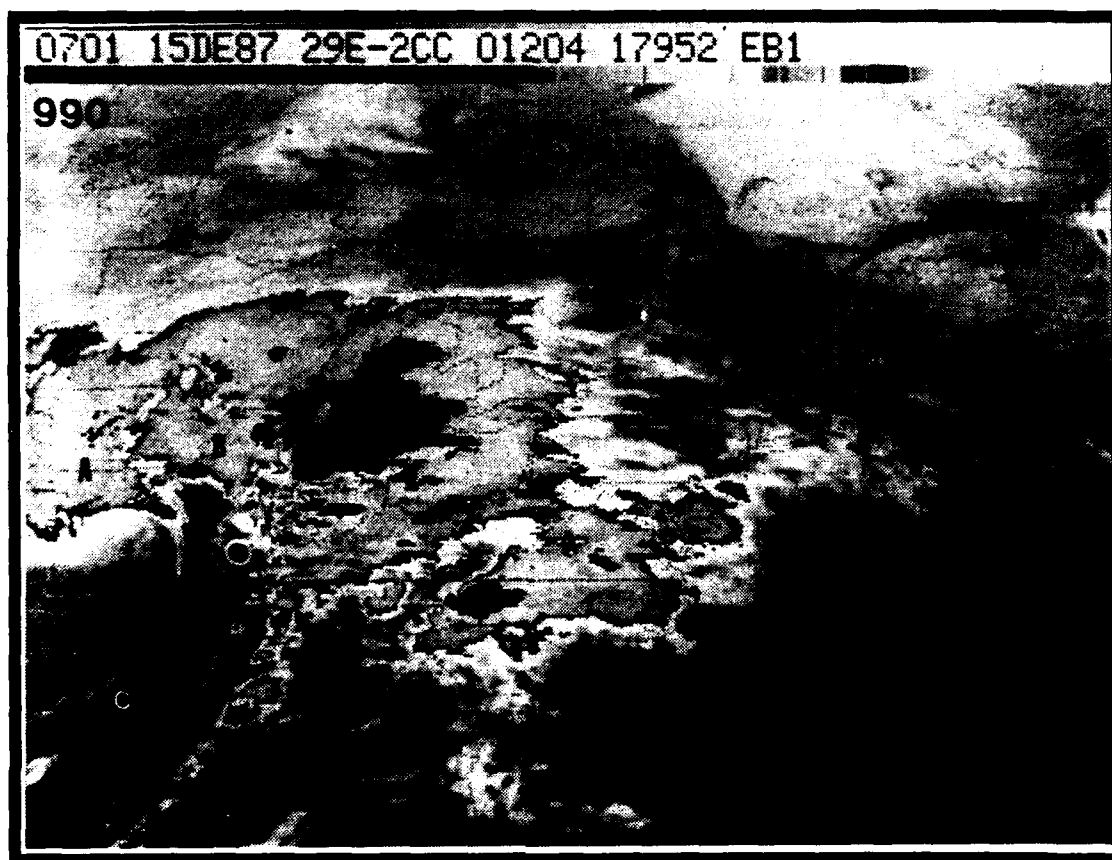


Figure 4.5. GOES-East infrared satellite imagery for 0701 UTC 15 December 1987. Surface cyclone position indicated by the black dot over southern Illinois while the sea-level pressure value is located beneath the date/time in the upper left. Lettered areas are referenced in the text.

upper air disturbance is located  $< 400$  km west of the surface cyclone, conducive to rapid development (Sanders, 1980). The head of the vorticity comma cloud has begun to emerge from under the thick cirrus deck, as the higher cirrus is advected east by higher winds aloft. The SWT has become negatively tilted resulting in an "S" shape along the western edge of the baroclinic zone cirrus shield at this time (area "B"). The ridge has built out ahead and has begun wrapping around the system. The subtropical jet runs along the cirrus streak in southern Arkansas (labeled "C") cyclonically into southwest Illinois. It is here that we begin to see a merging of the polar and subtropical jets.

The comma cloud over Missouri has undergone significant development as it enters the latter stages of Weldon's "rear of trough" model. The most striking feature at this point

is the well developed comma cloud pattern. Weldon (1979) attributes the development of the comma cloud to "differential rotation" as depicted in Figure 4.6. Initially, a straight border separates the two halves of the circle. The shaded region represents the visible cloud pattern. The strongest tangential winds are located at the inner circle and decrease radially in either direction. As the cloud system evolves from phase "I" to "IV", the shaded region takes on the observed "S" shape with the cyclonic vorticity maximum located at the inflection point of the border.

The development of the comma cloud coincides with the rotation of the trough axis as the jet streak comes around the base of the trough. The axis of the associated polar jet runs from western Arkansas into central Missouri closely paralleling the subtropical jet stream. The cirrus cloud tops have increased to 10.5 km and have taken on a well defined appearance with a sharp northern edge. At this point in time, the two cloud masses are still distinguishable.

During the next two hours the two cloud features merged into one broad cloud shield producing a classic cloud signature typical of an occluded cyclone. Such a process has been termed as an "instant occlusion", where the approaching vortex provides the occluded element and the baroclinic wave provides the warm and cold frontal boundaries (Anderson *et al.* 1969). During this process rapid pressure falls in excess of  $2.5 \text{ mb hr}^{-1}$  are experienced. The cloud signature rapidly takes on the characteristics of Weldon's "type B" cyclone. During this same period the polar and subtropical jets also merged into a

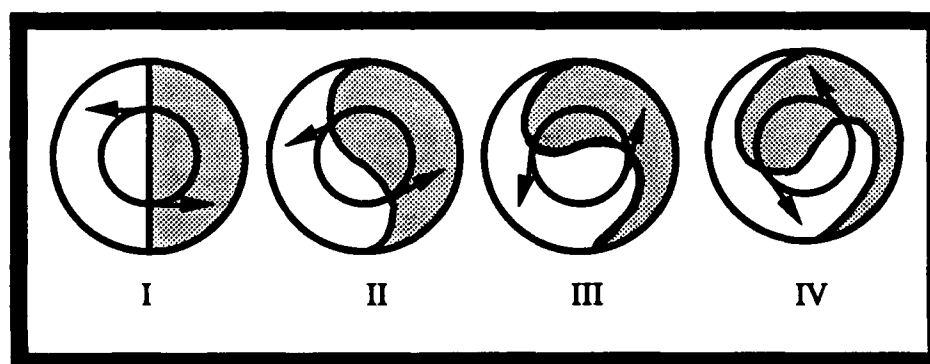


Figure 4.6. Evolution of a comma cloud pattern over a period of time as the result of differential rotation. Arrows represent the tangential wind speed that decreases in either direction. Shaded region represents the evolution of the cloud signature (Weldon, 1979).

single jet with increased winds of to  $85 \text{ m s}^{-1}$  over the Mississippi Valley.

The satellite photograph for 1201 UTC 15 December (Fig. 4.7) shows the cloud signature of a mature winter cyclone. The surface cyclone, over northeast Illinois, has reached its lowest central pressure (976 mb). The cloud pattern to the north and east of the cyclone have merged with that associated with the advancing upper-level vortex and extends to the west-southwest of the circulation center. The merging of the deformation and the baroclinic cirrus shields results in an expansive cloud pattern that covers the eastern United States. The  $85 \text{ m s}^{-1}$  jet stream level winds rapidly advance the cirrus shield eastward exposing the slower moving mid-level vorticity comma cloud feature. A north-south line of convection has developed on the rear edge of the vorticity comma cloud

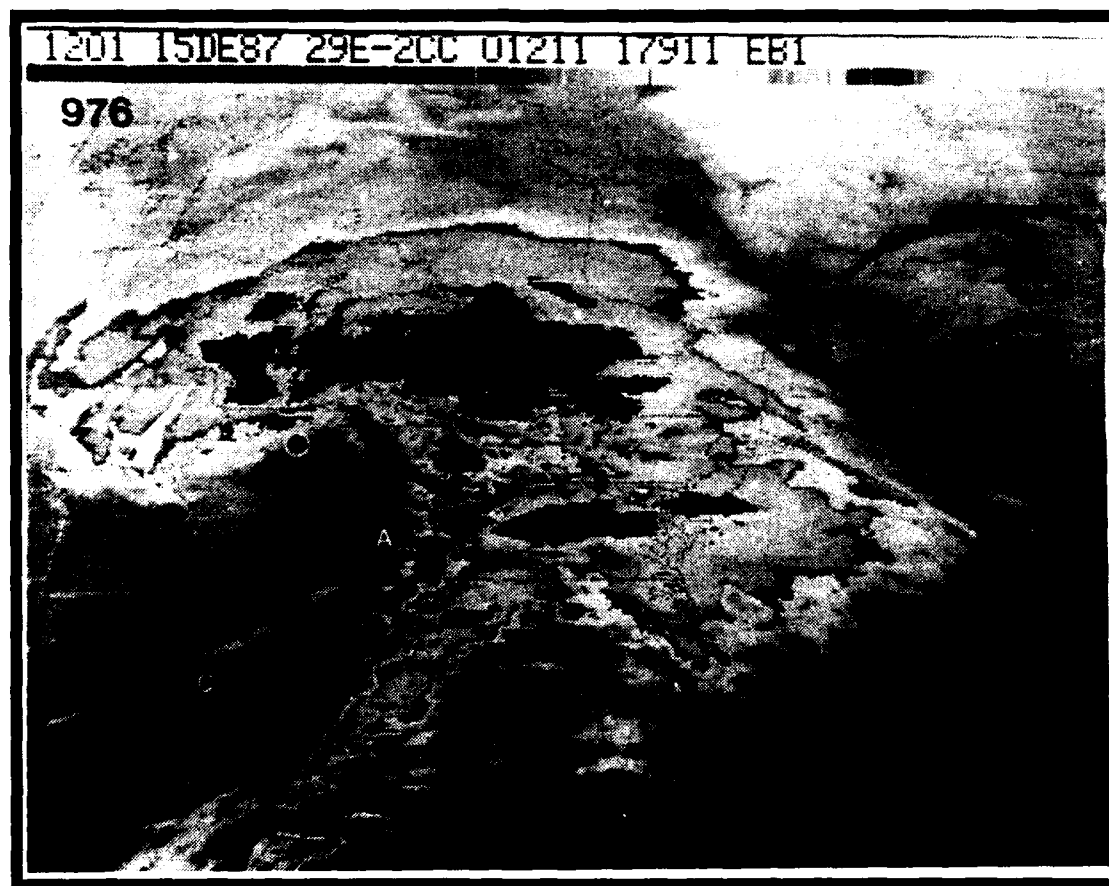


Figure 4.7. GOES-East infrared satellite imagery for 1201 UTC 15 December 1987. Surface cyclone position indicated by the black dot over northern Illinois while the sea-level pressure value is located beneath the date/time in the upper left. Lettered areas are referenced in the text.

(area "A"). A well defined dry slot has formed over area "B", indicative of dry stratospheric air descending to the lower troposphere. A streak of jet cirrus at location "C", evidence of the jet axis, is in agreement with the location of the jet in the 200 mb analysis. The jet axis extends from this cirrus streak northeastward to the Ohio Valley, and then west to Virginia ("D"). A secondary development occurs off the coast of New Jersey during the next 12 hours, perhaps triggered by the crossing of the exit region associated with this jet.

Figure 4.8 provides a sequence of development for the 14-15 December cyclone. Phase I of development is associated with a high-amplitude trough running north-south. To the west, a developing mid-tropospheric vortex has a jet streak entering the base its trough. An anticyclonic shield of cirrus is the precursor to development. A region of deformation cirrus, area "A", is located to the north and east of the circulation. The cirrus lies in a region of relatively weak upper-level winds due to the diffluent pattern. As the pattern develops, a closed circulation is observed in the mid-troposphere. The cloud signature is influenced by the developing circulation pattern as it builds into the upper troposphere prior to any surface development. A developing vorticity comma-cloud feature (area "C") is located under the cirrus shield. The feature is composed of mid-level clouds along with some embedded convective activity. A strong southwesterly subtropical jet provides weak PVA to initiate a line of convection ("D") and subsequent cyclone development. A comma cloud associated with the developing cyclone is found at "C". A large band of baroclinic zone cirrus ("B") is located on the east side of the trough south of the jet stream. The bulk of this cloud mass is associated with moisture transported into the upper levels through convection. The jet parallels the western edge of this cirrus shield.

During Phase II, the polar jet streak comes around the base of the trough resulting in a negatively tilted trough. This configuration favors development through increased advection of vorticity, temperature and moisture into the region of developing low pressure. The cloud shield of the upper-level vortex has become well defined. The SWT has increased in amplitude allowing a short-wave ridge to build out ahead of it. The vorticity comma cloud (area "C") takes on a more characteristic "S" shape, indicative of development. The northward progression and intensification of the jet results in further expansion of the baroclinic-zone cirrus in area "B". The northern edge of the deformation



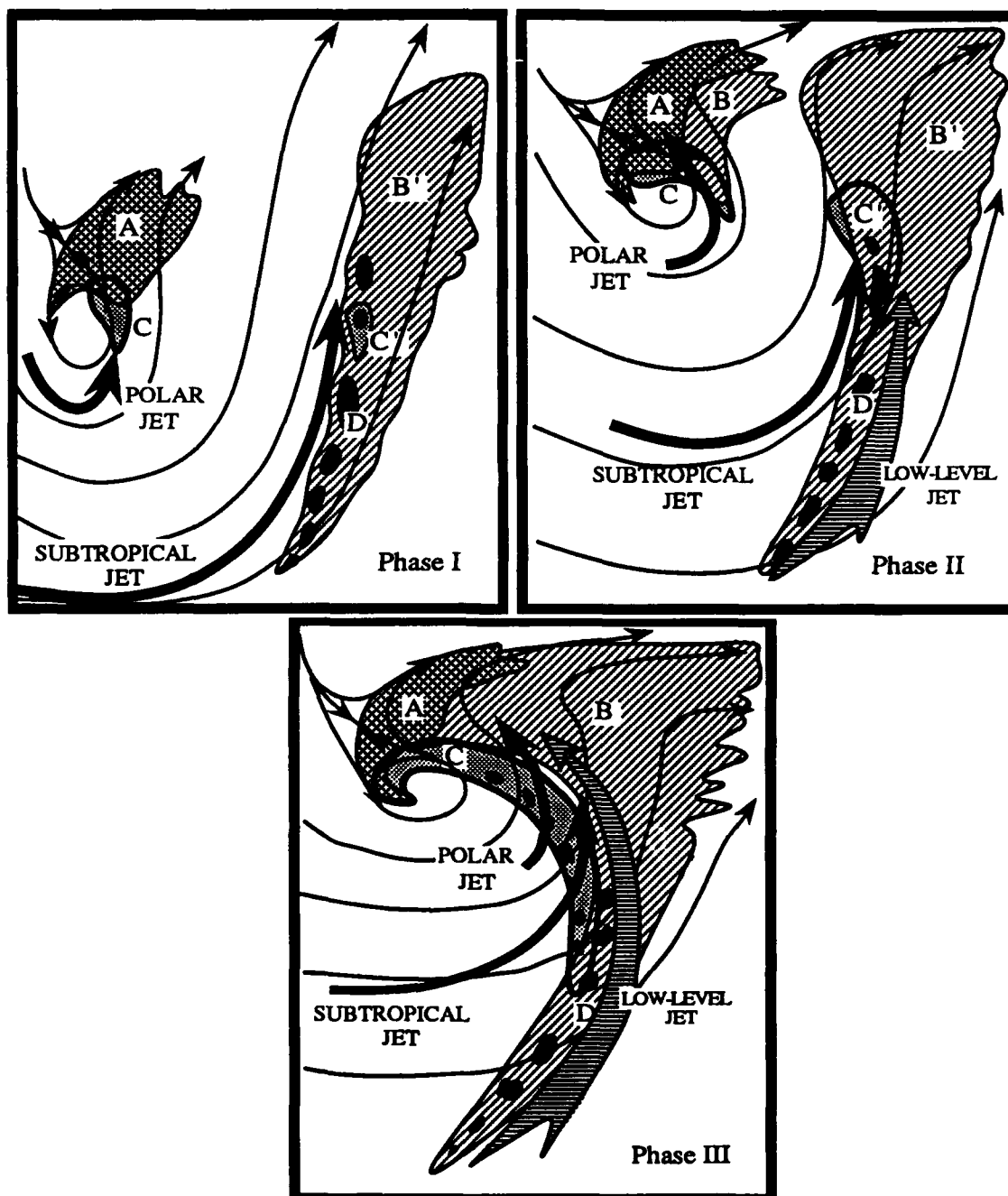


Figure 4.8. Evolution of the cloud signature for the 14-15 December 1987 explosive cyclogenesis event. Phasing of the upper and lower tropospheric features result in a cloud shield typical of a mature mid-latitude cyclone. Cloud element "A" is associated with deformation zone cirrus, "B" and "B'" are baroclinic zone cirrus, "C" and "C'" are the mid-level vorticity comma cloud element, and "D" is convective activity. Thick arrows are the upper tropospheric jet axis, thin arrows represent upper level streamlines, and the broad hatched arrow depicts the low-level jet.

zone cirrus shield (area "A") has sharpened as it rotates cyclonically towards the circulation center. The progression of the jet begins to produce an indentation and an inflection point along the back edge of the cloud shield. The inflection point is where the surface cyclone is found. The comma cloud has grown (area "C") and is beginning to appear from under the higher cirrus. Convection, area "D", is found along the western edge of the baroclinic cirrus shield south of the jet resulting in the formation of a low-level jet.

During the final phase of development the two cloud features merge. The two jet streaks merge as the trough continues to become more negatively tilted. An expansive cirrus shield forms as the baroclinic and deformation zone cirrus merge. The deformation cirrus, area "A", has wrapped around the circulation center. The vortex comma cloud (area "C") is fully exposed as the cirrus shield races out ahead of the slower moving mid-level cloud. Some limited convection (area "D") is found at the rear edge of the comma cloud, while more vigorous convection is found south of the jet axis. A well developed low-level jet extends along the cold front towards the cyclone center.

#### **4.2 Water-Vapor Imagery Interpretation**

Water-vapor imagery from the  $6.7\ \mu\text{m}$  channel on the Temperature-Humidity Infrared Radiometer (THIR) aboard the GOES satellite is a very useful product for understanding upper atmospheric processes. Rodgers *et al.* (1976) describes the use of the THIR as a tool to measure mid and upper atmospheric water-vapor content, generally between 500 and 300 mb. A number of processes may be inferred such as dynamical processes, moisture advection, and vertical motion patterns associated with synoptic scale systems. The precise altitudes of water vapor signals in the  $6.7\ \mu\text{m}$  imagery can be somewhat ambiguous since the amount of infrared radiation received by the satellite is a function of both temperature and water-vapor content. Where very dry regions are observed, the maximum radiance for the  $6.7\ \mu\text{m}$  channel shifts downward from 300-500 mb to a level closer to 700 mb. Thus, regions of strong dry intrusions represent pronounced dry conditions in the lower troposphere (Petersen *et al.*, 1984).

The concepts used in interpreting infrared-satellite imagery can be applied to water vapor imagery. The advantage to water-vapor imagery is that water vapor is present where clouds may not be located. Locating the position of the jet-stream axis is aided by viewing such imagery. The jet-stream axis is often found along the border separating moist from

dry air. This relationship is dependent on the origin and evolution of the dry region. Weldon (1985) has observed water-vapor boundaries associated with the jet axis to have only a narrow dry zone poleward of the water-vapor boundary. Well defined jets on the back side of a deepening trough tend not to have a discernible water vapor signature. In situations in which two jets are adjacent to one another, the equatorward jet is likely to have a strong water-vapor boundary.

Figure 4.9 shows the  $6.7\ \mu\text{m}$  water-vapor imagery for (a) 2201 UTC 14 December and (b) 1001 UTC 15 December. In the early stages of development (Fig. 4.9a) two distinct dry slots are observed in association with the polar and subtropical jets, respectively. The polar jet is associated with the dry slot denoted as "A" and the subtropical jet is associated with dry slot "B". Consistent with Weldon's observation, the extension of the polar jet on the back side of the trough does not have a sharp moisture

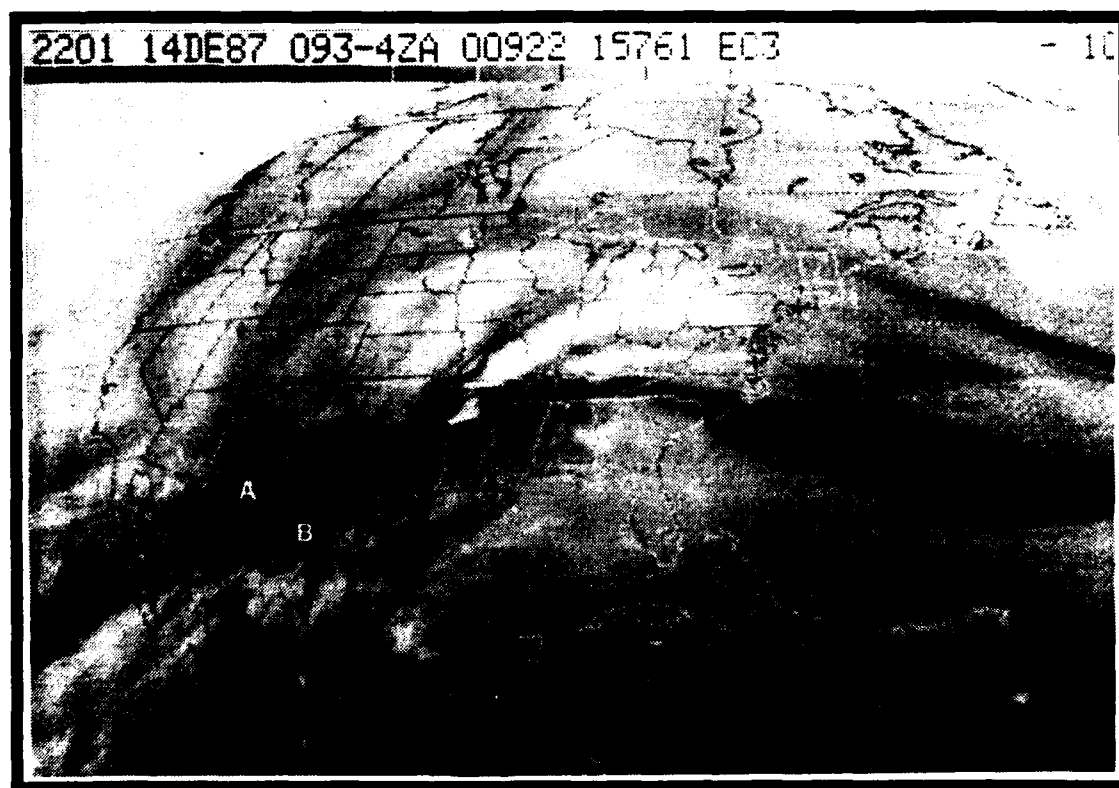


Figure 4.9a. GOES-East  $6.7\ \mu\text{m}$  water vapor satellite imagery for 2201 UTC 14 December 1987. Lettered areas are referenced in the text.

discontinuity, where as the southern jet does have a sharp distinctive moisture boundary. The surface cyclone that is beginning to develop at this time is located at point "C". The upper-level vortex moving out of the southern Rockies is apparent in the moisture channel as a bright white region of moisture over the central Plains. The dry intrusion evident from Texas into Tennessee provide the conditions necessary to fuel convective development.

During the cyclone's most rapid phase of development (Fig. 4.9b) the water-vapor imagery shows the polar jet's dry intrusion,"A", and the subtropical jet dry intrusion extending up from Alabama,"B", merging over western Tennessee. The two dry slots have combined into an expansive region of dry air throughout the Mississippi Valley. Inspection of Skew-T data and horizontal constant pressure charts indicate a significant layer of dry air extending down to the 700 mb level. During the expansion of the region of dry air, the surface cyclone located at "C", undergoes rapid deepening. A broad band of moisture from the Gulf of Mexico spirals in towards the cyclone center.



Figure 4.9b. GOES-East 6.7  $\mu\text{m}$  water vapor satellite imagery for 10:00 UTC 15 December 1987. Lettered areas are referenced in the text.

## CHAPTER 5

### STORM STRUCTURE

#### 5.1 Conventional Vertical Cross Section Display

To supplement the horizontal depiction of the cyclone development, vertical cross sections were constructed in the vicinity of the cyclone center for 0000 and 1200 UTC 15 December 1987. The use of vertical cross sections provide a valuable third dimension in viewing the atmospheric structure associated with the developing cyclone. Figure 5.1 shows the orientation of the axes of the cross sections and the rawinsonde stations used. The analysis was constructed by using a combination of NWS synoptic radiosonde data, with vertical wind measurements at one minute intervals, and constant pressure charts to interpolate data between stations along the cross section axes. An east/west orientation through the cyclone center was chosen in order to capture the surface development in relation to the approaching mid-tropospheric disturbance.

Potential temperature provides a convenient means of analyzing the thermal structure of the atmosphere. Identification of stable layers is an important means of resolving synoptic scale boundaries of discontinuity. Such stable layers are found in areas

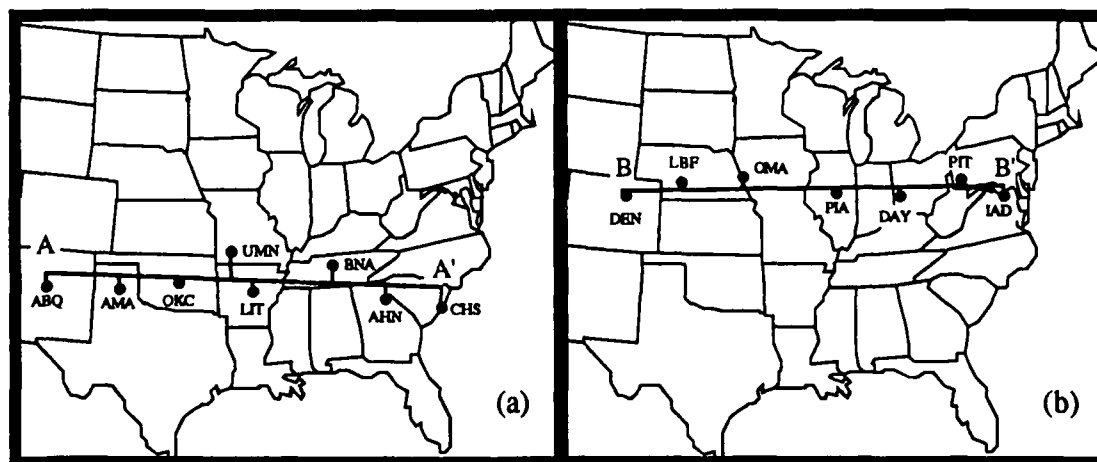


Figure 5.1. Orientation of cross section axis for (a) 0000 UTC and (b) 1200 UTC 15 December 1987.

were  $\delta\theta/\delta p$  is large. Consequently, stable layers associated with frontal zones and the stratosphere are indicated by an increased packing of potential temperature. Consistent with the work of earlier researchers (Saucier, 1955), it will be inferred in this section that the stable layers maintain both a spatial and temporal integrity.

The observed structure of the atmosphere will depend upon the orientation of the axis of the cross section in relation to the upper-level jet stream. Figure 5.2 provides a depiction of the structure of the atmosphere dependent upon the orientation of the cross section axis. Figure 5.2a provides a view of the upper-level jet pattern in the X-Y plane. Figures 5.2b-d provides the vertical structure that corresponds to the referenced axis orientation for each cross section. The cross section for 0000 UTC 15 December 1987 (Fig. 5.3) is orientated similarly to that depicted in Figure 5.2d. This orientation cuts across the upper-level trough and captures the relationship between the surface cyclone and the approaching upper-air vortex.

An analysis of the potential temperature field for 0000 UTC (Figure 5.3), reveals the strong stable layer associated with the frontal boundary. The frontal zone associated with the cold front slopes from Little Rock, Arkansas westward to the dome of cold air over Amarillo, Texas. Vertically, the temperature gradient of the frontal zone is  $13^{\circ}\text{C } 0.5 \text{ km}^{-1}$  over Little Rock and becomes less stable over Oklahoma City, Oklahoma where the gradient weakens to  $2.5^{\circ}\text{C } \text{km}^{-1}$ . Once over Amarillo, the stable layer splits into three separate layers. A squall line is observed along the sharp slope of the frontal surface near Little Rock at this time, consistent with the lower static stability seen in the cross section in the warm sector to the east. Further eastward, a stable layer associated with a cold dome of air over the Appalachian Mountains is intersected by the cross section. Cold air damming over the coastal plane is suppressing the advancement of the surface warm front over the south east (Fig. 3.7d).

The analysis of the tropopause was constructed using reported levels by the NWS. Over the Midwest, the tropopause descends to 335 mb in association with the upper-level trough. East of Little Rock, a significant increase in the height of the tropopause is seen. Tropopause levels range from 115 mb at Nashville, Tennessee to 106 mb reported at Charleston, South Carolina. The higher tropopause is indicative of the amplifying ridge building ahead of the advancing trough.

In the upper troposphere a double jet structure is evident at this time. A polar jet at 275 mb with maximum winds  $> 75 \text{ m s}^{-1}$  is observed over Oklahoma City. This feature is associated with the mid-tropospheric vortex. To the left of this jet core, the transition from heavy solid to dashed lines depicts formation of an upper-level front. As the slope of this front becomes vertical over Oklahoma City the horizontal temperature gradients weaken and the front is more clearly defined by the strong cyclonic shear observed between 200 and

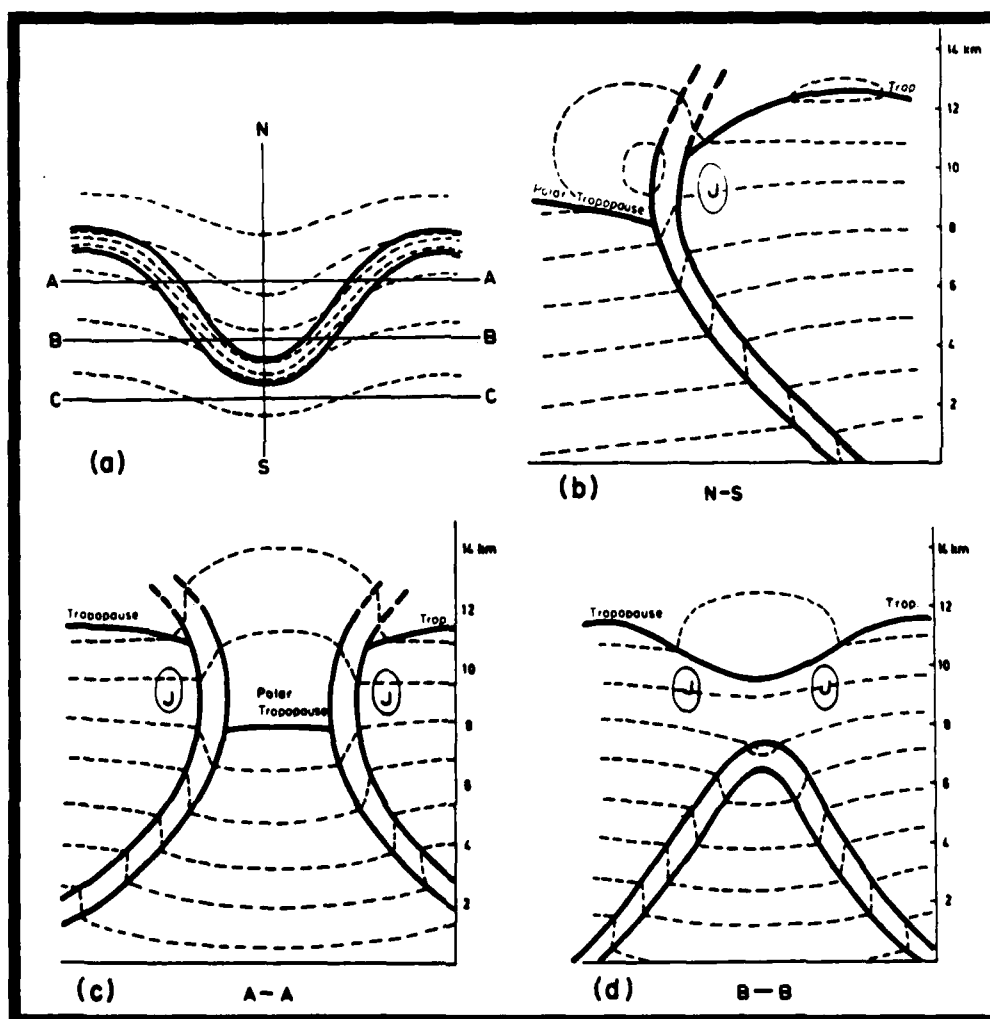


Figure 5.2. (a) Middle-tropospheric jet pattern in the X-Y plane. Isotherms are dashed lines. Thick solid lines are boundaries of jet axis. Thin solid lines are cross section axis. (b) fronts and tropopause (thick solid lines), isotherms (dashed lines), jet core (denoted by "J") in vertical cross section along axis N-S; (c) along axis A-A; (d) along axis B-B (Palmen and Newton, 1969).

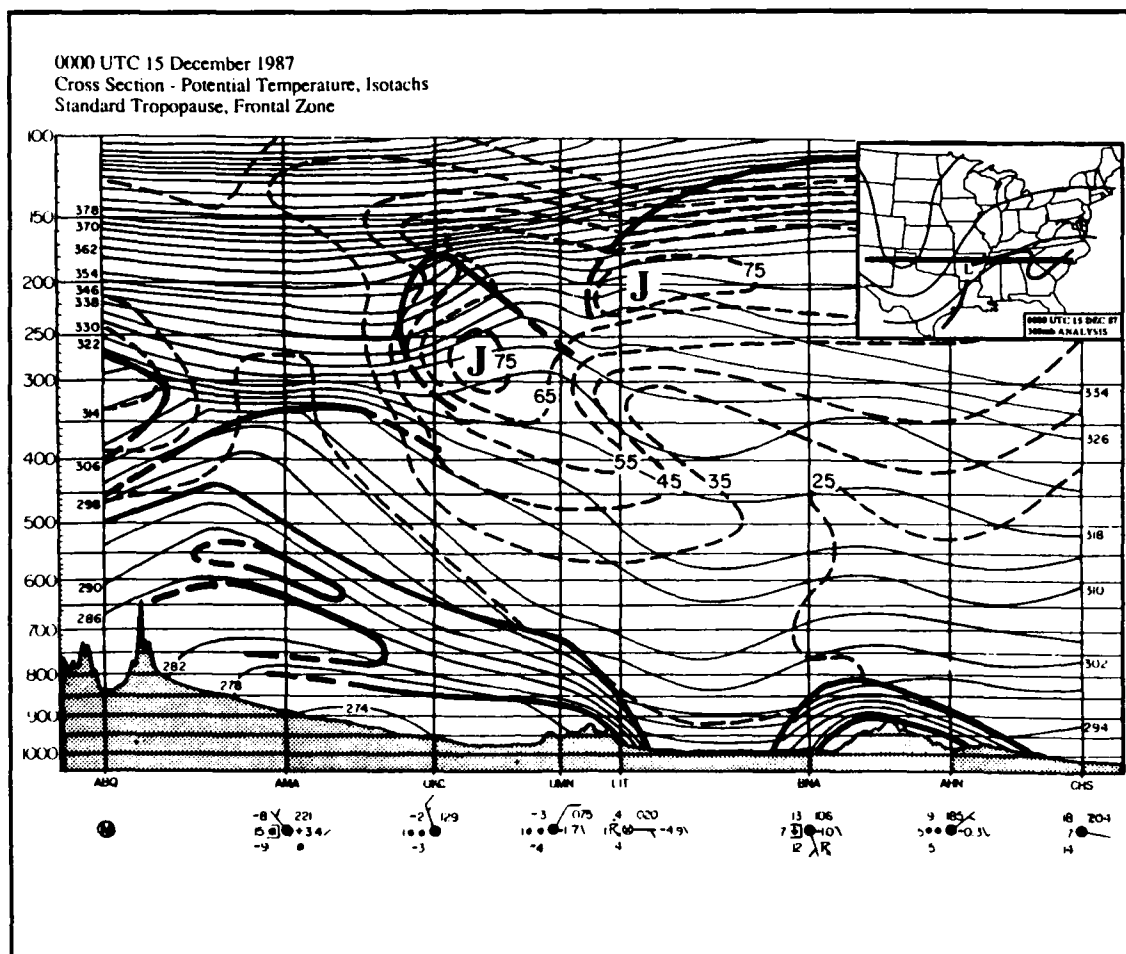


Figure 5.3. East-west vertical cross section at 0000 UTC 15 December 1987. Stations along the cross section are Albuquerque, New Mexico (ABQ), Amarillo, Texas (AMA), Oklahoma City, Oklahoma (OKC), Monett, Missouri (UMN), Little Rock, Arkansas (LIT), Nashville, Tennessee (BNA), Athens, Georgia (AHN), and Charleston, South Carolina (CHS). Vertical pressure axis is in millibars. Thin solid lines depict potential temperature at intervals of  $4^{\circ}\text{K}$ . Thick solid lines represent frontal zone in the lower troposphere and the tropopause in the upper troposphere. Dashed lines depict isotachs for the total wind speed at intervals of  $10\text{ m s}^{-1}$ . Jet core denoted by "J". Stippled area depicts ground. Reported surface observation displayed beneath station three letter identifier. Temperature is in  $^{\circ}\text{C}$ , winds are in  $\text{m s}^{-1}$ , and visibility is in statute miles. Map insert shows orientation of cross section axis (thick line) in relation to the 300 mb pattern (thin lines) and the surface frontal position.



300 mb (Palmen and Newton, 1969). A second jet, with a maximum wind speed  $>75 \text{ m s}^{-1}$ , is located over Little Rock at the 200 mb level. This jet has been identified as the subtropical jet as discussed in Chapter 3. Only weak shear is associated with this front.

By 1200 UTC the storm system has completed its most rapid phase of deepening. Figure 5.4 depicts the cross section B to B' in Figure 5.1b. The cross section intersects the surface cyclone and passes near the exit region of the upper-level jet streak. The vertical structure is similar to that displayed in Figure 5.2b. The merging of the sloping frontal boundary with the descending tropopause is similar to the classic "water spout model" developed by Danielsen (Reed and Danielsen, 1959). Throughout the frontal zone strong cyclonic shear is evident. The merging of the polar and subtropical jets have resulted in a single upper-level jet core located at 250 mb with a speed  $>75 \text{ m s}^{-1}$ . The organization of the jet structure results in increased horizontal shear within the frontal zone. A low-level jet has formed and ascends from the 750 mb level over the Gulf and intersects the plane of the cross section at  $\approx 575 \text{ mb}$ . A single broad stable layer is analyzed extending over Peoria towards Omaha indicative of the strong surface ridge over the central United States.

## 5.2 Stratospheric Influences

### 5.2.1 Role of Stratospheric Intrusion In Cyclogenesis

Work conducted by Reed and Sanders (1953), Newton (1954), and Reed and Danielsen (1959), on the concept of "tropopause folding" brought about an increased appreciation on the importance of subsidence in the upper and mid troposphere as a mechanism for upper-level frontogenesis. Further work by Danielsen (1968), Bosart (1970), Shapiro (1976), and Uccellini (1985), discuss the importance of tropopause folding in the exchange of air between the stratosphere and the troposphere. Research has shown that stratospheric air can be advected along isentropic surfaces down into the lower troposphere. The tropopause folding process as defined by Reed (1955) is considered to be the mechanism that transports stratospheric air to the mid and lower troposphere along the axis of the jet stream. The cross-stream circulation associated with the ageostrophic motion produces a horizontal convergence and vertical divergence resulting in subsidence poleward of the jet core. This results in the formation of the upper front and the descent of stratospheric air to lower levels (Fig. 5.5). Cyclogenesis has been documented to occur

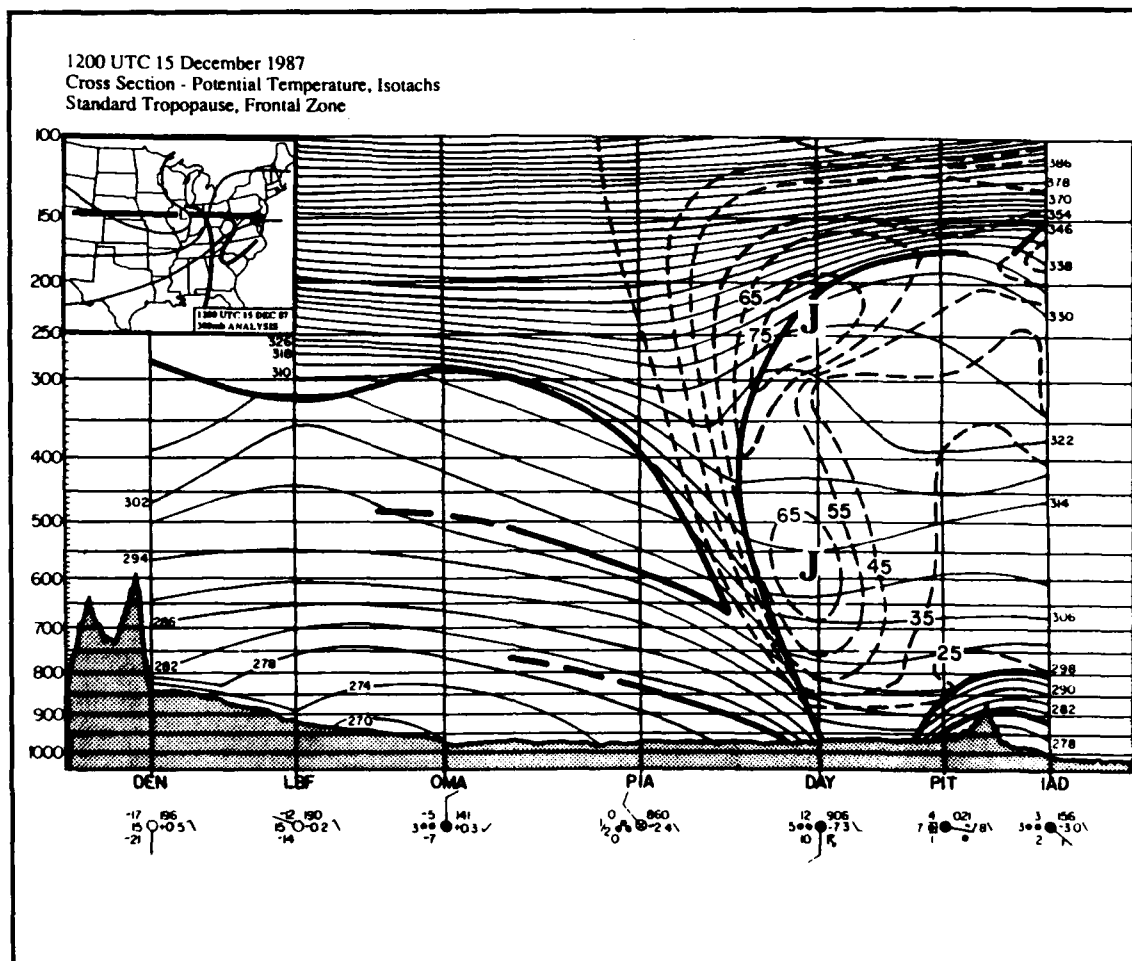


Figure 5.4. East-west vertical cross section at 1200 UTC 15 December 1987. Stations along the cross section are Denver, Colorado (DEN), North Platte, Nebraska (LBF), Omaha, Nebraska (OMA), Peoria, Illinois (PIA), Dayton, Ohio (DAY), Pittsburgh, Pennsylvania (PIT), and Washington D.C. (IAD). Vertical pressure axis is in millibars. Thin solid lines depict potential temperature at intervals of  $4^{\circ}\text{K}$ . Thick solid lines represent frontal zone in the lower troposphere and the tropopause in the upper troposphere. Dashed lines depict isotachs for the total wind speed at intervals of  $10\text{ m s}^{-1}$ . Jet core denoted by "J". Stippled area depicts ground. Reported surface observation displayed beneath station three letter identifier. Temperature is in  $^{\circ}\text{C}$ , winds are in  $\text{m s}^{-1}$ , and visibility is in statute miles. Map insert shows orientation of cross section axis (thick line) in relation to the 300 mb pattern (thin lines) and the surface frontal position.

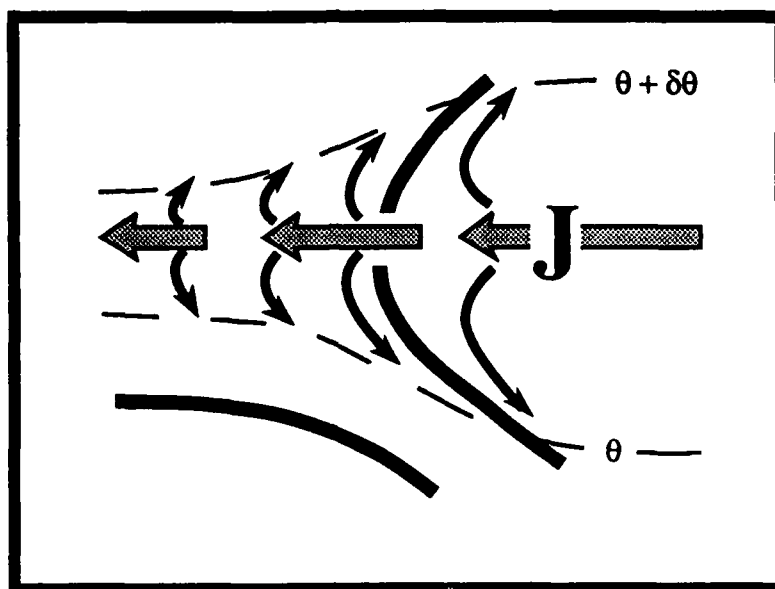


Figure 5.5. Schematic illustration of cross-stream circulation near upper-level jet axis resulting in upper level frontogenesis and stratospheric intrusion. Thick solid line is tropopause. The jet axis is directed into the paper at "J", dashed lines depict potential temperature, thin arrows represent the vertical divergence in association with the ageostrophic flow depicted by the large arrows (Palmen and Newton, 1968).

simultaneously with the development of the tropopause fold (Reed, 1955). Others have related the the upper-level frontogenesis and tropopause folding associated with the jet streak prior to the subsequent development of the surface cyclone (Uccellini, 1985). The intrusion of stratospheric air into the troposphere is characterized by high values of potential vorticity, ozone concentration, and radioactive material, all of which act as tracers in observing the atmospheric dynamics (Danielsen, 1968).

### 5.2.2 Conservation of Potential Vorticity

Kleinschmidt (1950, 1955) was the first to emphasize that the advection of a stratospheric reservoir of high potential vorticity associated with a lowering tropopause is important to cyclone development. In order to show the relationship between the stratospheric intrusion and cyclogenesis for the case described in this thesis, the principal of conservation of potential vorticity will be employed.

The historical development and use of potential vorticity is well documented by Hoskins *et al.* (1985). Rossby (1939) was the first to recognize that the vertical component of absolute vorticity is most important in describing the synoptic scale flow. He further concluded that the conservation of potential vorticity can be described simply by the ratio of the absolute vorticity to the depth of the fluid column in a barotropic model. This relation is comprised of the advection of absolute vorticity and the creation / destruction of vorticity through the vertical stretching / compression of vortex tubes. These two processes dominate the vorticity budget (Rossby, 1940).

The atmospheric response to cyclonic and anticyclonic potential vorticity anomalies introduced to an isentropic field are depicted in Figure 5.6. The introduction of a positive potential vorticity anomaly results in a contraction of isentropic surfaces towards the anomaly, producing increasingly unstable layers above and below. Anticyclonic anomalies result in diverging isentropes in the region of the anomaly, producing an area of increased stability above and below (Hoskins, 1988).

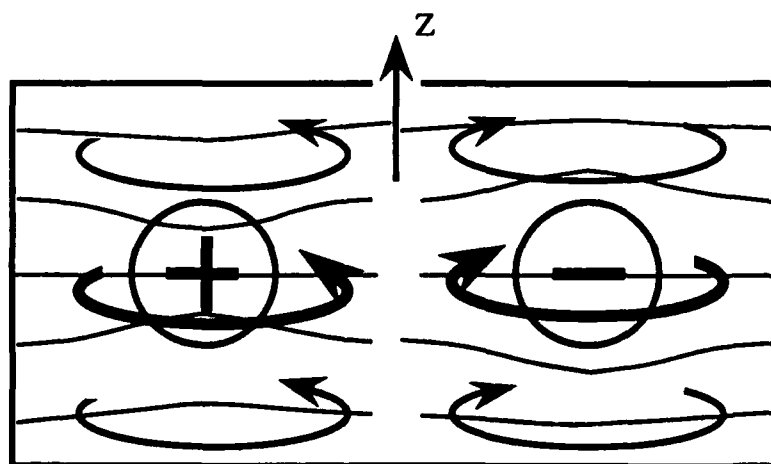


Figure 5.6. The atmospheric response to cyclonic (left) and anticyclonic (right) potential vorticity anomalies embedded in the flow. Cyclonic potential vorticity results in the convergence of the isentropes resulting in weaker static stability above and below the parcel. Anticyclonic potential vorticity produces a greater stable region above and below the parcel. Thin lines represent isentropes. Arrows depict circulation throughout the region of positive/negative potential vorticity (Hoskins, 1988).

The principle of the conservation of potential vorticity along an isentropic surfaces allows the adiabatic transport of stratospheric air to be tracked. Conservation of potential vorticity in isentropic coordinates can be expressed:

$$\text{CONSTANT} = (\zeta_{\theta} + f) (-\partial\theta/\partial p) \quad (5.2.1)$$

where  $\zeta_{\theta}$  is the absolute vorticity calculated on an isentropic surface,  $f$  is the coriolis parameter,  $\theta$  is the potential temperature, and  $p$  denotes pressure (Holton, 1979). As stratospheric air protrudes into the troposphere, vortex tube stretching occurs producing an increased cyclonic vorticity tendency due to the decrease in static stability (Fig. 5.7).

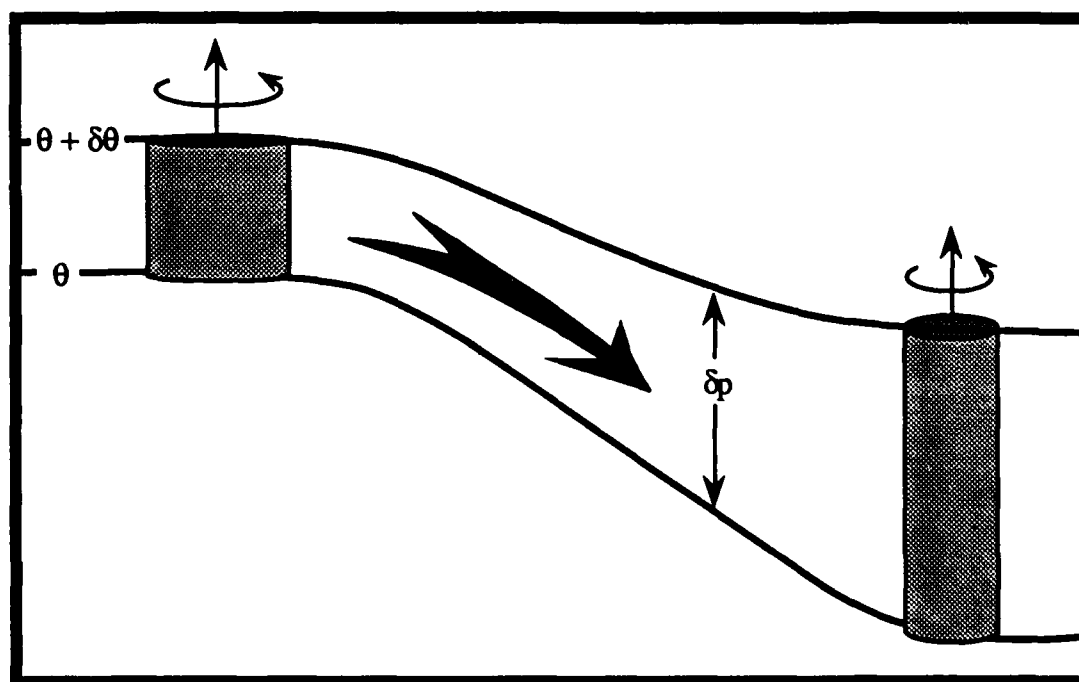


Figure 5.7. Parcel of air (cylinder) acquires more cyclonic vorticity (thin circular arrows) as it moves (thick arrow) into a region of lower static stability as a result of vortex tube stretching. The isentropic surfaces (thin solid lines) diverge producing a vertical expansion of the air parcel. The principle of the conservation of potential vorticity requires the generation of cyclonic vorticity. (Holton, 1979)

Hoskins (1988) points out that the principal of the conservation of potential vorticity is a reasonable assumption over a period of a few days except in regions where appreciable condensation is occurring. Here, the release of latent heat is sufficient to effect the stability of the surrounding atmosphere resulting in a change in potential vorticity.

To gain an appreciation for the numerical distribution of potential vorticity Hoskins *et al.* (1985) made calculations, using a modified form of equation 5.2.1, based on an idealized-standard atmosphere for a fictitious atmosphere at rest. Consequently, the relative vorticity is set to zero. Figure 5.8 displays the results of the calculations of potential vorticity profiles for 15°N, 45°N, and 75°N.

The tropospheric variation in potential vorticity values are associated latitudinally with  $f$  and vertically with density. Tropospheric air parcels are associated with values  $<1.5 \times 10^{-6} \text{ m}^2 \text{ s}^{-1} \text{ } ^\circ\text{K kg}^{-1}$ . At the tropopause the values jump to stratospheric values  $>1.5 \times 10^{-6} \text{ m}^2 \text{ s}^{-1} \text{ } ^\circ\text{K kg}^{-1}$ . The crosses represent points on the 350° K isentropic surface. Though varying little with height, the 350° K surface is associated with stratospheric air in the middle and high latitudes and tropospheric air in the lower latitudes. The 330°K surface

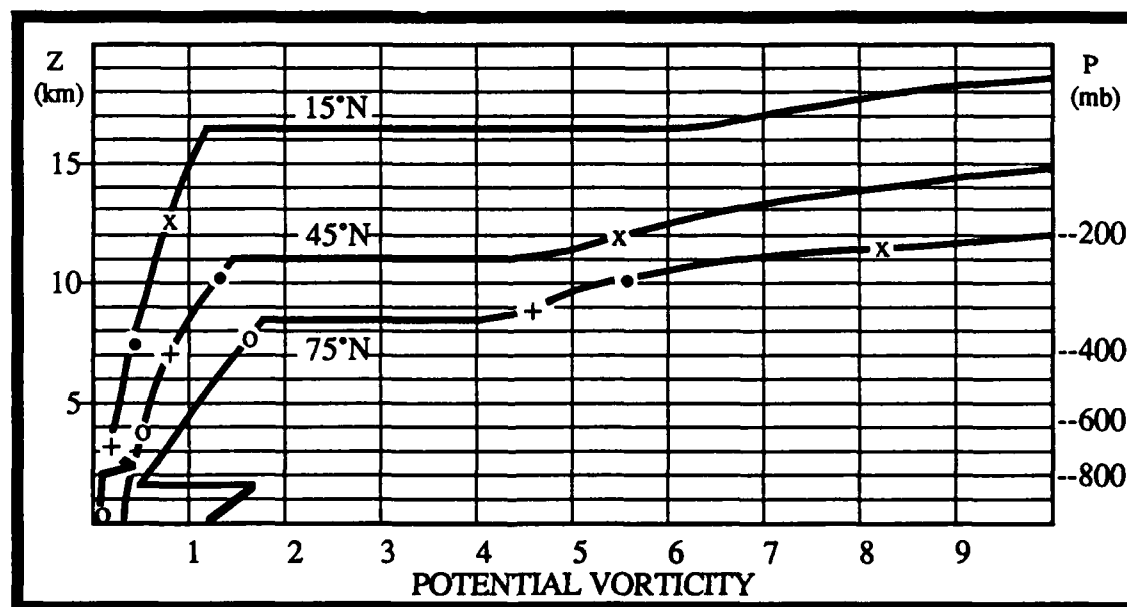


Figure 5.8. The potential vorticity associated with standard temperature profiles and zero relative vorticity. The profiles are the U.S. Standard Atmosphere 15°N annual, mid-latitude spring/autumn (labeled 45°N) and 75°N January (cold). The units of the abscissa is  $10^{-6} \text{ m}^2 \text{ s}^{-1} \text{ } ^\circ\text{K kg}^{-1}$ . The position of various isentropic surfaces are indicated by x (350° K), • (330° K), + (315° K), and o (300° K). (From Hoskins, 1985).

surface (dots) and the 315° K (pluses) also are associated with both troposphere and the stratosphere. The 300° K surface remains in the troposphere throughout.

Work by Reed and Danielsen (1959) and Shapiro (1976) describe the transition zone between stratospheric and tropospheric air to be associated with potential vorticity values  $>10 \times 10^{-6} \text{ }^\circ\text{K mb}^{-1} \text{ s}^{-1}$ . Such values are consistent with observations made by Bosart *et al.* (1984), Uccellini *et al.* (1985), and Young *et al.* (1987), and Hoskins *et al.*, (1988).

### 5.2.3 Eulerian Perspective of Potential Vorticity

The transport of potential vorticity rich air from one pressure level to another during the explosive development of the storm system is investigated from a Eulerian perspective. Figure 5.9 displays the potential vorticity, absolute vorticity, and static stability for the 325° K surface for 0000 and 1200 UTC 15 December 1987. The isentropic surface closest to the level of the polar jet core (325° K in Figs 5.3 and 5.4) was chosen to analyze changes in the potential vorticity field associated with the evolution of the jet.

Figure 5.9a shows a reservoir of high potential vorticity ( $>75 \times 10^{-6} \text{ }^\circ\text{K mb}^{-1} \text{ s}^{-1}$ ) over the northern Plains at 0000 UTC. A lobe of high potential vorticity extends southward into the Texas panhandle. This area is vertically aligned with the long-wave trough position and extends from the 250 mb level in South Dakota to 350 mb in Texas. The transition zone between stratospheric to tropospheric air has been shown to be associated with potential vorticity values  $>10 \times 10^{-6} \text{ }^\circ\text{K mb}^{-1} \text{ s}^{-1}$  (Reed and Danielsen, 1959; Shapiro, 1976). The developing surface cyclone is located near Little Rock, Arkansas with a tropospheric value of potential vorticity  $<10 \times 10^{-6} \text{ }^\circ\text{K mb}^{-1} \text{ s}^{-1}$ . The 15 to  $30 \times 10^{-6} \text{ }^\circ\text{K mb}^{-1} \text{ s}^{-1}$  potential vorticity isopleth is located along the axis of the polar jet (Fig 3.7b) and is associated with the tropopause fold (Reed, 1955). Data in this region show winds of  $65 \text{ m s}^{-1}$  in the vicinity of Oklahoma with the jet axis extending up towards the Great Lakes. The wind observations over Texas indicate the presence of a sharp trough and a significant jet resulting in high values of absolute vorticity (Fig. 5.9b). The associated stability parameter is illustrated in Figure 5.9c. The strong static stability associated with the stratosphere is evident in the northern Plains. Over Texas the stability reduces to  $10 \times 10^{-2} \text{ }^\circ\text{K mb}^{-1}$  near the 350 mb level. Thus, the potential vorticity pattern observed in Figure 5.9a is primarily the result of cyclonic absolute vorticity to the south and large static stability to the north.

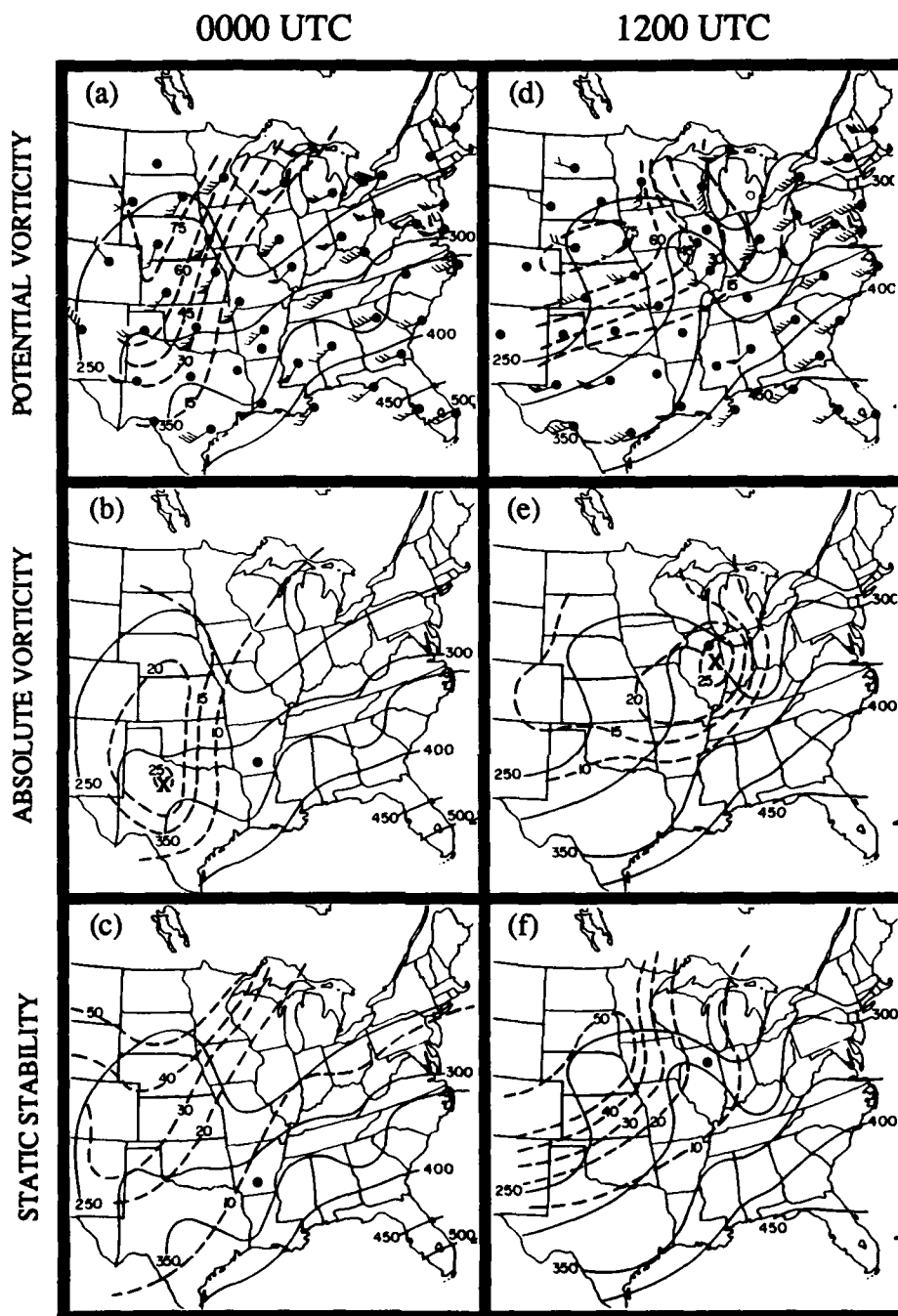


Figure 5.9. 325° K isentropic surface for 0000 UTC (a-c) and 1200 UTC 15 December 1987 (d-f). In all figures solid lines are isobars (mb) and the position of the surface cyclone is depicted by a dot. In "a" and "d" dashed lines depict potential vorticity ( $\times 10^{-6} \text{ } ^\circ\text{K mb}^{-1} \text{ s}^{-1}$ ) and winds are plotted in  $\text{m s}^{-1}$ . In "b" and "e" dashed lines are isopleths of absolute vorticity ( $\times 10^{-5} \text{ s}^{-1}$ ). A maxima of absolute vorticity is denoted by "X". In "c" and "f" dashed lines depicts static stability ( $\times 10^{-2} \text{ } ^\circ\text{K mb}^{-1}$ ).



By 1200 UTC the cyclone has fully developed and is situated over north-central Illinois. The upper-level jet has fully rotated about the base of the trough resulting in an east-west orientated trough line. Figure 5.9d displays the 325° K isentropic surface with a potential vorticity overlay. The reservoir of potential vorticity  $>75 \times 10^{-6} \text{ } ^\circ\text{K mb}^{-1} \text{ s}^{-1}$  has maintained the same magnitude and is now situated over Nebraska with a potential vorticity lobe extending eastward towards Indiana. This orientation is aligned similar to that of the upper trough. The position of the potential vorticity reservoir continues to be strongly tied to the 250 mb level. The  $15 \times 10^{-6} \text{ } ^\circ\text{K mb}^{-1} \text{ s}^{-1}$  potential vorticity isopleth still shows a strong relationship to the polar-jet axis and the tropopause fold. The surface cyclone is now associated with a potential vorticity value between  $30$  and  $45 \times 10^{-6} \text{ } ^\circ\text{K mb}^{-1} \text{ s}^{-1}$ . The increase in potential vorticity over the cyclone center is indicative of the lowering tropopause and stratospheric influence on cyclone development.

The absolute cyclonic vorticity maximum earlier located over Texas is now situated over Illinois (Fig. 5.9e). The vorticity maximum has not changed in magnitude as a sharp east-west trough, with an intensifying jet, is observed in the wind field plotted in Figure 5.9d. The surface cyclone, previously associated with an absolute vorticity value  $<10 \times 10^{-5} \text{ s}^{-1}$  (Fig. 5.9b), is now associated with a cyclonic vorticity value  $>25 \times 10^{-5} \text{ s}^{-1}$  (Fig. 5.9e). The static stability maintains the same magnitude but the gradient has increased significantly from northern Texas northward into Iowa (Fig. 5.9f). The increased static stability gradient is effective in vortex tube stretching. This results in increased cyclonic vorticity, as described in Figure 5.7, aiding in the spinup of the cyclone.

The 305° K isentropic surface was prepared to describe the lower tropospheric view of the potential vorticity pattern (Fig. 5.10). A strong pressure gradient is observed running north-south through the Midwest at 0000 UTC (Fig. 5.10a). Here, the flow nearly parallels the pressure gradient indicative of little vertical motion due to adiabatic lift (Saucier, 1955). Potential vorticity values  $>30 \times 10^{-6} \text{ } ^\circ\text{K mb}^{-1} \text{ s}^{-1}$  is found over the southern Rockies. The potential vorticity maxima is located near the 400 mb level in western New Mexico (not shown). In west central Texas a westerly flow at  $40 \text{ m s}^{-1}$  advects the higher values of potential vorticity into the central Plains. The strong cyclonic shear evident in the wind field (Fig. 5.10a) results in an absolute vorticity maxima of  $20 \times 10^{-5} \text{ s}^{-1}$  over northern Texas near the 375 mb level (Fig. 5.10b). The stability distribution is generally weaker in the lower troposphere than that observed on the 325° K surface (Fig. 5.10c). A static

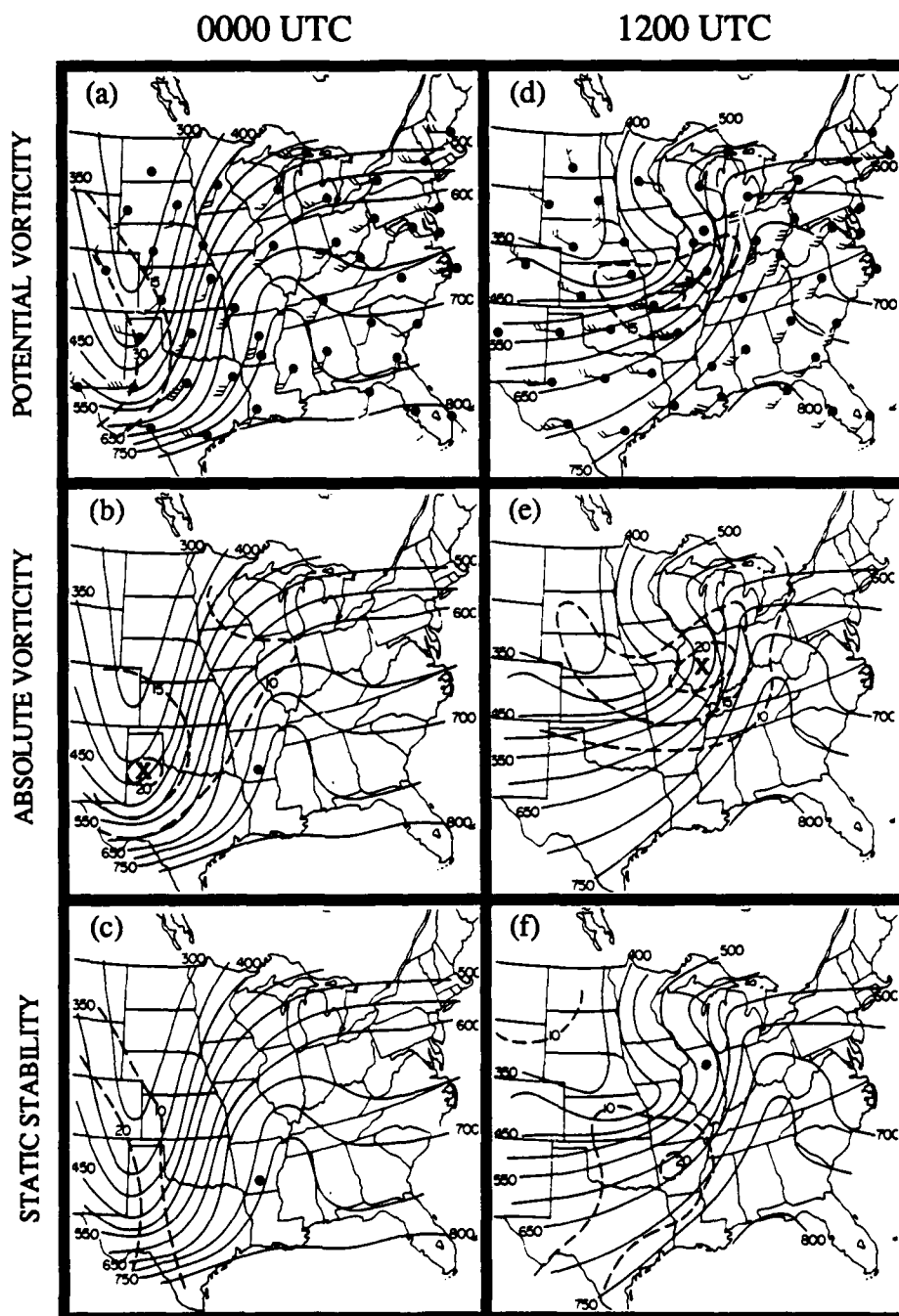


Figure 5.10. 305° K isentropic surface for 0000 UTC (a-c) and 1200 UTC 15 December 1987 (d-f). In all figures solid lines are isobars (mb) and the position of the surface cyclone is depicted by a dot. In "a" and "d" dashed lines depict potential vorticity ( $\times 10^{-6}$   $^{\circ}\text{K mb}^{-1} \text{ s}^{-1}$ ) and winds are plotted in  $\text{m s}^{-1}$ . In "b" and "e" dashed lines are isopleths of absolute vorticity ( $\times 10^{-5} \text{ s}^{-1}$ ). A maxima of absolute vorticity is denoted by "X". In "c" and "f" dashed lines depicts static stability ( $\times 10^{-2}$   $^{\circ}\text{K mb}^{-1}$ ).

stability parameter of  $20 \times 10^{-2} \text{ }^\circ\text{K mb}^{-1}$  is observed over the southern Rockies in response to the building ridge.

By 1200 UTC the potential vorticity maxima has descended from 400 mb to 550 mb and is situated over southern Missouri (Fig. 5.10d). The region encompassed by the  $15 \times 10^{-6} \text{ }^\circ\text{K mb}^{-1} \text{ s}^{-1}$  isopleth corresponds to the dry signature noted on the water-vapor satellite imagery (Fig. 4.9b). The descent of the potential vorticity is indicative of the stratospheric intrusion during the rapid phase of explosive cyclogenesis. The modest cross isobaric flow in the Kansas/Arkansas region depicts the advection of stratospheric air to the lower troposphere aiding cyclone development. The magnitude of the potential vorticity maxima is slightly weaker at this time either due to diabatic influences or the result of the nonuniform placement of radiosonde stations in the area (Uccellini *et al.*, 1985). The absolute vorticity maxima has descended from 375 mb over Texas to the 525 mb level. At 0000 UTC the surface cyclone was associated with an absolute vorticity value  $< 10 \times 10^{-5} \text{ s}^{-1}$  near 750 mb. After undergoing explosive development, the cyclone is associated with an absolute vorticity value  $> 20 \times 10^{-5} \text{ s}^{-1}$  near 525 mb (Fig. 5.10e) and stratospheric values of potential vorticity  $> 15 \times 10^{-6} \text{ }^\circ\text{K mb}^{-1} \text{ s}^{-1}$  (Fig. 5.10d). The stability plot shows a static stability maxima moving from the southern Rockies into Arkansas (Fig. 5.10f). The transport of stratospheric values of potential vorticity to the lower troposphere results in the generation of cyclonic vorticity over the developing cyclone.

The advection of stratospheric values of potential vorticity along isentropic surfaces to the lower troposphere was observed during the process of cyclone development as described by Reed and Danielsen (1959), Shapiro (1976), and Hoskins *et al.*, (1988). The surface cyclone was initially associated with tropospheric values of potential vorticity less than  $10 \times 10^{-6} \text{ }^\circ\text{K mb}^{-1} \text{ s}^{-1}$  at the 325° K surface. The development of the cyclone is associated with enhanced upper-level frontogenesis and a descending tropopause to the lower troposphere. Over the cyclone center, the lowering tropopause results in a significant dry intrusion and stratospheric values of potential vorticity extending down to the 305° K surface. The descending tropopause resulted in the generation of cyclonic vorticity aiding resulting in the rapid spinup of the cyclone. The review of satellite imagery illustrates the expanding dry slot, associated with the stratospheric dry intrusion, coincides with the explosive phase of cyclone development from 0600-1200 UTC.

#### 5.2.4 Vertical Cross Section of Potential Vorticity Structure

The vertical cross section depicting the distribution of the potential vorticity structure of the atmosphere provides insight on the influence of the exchange of air between the stratosphere and the troposphere in cyclone development. Potential vorticity cross sections were constructed using the same axis as those depicted in Figure 5.1. Barnes analyzed fields of theta at  $5^{\circ}$  K intervals were computed. From these theta surfaces the absolute vorticity and static stability were computed to obtain potential vorticity. Wind data for the theta surfaces is obtained through a routine that interpolates the wind speed and direction from the nearest significant-level wind report to that theta surface. The static stability is computed by comparing the change in pressure at an interval of  $5^{\circ}$  K above and below the theta surface. The horizontal displays of potential vorticity were then transferred into the plane of the cross section.

Figure 5.11 depicts the cross section of potential vorticity for 0000 UTC 15 December 1987. The cross section is similar to that displayed in Figure 5.3 in that it shows the potential temperature structure of the atmosphere and the observed winds. Omitted are the stable layers associated with the frontal zone and the NWS reported tropopause levels while isopleths of potential vorticity are included.

As discussed earlier, the transition between the troposphere to the stratosphere occurs above potential vorticity values of  $10 \times 10^{-6} \text{ }^{\circ}\text{K mb}^{-1} \text{ s}^{-1}$ . The  $15 \times 10^{-6} \text{ }^{\circ}\text{K mb}^{-1} \text{ s}^{-1}$  potential vorticity isopleth is first analyzed to depict the "calculated" position of the tropopause. The use of potential vorticity provides a useful means of determining the position of the tropopause especially in areas in which the environmental lapse rate is inconclusive in its placement. The Oklahoma City, Oklahoma radiosonde reported the tropopause at 175 mb while stratospheric values of potential vorticity places it at 370 mb. Investigation of the Skew-T chart shows a change in the slope of the temperature curve above 370 mb and again above 175 mb. Below 370 mb the lapse rate averages  $-6.4^{\circ} \text{ C km}^{-1}$ , at which point it decreases to  $-2.8^{\circ} \text{ C km}^{-1}$  till 175 mb where it then becomes nearly isothermal. Consequently, the ridged definition of the tropopause, established by the World Meteorological Organization, is not always representative of the processes taking place. Similarly, the location of the tropopause for Nashville varies from a NWS position of 115 mb to the potential vorticity calculated position of 165 mb. The later position fits the overall pattern better with strong stability and vertical shear found above the tropopause.

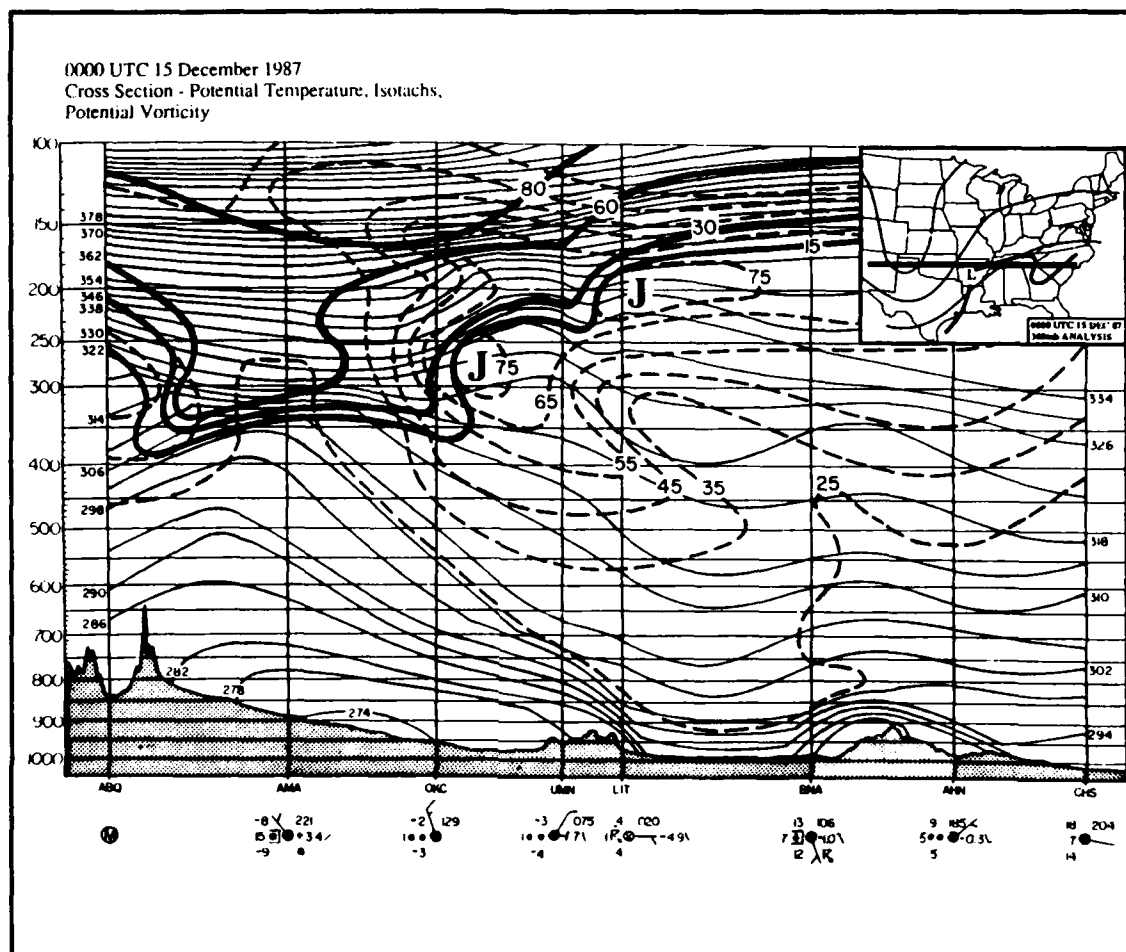


Figure 5.11 East-west vertical cross section at 0000 UTC 15 December 1987. Stations along the cross section are Albuquerque, New Mexico (ABQ), Amarillo, Texas (AMA), Oklahoma City, Oklahoma (OKC), Monett, Missouri (UMN), Little Rock, Arkansas (LIT), Nashville, Tennessee (BNA), Athens, Georgia (AHN), and Charleston, South Carolina (CHS). Vertical pressure axis is in millibars. Thin solid lines depict potential temperature at intervals of 4° K. Thick solid lines are isopleths of potential vorticity ( $^{\circ}\text{K mb}^{-1} \text{s}^{-1}$ ). Dashed lines depict isotachs for the total wind speed at intervals of 10  $\text{m s}^{-1}$ . Jet core denoted by "J". Stippled area depicts ground. Reported surface observation displayed beneath station three letter identifier. Temperature is in °C, winds are in  $\text{m s}^{-1}$ , and visibility is in statute miles. Map insert shows orientation of cross section axis (thick line) in relation to the 300 mb pattern (thin lines) and the surface frontal position.

The cross section provides a useful means of visualizing the irregularities of the stratosphere in relation to the cyclone development and the associated reservoirs of potential vorticity. The protrusion of stratospheric air into the troposphere, associated with the tropopause folding process, is easily visualized as lobes of high values of potential vorticity extend into the troposphere. The axis of the upper-level trough is situated over the panhandle of Texas resulting in a significantly lower tropopause than that observed east of Little Rock. The ageostrophic flow and vertical divergence associated with the jet core enhances the upper-level frontogenesis and descent of stratospheric air. The presence of two jet axis result in two separate protrusions over the southern Plains. Stratospheric air extends down to the 365 mb level in association with the polar jet and to the 240 mb level in response to the subtropical jet.

During the next twelve hours the cyclone's explosive development coincides with significant changes in the composition of the vertical structure of the atmosphere. Figure 5.12 depicts the cross section of potential vorticity for 1200 UTC.

The merging of the polar and subtropical jets and the vertically coupled lower level jet result in a significant single protrusion of stratospheric air down to the 700 mb level. The organization of the jet structure encourages the ageostrophic flow resulting in the significant descent of stratospheric air over the cyclone center, located just east of Peoria, Illinois. The advection of stratospheric values of potential vorticity down to the lower troposphere is responsible for the rapid spinup of the surface cyclone.

The location of the tropopause over Peoria differs significantly from the NWS placement and that calculated from potential vorticity, which place the tropopause at 375 mb. The NWS position is nearly 200 millibars higher at 183 mb. Investigation of the 1200 UTC Skew-T for Peoria displays the thermal structure of the atmosphere (Fig. 5.13). The lapse rate above 183 mb averages  $-1^{\circ} \text{ C km}^{-1}$ , between 375 mb and 183 mb it averages  $-2.5^{\circ} \text{ C km}^{-1}$ , and below 375 mb the lapse rate averages  $-6^{\circ} \text{ C km}^{-1}$ . The placement of the tropopause at the 183 mb level puts it well within stratospheric values of potential vorticity as discussed by Hoskins (1988). The positioning of the tropopause is difficult at best by simple inspection of the Skew-T plot. The aid of potential vorticity calculations provide an effective means of determining the more precise location of the tropopause.

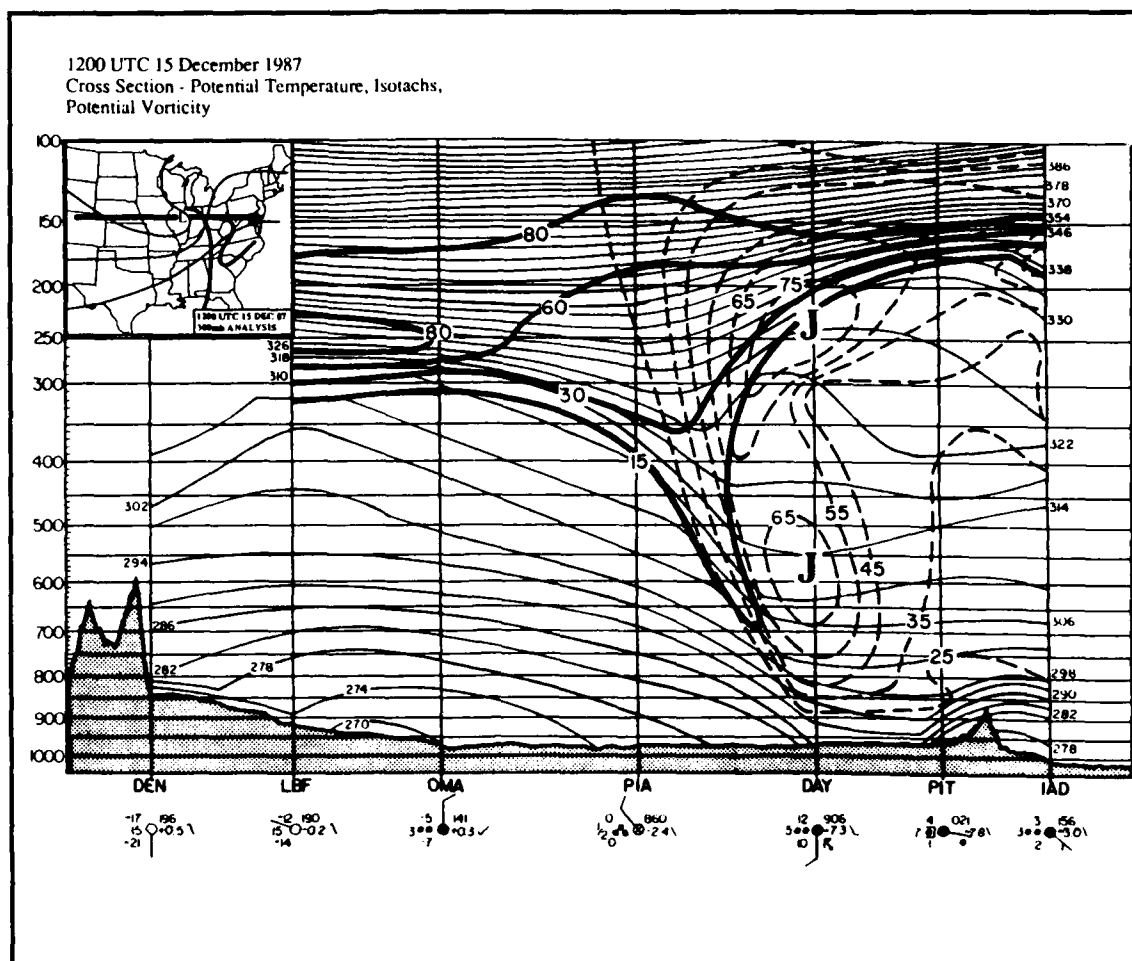
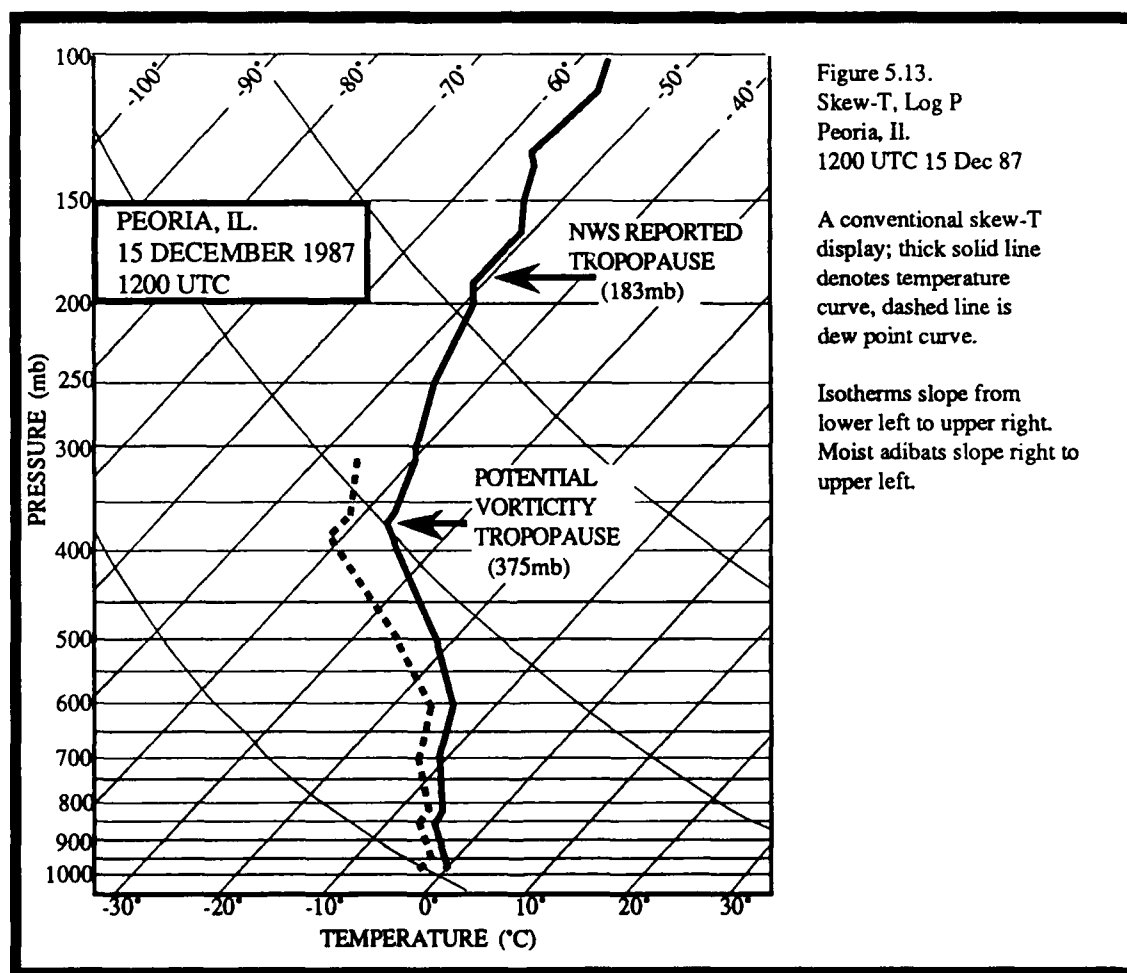


Figure 5.12. East-west vertical cross section at 1200 UTC 15 December 1987. Stations along the cross section are Denver, Colorado (DEN), North Platte, Nebraska (LBF), Omaha, Nebraska (OMA), Peoria, Illinois (PIA), Dayton, Ohio (DAY), Pittsburgh, Pennsylvania (PIT), and Washington D.C. (IAD). Vertical pressure axis is in millibars. Thin solid lines depict potential temperature at intervals of  $4^{\circ}$  K. Thick solid lines are isopleths of potential vorticity ( $^{\circ}\text{K mb}^{-1} \text{s}^{-1}$ ). Dashed lines depict isotachs for the total wind speed at intervals of  $10 \text{ m s}^{-1}$ . Jet core denoted by "J". Stippled area depicts ground. Reported surface observation displayed beneath station three letter identifier. Temperature is in  $^{\circ}\text{C}$ , winds are in  $\text{m s}^{-1}$ , and visibility is in statute miles. Map insert shows orientation of cross section axis (thick line) in relation to the 300 mb pattern (thin lines) and the surface frontal position.

The surface cyclone has just completed its most explosive phase of development. The vertical displacement of the tropopause, directly above the surface cyclone, has descended from 180 mb (at 0000 UTC) to the 450 mb level (at 1200 UTC). Nearly a 7 km descent in the tropopause was observed in this twelve hour period. The surface pressure rapidly decreases as the stable stratospheric air extends further into the troposphere occupying a greater mass in the vertical column above the surface cyclone.





### 5.3 Thermodynamic Omega

#### 5.3.1 Thermodynamic Calculations of Vertical Motion

The area of clouds and precipitation associated with the upper-air vortex has been associated with vertical motion driven by the advection of cyclonic vorticity by the thermal wind. The stratiform precipitation to the north and east of the developing cyclone is primarily the result of adiabatic lift. To determine the vertical motion distribution associated with this area the thermodynamic method is employed.

This method states that the vertical motion at a point on an isentropic surface is proportional to the wind speed relative to the motion of the isentropic surface multiplied by the isentropic pressure gradient in the direction of the relative wind vector (Durran and Snellman, 1987). On an isentropic surface, we can express the vertical motion along an isentropic surface as (Homan and Uccellini, 1987):

$$\omega_{\theta} = \left( \frac{dp}{dt} \right)_{\theta} = \frac{\partial p}{\partial t} \Big|_{\theta} + \mathbf{V} \cdot \nabla_{\theta} p + \dot{\theta} \frac{\partial p}{\partial \theta} \quad \text{where } \dot{\theta} = \frac{d\theta}{dt} \quad \{5.3.1\}$$

where  $\omega_{\theta}$  is the vertical motion calculated on an isentropic surface,  $\theta$  is potential temperature,  $p$  is pressure,  $t$  is the time element, and  $\mathbf{V}$  is the wind vector. The drawback in using this method is that specifying the relative motion of an isentropic surface requires temporal resolution not usually available in sounding data. As discussed by Uccellini (1976), the offsetting nature between the local pressure tendency and the diabatic term in equation 5.3.1 has led Saucier (1955) to note that the pressure advection term provides a good approximation of the vertical motion. This is considered to be a tolerable approximation even in areas of extensive cloud and precipitation. Consequently, the vertical motion associated with adiabatic lift can be calculated using the relationship:

$$\omega_{\theta} \approx \mathbf{V} \cdot \nabla_{\theta} p \quad \{5.3.2\}$$

The thermodynamic omega calculations were made using the Barnes objective analysis scheme. Calculations were made for the 300° K and 325° K surface at 0000 UTC 15 December (Fig. 5.14). The 300° K surface was chosen to depict the lift of air parcels near the surface and the 325° K surface depicts the vertical motion near the jet stream.

The vertical motion pattern at the 300° K surface shows a large area of ascent over the eastern United States (Fig. 5.14a). The vertical motion pattern aligns well with the stratiform cloud and precipitation associated with the developing surface cyclone. Over Oklahoma and Kansas an area of strong subsidence is calculated where clouds and precipitation are observed. However, an inspection of the 325° K surface shows strong upward vertical motion in this area in association with the polar jet and over Missouri in response to the subtropical jet (Fig. 5.14b). Consequently, we again see evidence of two separate mechanisms at work in the development of the synoptic growth of the cyclone.

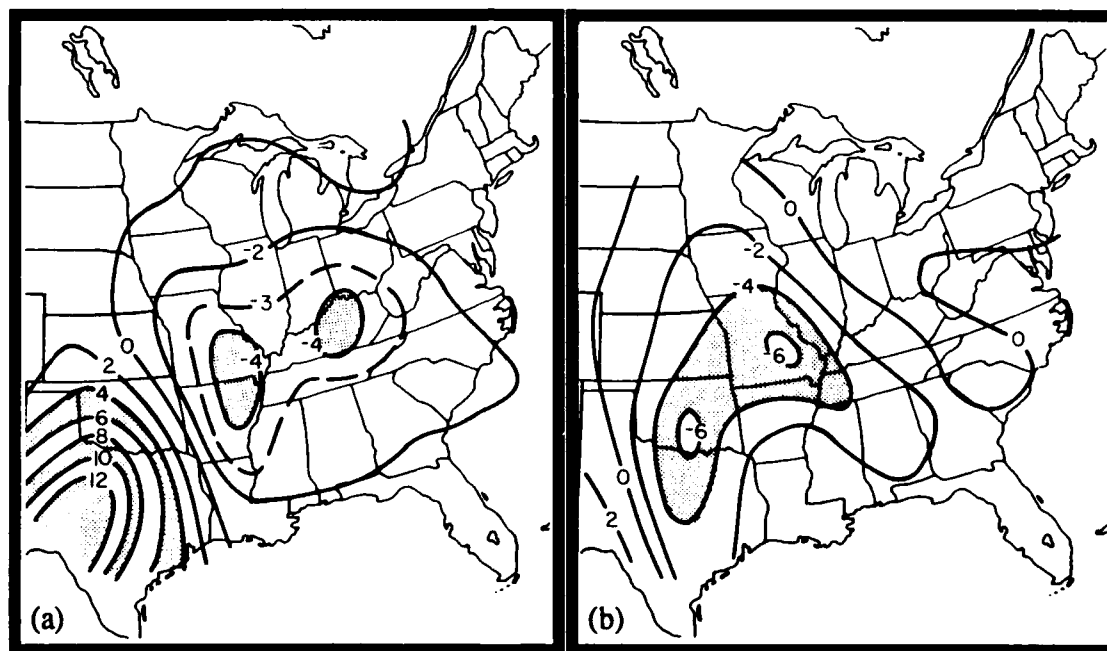


Figure 5.14. Thermodynamic omega calculations for 0000 UTC 15 December 1987. a) vertical motion along the 300° K isentropic surface, b) vertical motion along the 325° K isentropic surface. Solid lines depicts vertical motion isopleths in  $\mu\text{bars s}^{-1}$ . Shaded region depicts vertical motion of  $\pm 4 \mu\text{bars s}^{-1}$  at an interval of  $4 \mu\text{bars s}^{-1}$ .

Calculations of the vertical motion fields for 1200 UTC are displayed in Figure 5.15. In the lower levels, Figure 5.15a shows strong subsidence,  $6 \mu\text{bars s}^{-1}$ , in the vicinity of the cyclone center while the upward vertical motion is shunted to the east over the Mid-Atlantic region. The introduction of such strong subsidence over the cyclone center suppresses deepening resulting in the subsequent filling of the system. At the  $325^\circ \text{K}$  level we continue to see strong upward vertical motion over the cyclone that has increased in magnitude to  $-8 \mu\text{bars s}^{-1}$  (Fig. 5.15b). This pattern is consistent of the vertical motion associated with the left exit region of a jet streak.

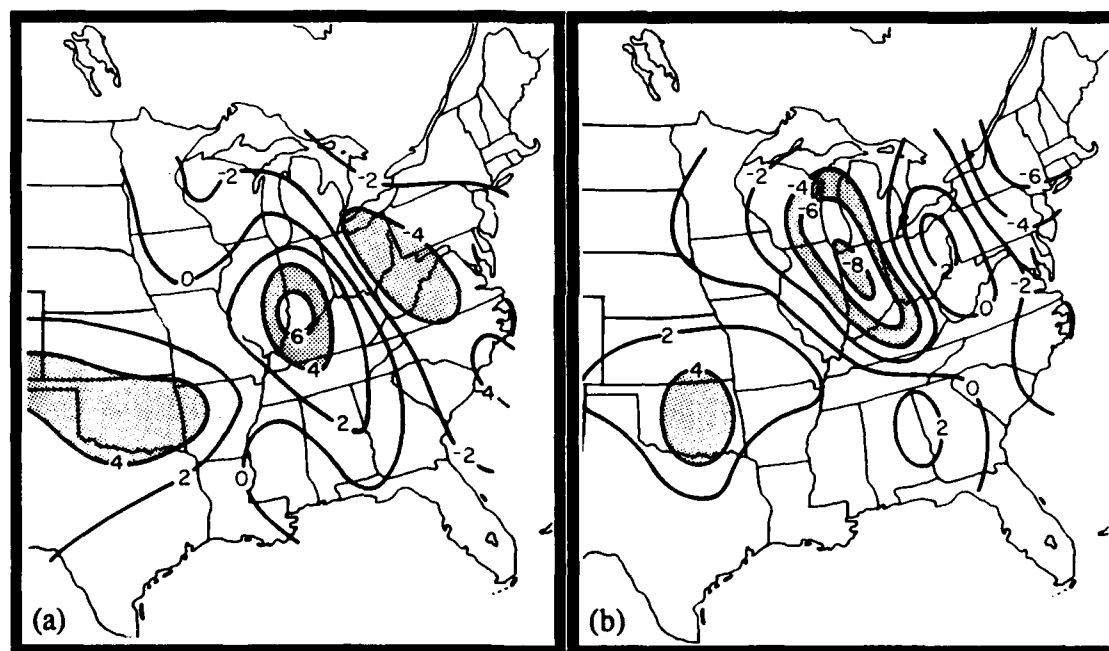


Figure 5.15. Thermodynamic omega calculations for 1200 UTC 15 December 1987. a) vertical motion along the  $310^\circ \text{K}$  isentropic surface, b) vertical motion along the  $325^\circ \text{K}$  isentropic surface. Solid lines depicts vertical motion is  $\mu\text{bars s}^{-1}$ . Shaded region depicts vertical motion of  $\pm 4 \mu\text{bars s}^{-1}$  at an interval of  $4 \mu\text{bars s}^{-1}$ .

### 5.3.2 Vertical Cross Section of Thermodynamic Omega

Horizontal displays of thermodynamic vertical motion patterns were analyzed and then transferred into the plane of the cross sections depicted in Figure 5.1. This depiction provides insight into the structure of the vertical motion pattern associated with the descending tropopause during the explosive development of the cyclone

Figure 5.16 depicts the vertical motion pattern for 0000 UTC 15 December 1987. Upward vertical motion is found in the left exit and right entrance region of a jet streak, as discussed in section 3.1. Consistent with that work, upward vertical motion of  $-6 \mu\text{bars s}^{-1}$  is found to the left of both the polar and subtropical jets. The upward motion is most pronounced in the upper and mid troposphere where values of  $-4 \mu\text{bars s}^{-1}$  extends down to 530 mb. A maxima of  $-6 \mu\text{bars s}^{-1}$ , in association with the polar jet, is related to the development of the upper-level vortex observed over Oklahoma. Near the surface, a second region of significant upward vertical motion is found in response to the frontal zone. The upward vertical motion throughout the troposphere allows the formation of significant thunderstorm activity and cyclone development near Little Rock, Arkansas. A region of significant subsidence is observed in the middle troposphere between Amarillo and Oklahoma City. This region extends from the tropopause to the top of the frontal surface. The subsidence weakens as it extends eastward separating the upward vertical maximums in the lower and upper troposphere.

The vertical motion profile at 1200 UTC is depicted in Figure 5.17. The increase in the organization of the jet structure results in an enhanced ageostrophic flow and vertical divergence. The result is the transport of stratospheric air down to the 700 mb level. The stratospheric protrusion observed in Figure 5.12 is associated with a significant region of subsidence in the order of  $+6 \mu\text{bars s}^{-1}$ . The vertical motion distribution about the jet in the low levels is consistent with that found in the jet entrance region. Here, subsidence is found in the left entrance region further aiding the descent of stratospheric air. The vertical extent of the strong subsidence over the cyclone center works towards the demise of the system. The consolidation of the polar and subtropical jets result in an increase in the upward vertical motion field from  $-6 \mu\text{bars s}^{-1}$ , twelve hours earlier, to  $-8 \mu\text{bars s}^{-1}$ .

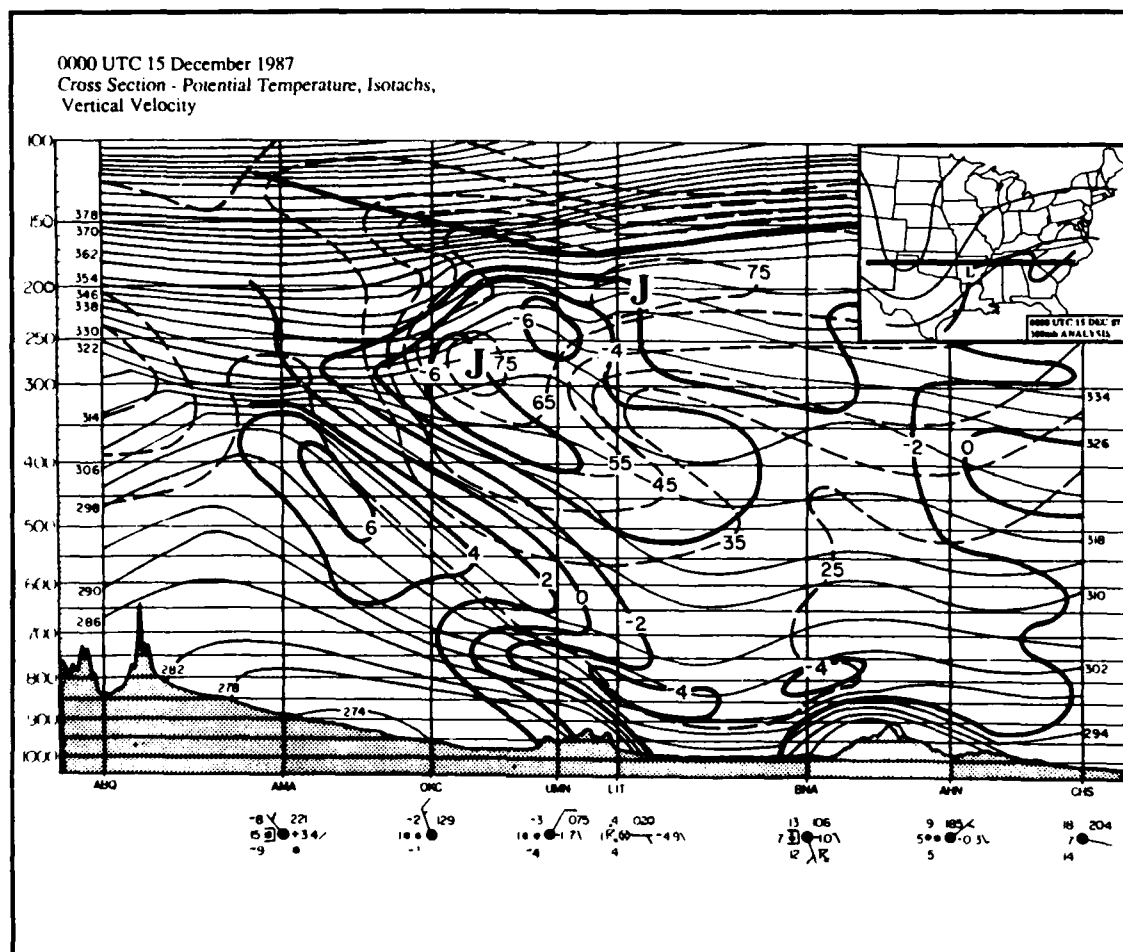


Figure 5.16. East-west vertical cross section at 0000 UTC 15 December 1987. Stations along the cross section are Albuquerque, New Mexico (ABQ), Amarillo, Texas (AMA), Oklahoma City, Oklahoma (OKC), Monett, Missouri (UMN), Little Rock, Arkansas (LIT), Nashville, Tennessee (BNA), Athens, Georgia (AHN), and Charleston, South Carolina (CHS). Vertical pressure axis is in millibars. Thin solid lines depict potential temperature at intervals of 4°K. Thick solid lines are isopleths of thermodynamic vertical motion ( $\mu\text{bars s}^{-1}$ ). Dashed lines depict isotachs for the total wind speed at intervals of 10 m s<sup>-1</sup>. Jet core denoted by "J". Stippled area depicts ground. Reported surface observation displayed beneath station three letter identifier. Temperature is in °C, winds are in m s<sup>-1</sup>, and visibility is in statute miles. Map insert shows orientation of cross section axis (thick line) in relation to the 300 mb pattern (thin lines) and the surface frontal position.

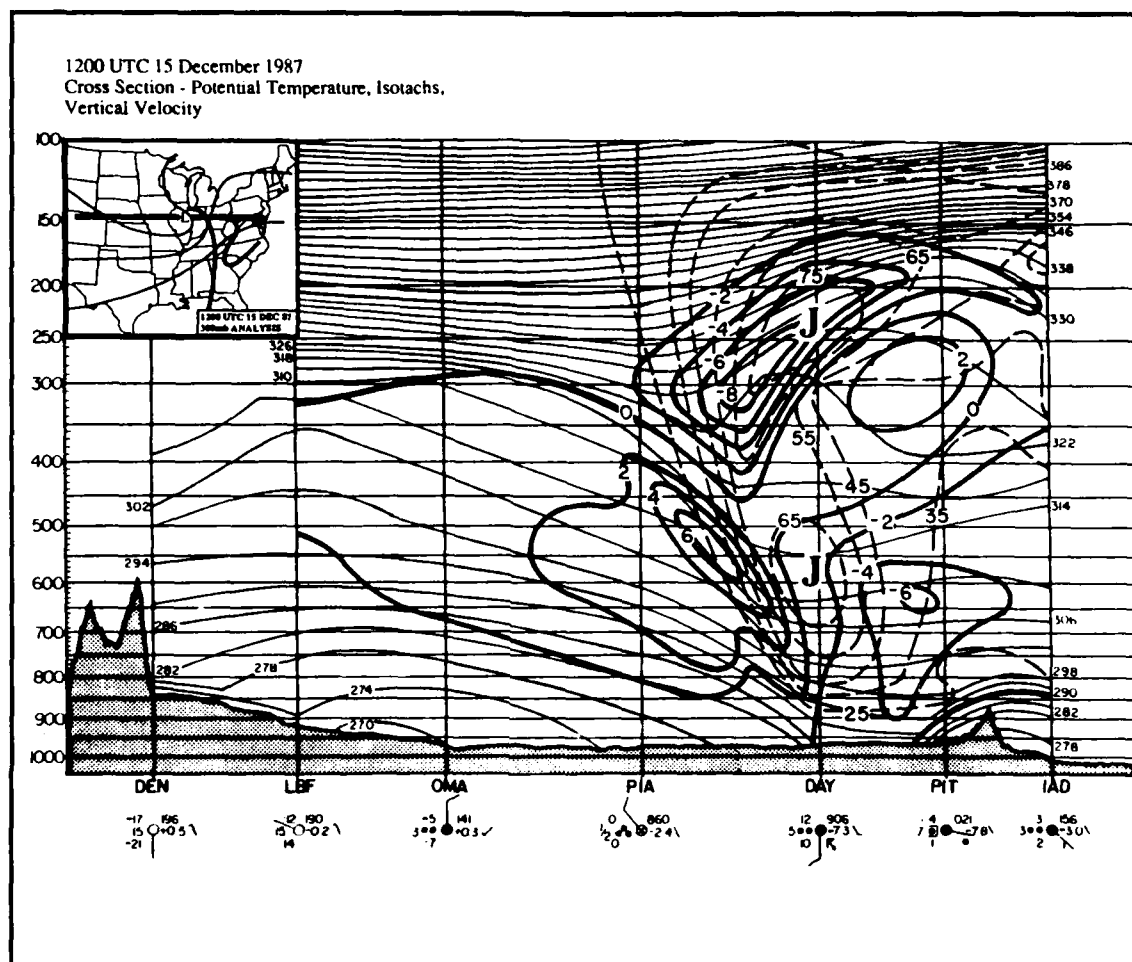


Figure 5.17. East-west vertical cross section at 1200 UTC 15 December 1987. Stations along the cross section are Denver, Colorado (DEN), North Platte, Nebraska (LBF), Omaha, Nebraska (OMA), Peoria, Illinois (PIA), Dayton, Ohio (DAY), Pittsburgh, Pennsylvania (PIT), and Washington D.C. (IAD). Vertical pressure axis is in millibars. Thin solid lines depict potential temperature at intervals of 4°K. Thick solid lines are isopleths of thermodynamic vertical motion ( $\mu\text{bars s}^{-1}$ ). Dashed lines depict isotachs for the total wind speed at intervals of 10  $\text{m s}^{-1}$ . Jet core denoted by "J". Stippled area depicts ground. Reported surface observation displayed beneath station three letter identifier. Temperature is in °C, winds are in  $\text{m s}^{-1}$ , and visibility is in statute miles. Map insert shows orientation of cross section axis (thick line) in relation to the 300 mb pattern (thin lines) and the surface frontal position.

## CHAPTER 6

## SUMMARY AND CONCLUSIONS

## 6.1 Summary

A study was conducted to document the development of explosive cyclogenesis over the Mid-West United States during 14-15 December 1987. The storms development was marked by two distinctive phases of deepening. Figure 6.1 summarizes the observed changes in surface pressure, surface-geostrophic relative vorticity, and the distance between the surface cyclone and the upper-tropospheric vorticity maximum.

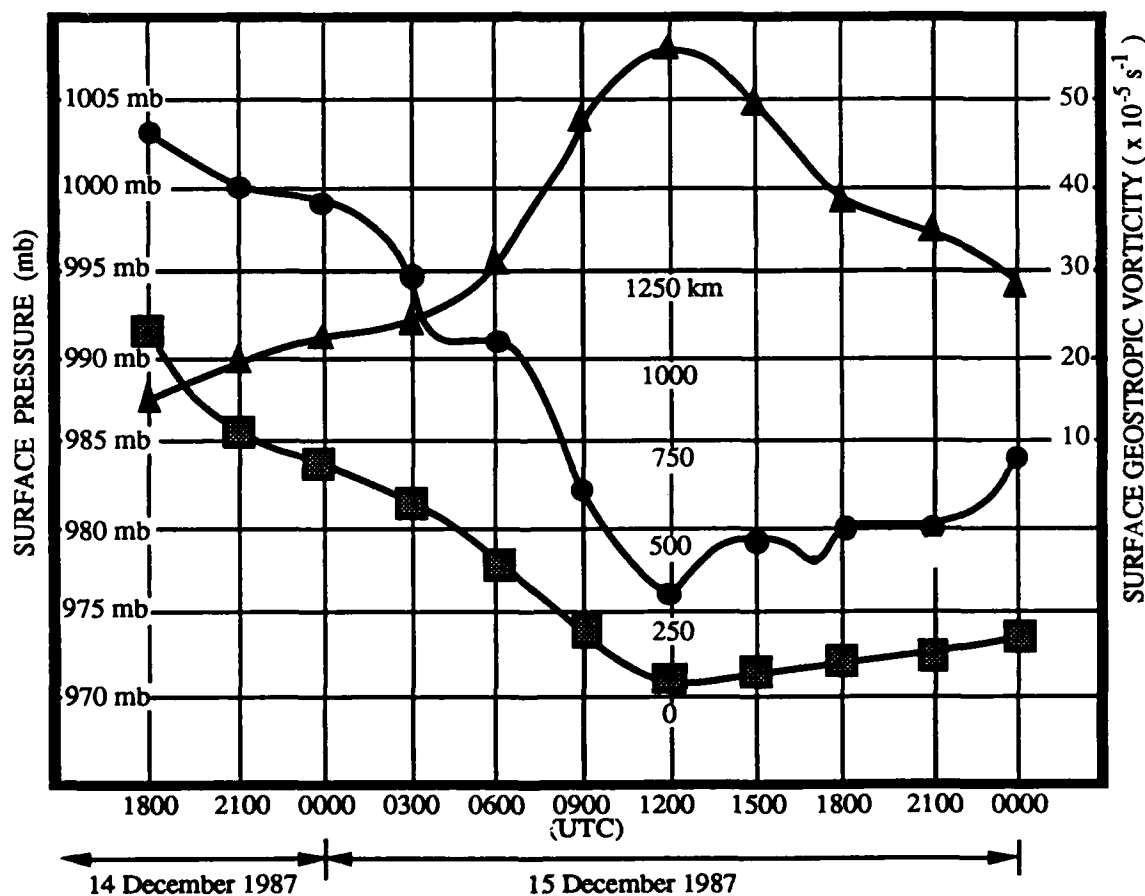


Figure 6.1. A Eulerian perspective for the 14-15 December 1987 cyclone development. Circles depict surface central pressure, Squares show distance between the cyclone center and the upper-level cyclonic vorticity maximum, and triangles depict the values of surface-geostrophic vorticity.

Cyclogenesis was initiated 100 km north of Houston, Texas at  $\approx 1800$  UTC 14 December. During the initial phase, 1800 UTC 14 December to 0400 UTC 15 December, the cyclone experienced a pressure fall of  $\approx 1 \text{ mb } \text{hr}^{-1}$ . Development was initiated in concert with the outbreak of deep convection over the cyclone center while only weak cyclonic vorticity advection aloft was observed in association with a propagating subtropical jet streak. A vigorous SWT, associated with the polar jet, was positioned over 1000 km to the west-northwest of the surface cyclone.

Figure 6.2 depicts the environment leading to development of the cyclone. The eastern Texas region was marked by a convectively unstable atmosphere. The boundary layer consisted of a large thermal and moisture gradient along the frontal zone in response to the southerly flow of warm-moist air from the Gulf of Mexico. Above 750 mb, a dry west-southwest intrusion was superposed over the region. Consequently, the environment in which cyclone development took place was marked by significant convective instability. The strong frontal zone and the advection of weak cyclonic vorticity aloft triggered the observed convection.

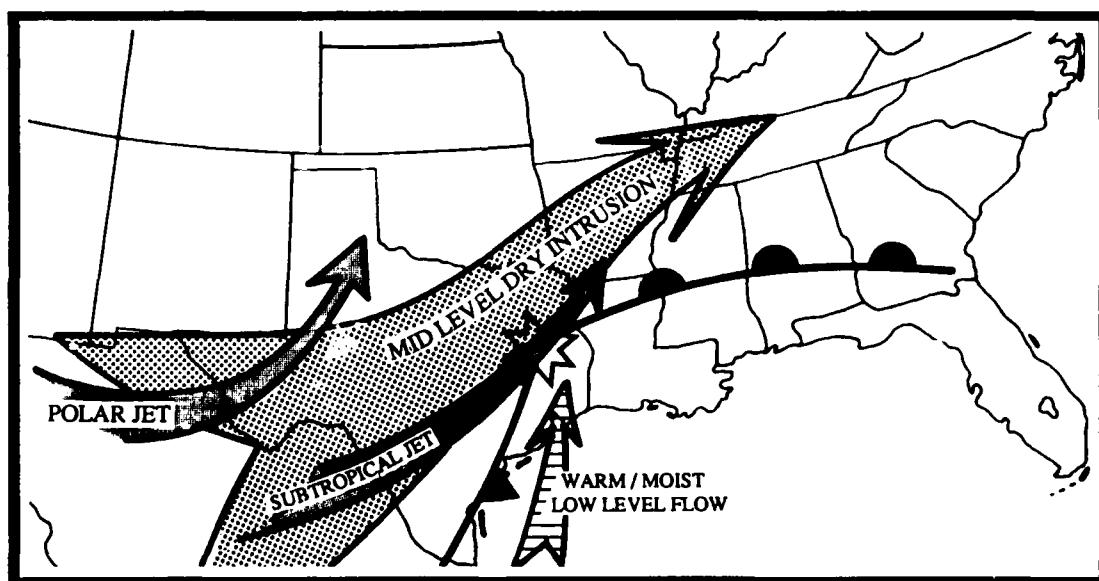


Figure 6.2. Environment for the development of the surface cyclone at 1800 UTC 14 December 1987.



A squall line developed along the cold front at 2100 UTC 14 December. Low-level convergence associated with the squall-line convection enhanced frontogenesis along the cold front and an associated low-level jet developed in the warm air just ahead of the front in response to thermal wind constraints. The low-level jet aided cyclogenesis through the advection of warm-moist Gulf air into the region of developing low pressure.

Calculations of surface-geostrophic relative vorticity ( $\zeta_g$ ) can be used to quantify the storm intensification (Petterssen, 1956). Calculations of surface-geostrophic relative vorticity were made using the form:

$$\zeta_g = \frac{\alpha}{f} \nabla^2 p \quad (6.1.1)$$

where  $\alpha$  is the specific humidity (value of  $0.8 \text{ m}^3 \text{ km}^{-1}$  was used) and calculations of  $\nabla^2 p$  were made using a grid spacing of 381 km. Vorticity generated during the first phase of development steadily increased 13 units to a value of  $28 \times 10^{-5} \text{ s}^{-1}$ .

The second phase of development, 0600-1200 UTC 15 December, was associated with a very rapid pressure fall ( $>2.5 \text{ mb hr}^{-1}$ )(Fig. 6.1). This explosive development coincides with the interaction of a progressive SWT superposed over the surface cyclone, the merging of the polar and subtropical jets, and the vertical coupling of the low and mid-level tropospheric jet streaks. Deep convection, which has been cited as a contributing factor to explosive development, is no longer observed over the cyclone center.

By 0600 UTC the SWT was located within 400 km of the surface cyclone (Fig. 6.1). The proximity of the upper-level vortex allows the associated differential vorticity advection by the thermal wind to be superposed over the surface cyclone promoting upward vertical motion. A merging of the polar and subtropical jets streaks results in very large dynamic forcing increasing the ageostrophic circulation pattern and the resultant vertical motion distribution. This process increases the observed upper-level subsidence forcing an intrusion of stratospheric air to the lower troposphere. An observed stratospheric intrusion to the 700 mb level generates substantial mid and upper tropospheric cyclonic vorticity advection that aids in the spinup of the storm.

The vertical coupling of the ageostrophic motion fields associated with the left exit region of the upper and lower-level jets streaks enhances the upward vertical motion throughout the troposphere. Figure 6.3 provides a conceptual model illustrating the vertical alignment of the two jet cores and their associated vertical motion patterns during the most rapid phase of development. The resultant vertical motion distribution produces pronounced ascent over the cyclone center while strong subsidence forces stratospheric air to the lower levels.

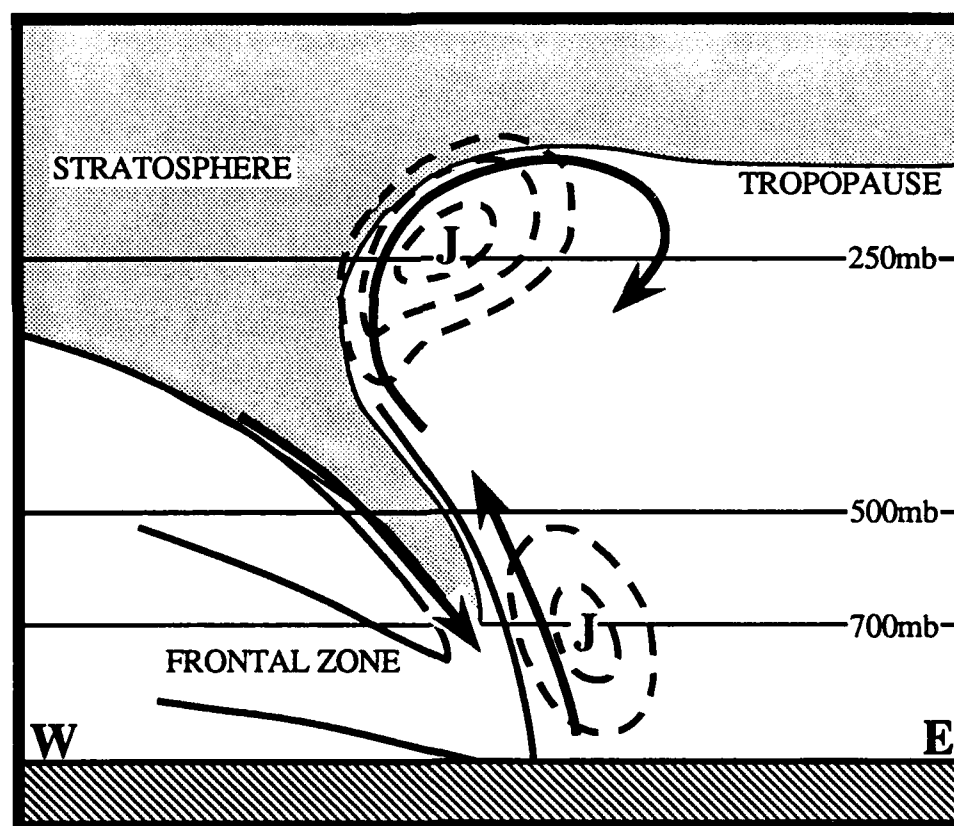


Figure 6.3. Conceptual model of the vertical cross section intersecting the center of the cyclone center during the most rapid phase of development. Thick arrow illustrates the vertical motion distribution. "J" denotes the jet axis and the dashed lines are isotachs. The stratosphere and the protrusion of stratospheric air to lower levels is stippled. Heavy solid lines define the stable layer associated with the frontal zone and the descending tropopause.

The explosive deepening results in a rapid increase in the generation of surface vorticity (Fig. 6.1). By 1200 UTC the surface-geostrophic relative vorticity doubles to  $56 \times 10^{-5} \text{ s}^{-1}$  as the storm deepens to a minimum central pressure of 976 mb. The cyclone development ceases as the surface cyclone becomes vertical with the upper-level low and the subsidence associated with the descending stratospheric air is superposed over the surface cyclone. The upward vertical motion over the surface cyclone is minimized and subsequent filling is noted. As the cyclone passes over the southern tip of Lake Michigan the influence of diabatic heating (Petterssen, 1956) acts to reduce the sea-level pressure between 1500-1700 UTC (Fig. 6.1). As the cyclone moves northeastward, diabatic heat sources are minimized and the system resumes its decay.

## 6.2 Conclusions

It has been suggested that the development of explosive cyclogenesis is the result of some additional process(es) other than typical baroclinic instability. In this research, explosive development was observed in response to several processes coming together providing optimal conditions of baroclinic instability. No evidence was found to suggest that additional process(es) were responsible for the explosive development of the cyclone. Important events in the explosive development include:

- Development of convection coincident with initial cyclogenesis
- Rapid development of a squall line along the cold front enhancing frontogenesis
- Development of a low-level jet ahead of the cold front transporting warm-moist air to the region of developing low pressure
- Mid-tropospheric vortex moving to within 400 km of the surface cyclone
- Merging of the polar and subtropical jet streaks results in very large dynamic forcing
- Stratospheric intrusion to the 700 mb level generating substantial mid and upper tropospheric cyclonic vorticity advection that aids the spinup of the storm.
- Vertical coupling of the ageostrophic motion fields associated with the left exit region of the upper and lower-level jets streaks

### **6.3 Future Research**

The research presented in this thesis provides the synoptic development for a case of explosive cyclogenesis. Additional research is warranted to further our understanding and to quantify the mechanisms at work in explosive cyclogenesis. Such research should include:

- Compare Q-vectors and kinematic calculations of vertical motion.
- Compute the magnitude and evolution of frontogenesis associated with the developing cold front.
- Investigate the role of symmetric instability associated with heavy stratiform precipitation north of the occluded front.

## CHAPTER 7

## REFERENCES

- Achter, T. H., and L. H. Horn, 1986: Spring season Colorado cyclones. Part I: Use of composites to relate upper and lower tropospheric wind fields. *J. Climate Appl. Meteor.*, **25**, 732-743.
- Anderson, R. K., J. P. Ashman, F. Bittner, G. R. Farr, E. W. Ferguson, V. J. Oliver, and A. H. Smith, 1969: Application of meteorological satellite data in analysis and forecasting. ESSA Tech. Rep. NESC 51 U.S. Dept. of Commerce, Washington, D.C. [NTIS AD-697022.]
- Barnes, S. L., 1964: A technique for maximizing details in numerical weather map analysis. *J. Appl. Meteor.*, **3**, 396-409.
- \_\_\_\_\_, 1973: Mesoscale objective analysis using weighted time-series observations. NOAA Technical Memorandum ERL NSSL-62, Norman, OK., 60 pp.
- \_\_\_\_\_, 1985: Omega diagnostics as a supplement to LFM/MOS guidance in weakly forced convective situations. *Mon. Wea. Rev.*, **113**, 2122-2141.
- Bjerknes, J., and H. Solberg, 1921: Meteorological conditions for the formation of rain. *Geofys. Publikasjoner*, Norske Videnskaps-Akad. Oslo, **2**, No. 3, 60 pp.
- \_\_\_\_\_, and H. Solberg, 1922: Life cycle of cyclones and the polar front theory of atmospheric circulation. *Geofys. Publ.*, **9**, 30-45.
- \_\_\_\_\_, J. Bjerknes, H. Solberg, and T. Bergeron, 1933: Physikalische hydrodynamik mit anwendung auf die dynamische meteorologie, Springer, Berlin.
- \_\_\_\_\_, 1937: Theorie der aussertropischen zyklonenbildung. *Meteorol. Z.*, **54**, 462-466.

- Bosart, L. F., 1970: Mid-tropospheric frontogenesis. *Quart. J. Roy. Meteor. Soc.*, **96**, 442-471.
- \_\_\_\_\_, 1981: The President's Day snowstorm of 18-19 February 1979: A subsynoptic scale event. *Mon. Wea. Rev.*, **109**, 1542-1566.
- \_\_\_\_\_, and S. C. Lin, 1984: A diagnostic analysis of the Presidents' Day storm of February 1979. *Mon. Wea. Rev.*, **112**, 2148-2177.
- Carleton, A. M., 1985: Satellite climatological aspects of the polar low and "instant occlusion." *Tellus*, **37**, 433-450.
- Charney, J. G., G. P. Cressman, D. Fultz, S. L. Hess, A. E. Nyberg, E. V. Palmen, H. Riehl, C. Rossby, Z. Sekera, V. P. Starr, and T. C. Yeh, 1947: On the general circulation of the atmosphere in middle latitudes. *Bull. Amer. Meteor. Soc.*, **28**, 255-280.
- Charney, J. G., 1947: The dynamics of long waves in a baroclinic westerly current. *J. of Meteor.*, **4**, 135-162.
- \_\_\_\_\_, and A. Eliassen, 1964: On the growth of hurricane depression. *J. Atmos. Sci.*, **21**, 68-75.
- Danielson, E. F., 1968: Stratospheric-tropospheric exchange based upon radioactivity, ozone, and potential vorticity. *J. Atmos. Sci.*, **25**, 502-518.
- Durran, D. R. and L. W. Snellman, 1987: The diagnosis of synoptic-scale motion in an operational environment. *Wea. and Forecasting*, **1**, 17-31.
- Fitz-Roy, R., 1863: Weather Book. A Manual of Practical Meteorology. London

- George, J. J., 1960: Weather Forecasting for Aeronautics. New York, Academic Press, 407-415 pp.
- Gyakum J. R., 1983: On the evolution of the QE II storm. I: Synoptic aspects. *Mon. Wea. Rev.*, **6**, 1137-1155.
- \_\_\_\_\_, and E. S. Barker, 1988: A case study of explosive subsynoptic-scale cyclogenesis. *Mon. Wea. Rev.*, **116**, 2225-2253.
- Haltiner, G. J., and F. L. Martin, 1957: Dynamical and Physical Meteorology. New York, McGraw-Hill Book Co, 470 pp.
- Holton, J. R., 1979: An Introduction to Dynamic Meteorology. International Geophysics Series, Vol. 23, Academic Press, New York, 391 pp.
- Homan, J. and L. W. Uccellini, 1987: Winter forecast problems associated with light to moderate snow events in the mid-Atlantic states on 14 and 22 February 1986. *Wea. and Forecasting*, **1**, 4-12.
- Hoskins, B. J., P. Berrisford, 1988: A potential vorticity perspective. *Weather*, **43**, 122-129.
- \_\_\_\_\_, M.E. McIntyre, and A. W. Robertson, 1985: On the use and significance of isentropic potential vorticity maps. *Quart. J. Roy. Meteor. Soc.*, **111**, 877-946.
- Hovanec, R. D., and L. H. Horn, 1975: Static stability and the 300 mb isotach field in the Colorado cyclogenetic area. *Mon. Wea. Rev.*, **103**, 628-638.
- Kleinschmidt, E., 1950: Uber aufban und entstehung von zyklonen (1. Teil). *Met. Rund.*, **3**, 1-6.

\_\_\_\_\_, 1955: Die entstehung einer hohenzyklone uber nordamerika, *Tellus*, **7**, 96-110.

Konrad, C. E., and S. J. Colucci, 1988: Synoptic climatology of 500 mb circulation changes during explosive cyclogenesis. *Mon. Wea. Rev.*, **116**, 1431-1443.

MacDonald, B. C., and E. R. Reiter, 1988: Explosive cyclogenesis over the eastern United States. *Mon. Wea. Rev.*, **116**, 1568-1586.

Mailhot, J. and C. Chouinard, 1989: Numerical forecasts of explosive winter storms: Sensitivity experiments with a meso- $\alpha$  scale model. *Mon. Wea. Rev.*, **117**, in print.

Moore, J. T., and P. D. Blakley, 1988: The role of frontogenetical forcing and conditional symmetric instability in the midwest snowstorm of 30-31 January 1982. *Mon. Wea. Rev.*, **116**, 2155-2171.

Mullen, S. L., 1983: Explosive cyclogenesis associated with cyclones in polar airstreams. *Mon. Wea. Rev.*, **111**, 1537-1553.

Miller, J. E., 1946: Cyclogenesis in the Atlantic coastal region of the United States. *J. Meteor.*, **3**, 31-44.

Miller, R. C., 1972: Notes on analysis and severe storm forecasting procedures of the Air Force Global Weather Central. AWS Tech. Rep 200 (Rev). [Available from AWS Headquarters, Scott AFB, IL 62225].

Newton, C. W., 1954: Frontogenesis and frontolysis as a three-dimensional process. *J. Meteor.*, **11**, 449-461.

Palmen, E., and C. W. Newton, 1969: Atmospheric Circulation Systems: Their Structure and Physical Interpretation, Academic Press, New York, 603 pp.



- Peppler, R. A., 1988: A Review of Static Stability Indices and Related Thermodynamic Parameters, Illinois State Water Survey Miscellaneous Publication 104, 87 pp.
- Petersen, R. A., L. W. Uccellini, A. Mostek and D. A. Keyser, 1984: Delineating mid- and low-level water vapor patterns in a preconvective environment using VAS moisture channels. *Mon. Wea. Rev.*, **112**, 2178-2198.
- Petterssen, S., 1956: Weather Analysis and Forecasting (Vol. I), New York: McGraw-Hill Book Co, 428 pp.
- Reed, R. J., and F. Sanders, 1953: An investigation of the development of a mid-tropospheric frontal zone and its associated vorticity field. *J. Meteor.*, **10**, 338-349.
- \_\_\_\_\_, 1955: A study of a characteristic type of upper-level frontogenesis. *J. Meteor.*, **12**, 226-237.
- \_\_\_\_\_, and E. F. Danielson, 1959: Fronts in the vicinity of the tropopause. *Arch. Meteorol. Bioklim*, **11A**, 1-17.
- \_\_\_\_\_, and M. D. Albright, 1986: A case study of explosive cyclogenesis in the eastern Pacific. *Mon. Wea. Rev.*, **114**, 2297-2319.
- \_\_\_\_\_, and Y. Kuo, 1988: Numerical simulation of an explosive deepening cyclone in the eastern Pacific. *Mon. Wea. Rev.*, **10**, 2081-2105.
- Riehl, H., and S. Teweles, 1953: A further study on the relation between the jet stream and cyclone formation. *Tellus*, **5**, 66-79.
- Rodgers, E. B., V. V. Solomonson and H. L. Kyle, 1976: Upper tropospheric dynamics as reflected in Nimbus 4 THIR 6.7- $\mu\text{m}$  data. *J. Geophys. Res.*, **81**, 5749-5758.

- Roebber, P. J., 1984: Statistical analysis and updated climatology of explosive cyclones. *Mon. Wea. Rev.*, **112**, 1577-1589.
- Rossby, C. G., 1939: Relation between variations in the intensity of the zonal circulation of the atmosphere and the displacement of the semi-permanent centers of action. *J. Marine Res.*, **2**(1), 38-55.
- \_\_\_\_\_, 1940: Planetary flow patterns in the atmosphere. *Quart. J. Roy. Meteor. Soc.*, **66**, Suppl., 68-87.
- Sanders, F., and J. R. Gyakum, 1980: Synoptic-dynamic climatology of the "bomb". *Mon. Wea. Rev.*, **108**, 1589-1606.
- \_\_\_\_\_, 1986: Explosive cyclogenesis in the west-central north Atlantic ocean, 1981-84. Part I: Composite structure and mean behavior. *Mon. Wea. Rev.*, **114**, 1781-1794.
- \_\_\_\_\_, 1987: A study of 500 mb vorticity maxima crossing the east coast of North America and associated surface cyclogenesis. *Wea. and Forecasting*, **2**, 70-83.
- Saucier, W.J., 1955: Principles of Meteorological Analysis, The University of Chicago Press, 438 pp.
- Shapiro, M. A., 1976: The role of turbulent heat flux in the generation of potential vorticity in the vicinity of upper-level jet stream systems. *Mon. Wea. Rev.*, **104**, 892-906.
- Storm Data, December 1987, Volume 29, Number 12, U. S. Department of Commerce / NOAA / NESDIS / National Climatic Data Center, Asheville, N.C.
- Tracton, M. S., 1973: The role of convection in the development of extratropical cyclones. *Mon. Wea. Rev.*, **101**, 573-593.

Trenberth, K. E., 1978: On the interpretation of the diagnostic quasi-geostrophic omega equation. *Mon. Wea. Rev.*, **106**, 131-137.

Uccellini, L.W., 1976: Operational diagnostic applications of isentropic analysis. *Nat. Wea. Dig.*, **1**, 4-12.

\_\_\_\_\_, and D. R. Johnson, 1979: The coupling of upper and lower tropospheric jet streaks and implications for the development of severe convective storms. *Mon. Wea. Rev.*, **107**, 682-703.

\_\_\_\_\_, 1980: Notes and Correspondence: On the role of upper tropospheric jet streaks and leeside cyclogenesis in the development of low-level jets in the great plains. *Mon. Wea. Rev.*, **108**, 1689-1696.

\_\_\_\_\_, P. J. Kocin, R. A. Petersen, C. H. Wash and K. F. Brill, 1984: The Presidents' Day cyclone of 18-19 February 1979: Synoptic overview and analysis of the subtropical jet streak influencing the pre-cyclogenetic period. *Mon. Wea. Rev.*, **112**, 31-55.

\_\_\_\_\_, D. Keyser, K. F. Brill and C. H. Wash, 1985: The Presidents' Day cyclone of 18-19 February 1979: Influence of a tropopause fold on rapid cyclogenesis. *Mon. Wea. Rev.*, **113**, 962-988.

\_\_\_\_\_, and P. J. Kocin, 1987: The interaction of jet streak circulation during heavy snow events along the east coast of the United States. *Wea. and Forecasting*, **1**, 289-308.

Young, M. V., G. A. Monk, and K. A. Browning, 1987: Interpretation of satellite imagery of a rapidly deepening cyclone. *Quart. J. Roy. Meteor. Soc.*, **113**, 1089-1115.

Weekly Weather and Crop Report, December 1987, Volume 74, Number 49, U.S. Department of Commerce, U.S. Department of Agriculture, Washington D.C.

Weldon, R., 1979: Satellite Training Course Notes, Applications Division, National Environmental Satellite Service, NOAA, 80 pp.

\_\_\_\_\_, 1983: Synoptic Scale Cloud Systems. Course training notes, Satellite Applications Laboratory, NOAA/NESDIS, Washington D.C.

\_\_\_\_\_, 1985: Conclusions and Generalizations of Water Vapor Imagery Gray Shades Versus Moisture Distribution, Course training notes, Satellite Applications Laboratory, NOAA/NESDIS, Washington D.C., 4 pp.

\_\_\_\_\_, 1987: Types of Cyclogenesis, Course training notes, Satellite Applications Laboratory, NOAA/NESDIS, Washington D.C.